NAVAL POSTGRADUATE SCHOOL

MONTEREY, CALIFORNIA

THESIS

A HYBRID, LARGE-SCALE WIRELESS SENSOR NETWORK FOR REAL-TIME ACQUISITION AND TRACKING

by

Panagiotis Katopodis

June 2007

Thesis Advisor:	Murali Tummala
Co-Advisor:	Gamani Karunasiri
Second Reader:	Bret Michael

Approved for public release; distribution is unlimited

THIS PAGE INTENTIONALLY LEFT BLANK

REPORT DOCUMENTATION PAGE			Form Approved OMB No. 0704-0188
Public reporting burden for this collection of information is estimated to average 1 hour per response, including the time for reviewing instruction, searching existing data sources, gathering and maintaining the data needed, and completing and reviewing the collection of information. Send comments regarding this burden estimate or any other aspect of this collection of information, including suggestions for reducing this burden, to Washington headquarters Services, Directorate for Information Operations and Reports, 1215 Jefferson Davis Highway, Suite 1204, Arlington, VA 22202-4302, and to the Office of Management and Budget, Paperwork Reduction Project (0704-0188) Washington DC 20503.			
1. AGENCY USE ONLY *(Leave blank)*	**2. REPORT DATE** June 2007	**3. REPORT TYPE AND DATES COVERED** Master's Thesis	
4. TITLE AND SUBTITLE A Hybrid, Large-Scale Wireless Sensor Network for Real-Time Acquisition and Tracking		**5. FUNDING NUMBERS**	
6. AUTHOR(S) Panagiotis Katopodis			
7. PERFORMING ORGANIZATION NAME(S) AND ADDRESS(ES) Naval Postgraduate School Monterey, CA 93943-5000		**8. PERFORMING ORGANIZATION REPORT NUMBER**	
9. SPONSORING /MONITORING AGENCY NAME(S) AND ADDRESS(ES) Missile Defense Agency		**10. SPONSORING/MONITORING AGENCY REPORT NUMBER**	
11. SUPPLEMENTARY NOTES The views expressed in this thesis are those of the author and do not reflect the official policy or position of the Department of Defense or the U.S. Government.			
12a. DISTRIBUTION / AVAILABILITY STATEMENT Approved for public release; distribution is unlimited		**12b. DISTRIBUTION CODE**	

13. ABSTRACT (maximum 200 words)

This thesis proposes a hybrid, large-scale wireless sensor network (WSN) designed to support real-time target detection and tracking of multiple ballistic missile threats. In particular, the proposed WSN consists of terrestrial as well as satellite nodes. The IR signatures presented by the target-background combination are explored and modern IR sensor technologies are examined in search of a suitable IR sensor for the proposed hybrid, large-scale WSN. A multicolor, Quantum Well Infrared Photodetector (QWIP), step-stare, large-format Focal Plane Array (FPA) is proposed and evaluated through performance analysis.

The thesis proposes an efficient data dissemination mechanism as well as a suitable medium access control (MAC) scheme for the proposed WSN, designed to meet the real-time and accuracy requirements without introducing excessive overhead and increased end-to-end time-delays. A clustering mechanism, called the "Area of Interest" (AOI) is introduced, which combines the "content based" feature of the data centric routing approach with the principles of in-network data aggregation and clustering. Simulation results verify that aggregation within the AOI improves the data throughput across the full range of network load. A contention based MAC scheme, Carrier Sense Multiple Access (CSMA), and a contention free approach, Time Division Multiple Access (TDMA), are examined. Performance analysis and simulation results indicate that a contention-free approach is suitable for implementation in wireless networks associated with large propagation delays and increased offered loads. Matlab and OPNET Modeler© software packages are used to simulate and evaluate the proposed schemes.

14. SUBJECT TERMS Wireless Sensor Networks, Real-Time Target Tracking, Multi-color Quantum-Well Infrared Photodetectors, Focal Plane Array, Data Centric Routing, Clustering, Data Aggregation, Medium Access Control, Carrier Sense Multiple Access (CSMA), Time Division Multiple Access (TDMA).			**15. NUMBER OF PAGES** 111
			16. PRICE CODE
17. SECURITY CLASSIFICATION OF REPORT Unclassified	**18. SECURITY CLASSIFICATION OF THIS PAGE** Unclassified	**19. SECURITY CLASSIFICATION OF ABSTRACT** Unclassified	**20. LIMITATION OF ABSTRACT** UL

NSN 7540-01-280-5500

Standard Form 298 (Rev. 2-89)
Prescribed by ANSI Std. 239-18

THIS PAGE INTENTIONALLY LEFT BLANK

Approved for public release; distribution is unlimited

A HYBRID, LARGE-SCALE WIRELESS SENSOR NETWORK FOR REAL-TIME ACQUISITION AND TRACKING

Panagiotis Katopodis
Lieutenant Junior Grade, Hellenic Navy
B.S., Hellenic Naval Academy, 1997

Submitted in partial fulfillment of the
requirements for the degree of

MASTER OF SCIENCE IN ELECTRICAL ENGINEERING
and
MASTER OF SCIENCE IN APPLIED PHYSICS

from the

NAVAL POSTGRADUATE SCHOOL
June 2007

Author: Panagiotis Katopodis

Approved by: Professor Murali Tummala
Thesis Advisor

Professor Gamani Karunasiri
Co-Advisor

Professor Bret Michael
Second Reader

Professor James H. Luscombe
Chairman, Department of Physics

Professor Jeffrey B. Knorr
Chairman, Department of Electrical and Computer Engineering

THIS PAGE INTENTIONALLY LEFT BLANK

ABSTRACT

This thesis proposes a hybrid, large-scale wireless sensor network (WSN) designed to support real-time target detection and tracking of multiple ballistic missile threats. In particular, the proposed WSN consists of terrestrial as well as satellite nodes. The IR signatures presented by the target-background combination are explored and modern IR sensor technologies are examined in search of a suitable IR sensor for the proposed hybrid, large-scale WSN. A multicolor, Quantum Well Infrared Photodetector (QWIP), step-stare, large-format Focal Plane Array (FPA) is proposed and evaluated through performance analysis.

The thesis proposes an efficient data dissemination mechanism as well as a suitable medium access control (MAC) scheme for the proposed WSN, designed to meet the real-time and accuracy requirements without introducing excessive overhead and increased end-to-end time-delays. A clustering mechanism, called the "Area of Interest" (AOI) is introduced, which combines the "content based" feature of the data centric routing approach with the principles of in-network data aggregation and clustering. Simulation results verify that aggregation within the AOI improves the data throughput across the full range of network load. A contention based MAC scheme, Carrier Sense Multiple Access (CSMA), and a contention free approach, Time Division Multiple Access (TDMA), are examined. Performance analysis and simulation results indicate that a contention-free approach is suitable for implementation in wireless networks associated with large propagation delays and increased offered loads. Matlab and OPNET Modeler© software packages are used to simulate and evaluate the proposed schemes.

THIS PAGE INTENTIONALLY LEFT BLANK

TABLE OF CONTENTS

LIST OF FIGURES

LIST OF TABLES

THIS PAGE INTENTIONALLY LEFT BLANK

ACKNOWLEDGMENTS

A *thesis*, from the Greek word *"θέσις"*, means position. Anyone is capable of providing an intellectual argument, however very few have the fortune of presenting a *thesis*. My co-advisors, Professor Murali Tummala, Professor Gamani Karunasiri, and Professor Bret Michael, as well as CDR Owens Walker, ensured that my work is a *thesis*. Any acknowledgement in my own words would not match their contribution; therefore I would like to share with them a quote by one of my ancestors:

"Those who educate children well are more to be honored than they who produce them; for these only gave them life, those the art of living well"

(**Aristotle** 384 - 322 BC)

Most importantly, I wish to thank my wife, Eleni, for her endless patience and invaluable support, as well as a little man, who not only inspired and encouraged me with his big smile but also made sure that I got enough rest throughout my thesis, my five-months old son, Thomas. It is to them that I dedicate this work.

THIS PAGE INTENTIONALLY LEFT BLANK

EXECUTIVE SUMMARY

In recent years, significant research advancements have occurred in the field of Wireless Sensor Networks (WSN), which consist of small nodes with sensing, computational, and wireless communications capabilities. These nodes may be deployed in large numbers in hazardous areas, incorporate a wide variety of sensors and self organize unattended to form a WSN that will disseminate the sensed data to a remote station. The military and civilian applications of WSN are vast and may include: target detection and tracking, security surveillance, weather and environmental condition monitoring, medical support, industrial monitoring and inventory management. However, these "traditional" WSN, due to their nature, impose considerable constraints on energy efficiency, on-board processing power and communication transmission ranges.

This thesis will leverage these recent advancements in the area of WSN by proposing a hybrid, large-scale wireless sensor network (WSN) designed to support real-time target detection and tracking of multiple ballistic missile threats of all ranges and in all phases of flight. Although the proposed hybrid, large-scale WSN does not share many of the constraints imposed on traditional WSN, particularly in terms of energy and on-board node processing, it still is a wireless network of sensors and exhibits one of their basic characteristics, in the sense that the data traffic is based on the sensed phenomena.

Critical factors in the design of the network topology and the deployment of the sensor nodes are those of sensor coverage and communication connectivity since they will guarantee early warning/detection, continuous tracking of the threat, and successful inter-communication among the sensor node platforms. Therefore, a hierarchical network architecture composed of three different tiers, defined by altitude above the earth, incorporating both terrestrial and satellite sensor nodes is considered.

This thesis has two main objectives. The first objective is the examination of the IR signatures presented by the target-background combination and the investigation of modern IR sensor technologies in search of a suitable IR sensor for the proposed hybrid, large-scale WSN. The singularities of such an IR sensor involve background competing

factors, such as solar and earth radiation (earthshine), large sensor footprints and a target-background combination, which is not constant throughout the target trajectory. To effectively resolve these issues, a multi-color quantum-well IR photodetector (QWIP) step-stare focal plane array (FPA) is proposed.

The hybrid nature of the WSN, which incorporates terrestrial and space based platforms, fixed and mobile nodes, and RF as well as IR sensors, presents a great challenge in the data dissemination. Additionally, the necessity for real-time target tracking generates a set of requirements that must be fulfilled. These include maximization of the network data throughput and minimization of the network end-to-end time-delay.

The second thesis objective involves the development of an efficient data dissemination mechanism as well as a suitable medium access control scheme for the proposed hybrid, large-scale WSN. A clustering mechanism, called the "Area of Interest" (AOI) is introduced, which combines the "content based" feature of the *data centric* routing approach with the principles of in-network data aggregation and clustering. Building upon this AOI mechanism, a data dissemination algorithm suitable for a hybrid large-scale WSN, designed to meet the real-time and accuracy operational requirements imposed by the nature and mission of the WSN without introducing excessive data overhead and increased time-delays is presented.

Medium access control (MAC) schemes are investigated since the nature of the proposed WSN necessitates for a shared medium consideration, rather than treating the node interconnections as dedicated point-to-point communication links. A contention based scheme, Carrier Sense Multiple Access (CSMA) MAC, and a contention free approach, Time Division Multiple Access (TDMA) MAC, are examined.

Although this thesis is immediately applicable to an IBMDS, the obtained results may be extended to tactical missile defense systems as well as "traditional" wireless sensor networks intended for real-time object surveillance, detection and tracking in military as well as civilian applications.

I. INTRODUCTION

In recent years, the theater of operations for missile defense has expanded from the "traditional" tactical boundaries, where the threat was limited to a confined geographical area, to a broader strategic domain where the threat involves Intercontinental Ballistic Missiles (ICBM). An ICBM is characterized by a global nature since an attack may be initiated from virtually any place on Earth posing a threat to a distant and wide geographical area. Additionally, the ICBM's high altitude, large speed, and increased range leave a defense system little room for error. This global nature of the threat unavoidably implies that the components of a defense system designed to counteract this threat, such as sensor / weapon platforms and Command & Control centers, will most probably be geographically dispersed. Therefore, to meet these challenges, the design of a Ballistic Missile Defense System (BMDS) must provide continuous surveillance, detection and tracking capabilities for a large threat volume and simultaneously guarantee an efficient and reliable communication / cooperation among the BMDS components in a real-time fashion.

The Missile Defense Agency (MDA) is developing an Integrated Ballistic Missile Defense System (IBMDS) to defend the United States, its deployed forces, allies and friends from ballistic missiles of all ranges and in all phases of flight. The IBMDS will be capable of destroying a ballistic missile in each of three distinct phases of its trajectory—boost, midcourse, and terminal phase. This requires the employment of advanced sensors and weapons as well as quick reaction times provided by reliable command and control, battle management, and communications [1].

The IBMDS incorporates a collection of sensor and weapon systems that are integrated to achieve the best possible performance. Terrestrial sensors involve systems such as the sea-based X-band radar (SBX) that is capable of detection, tracking, kill-assessment and countermeasure discrimination, the Aegis AN/SPY-1 S-band phased array radars onboard warships, and forward deployable X-band Radars (FDR) that enhance the probability of early warning by obtaining data from the initial phase of the

threat trajectory. Space-based sensors include the optical and IR sensor systems carried by the Geostationary (GEO) satellites of the Defense Support Program (DSP) and the Low-earth orbit (LEO) satellites of the Space Tracking and Surveillance System (STSS). Furthermore, weapon systems such as the airborne laser aircraft YAL-1A, the SM-3 sea-based short-range interceptors, the ground-based long-range interceptors, multiple kill-vehicles, and Patriot Advanced Capability-3 terminal defense system, are incorporated into the IBMDS. An artistic rendering of the IBMDS developed by the MDA is illustrated in Figure 1.

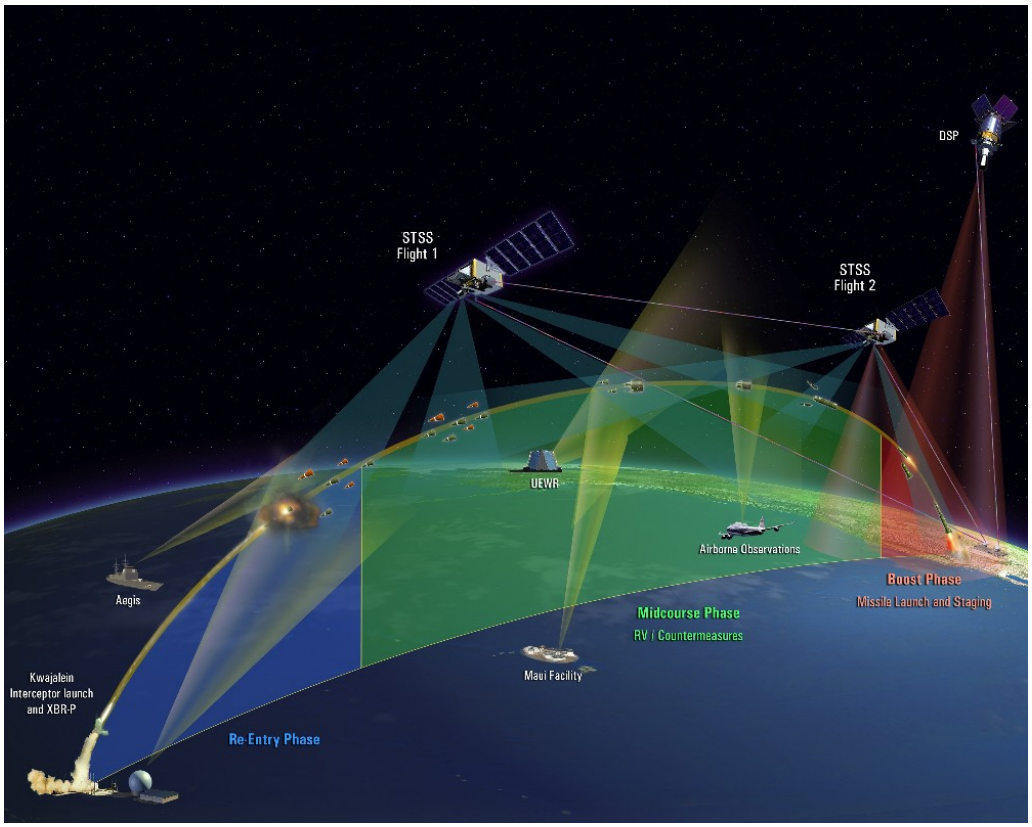

Figure 1. Integrated Ballistic Missile Defense System (IBMDS) developed by the MDA. The sensor and weapon systems incorporated into the IBMDS are presented with respect to the trajectory of the ballistic missile threat.

This thesis proposes a hybrid, large-scale wireless sensor network (WSN) designed to support real-time target detection and tracking of multiple ballistic missile threats of all ranges and in all phases of flight.

A hierarchical network architecture that is composed of three different tiers, defined by altitude above the earth, incorporating both terrestrial and satellite sensor nodes, is considered. The terrestrial nodes, which are both mobile and fixed RF and IR sensor platforms, reside in the lower tier. The second tier is formed by LEO satellites carrying search and track IR sensors with overlapping global coverage. The top tier consists of GEO satellites carrying search IR sensors that provide wider fields-of-view and redundancy in the sensor network. An example of this architecture is illustrated in Figure 2.

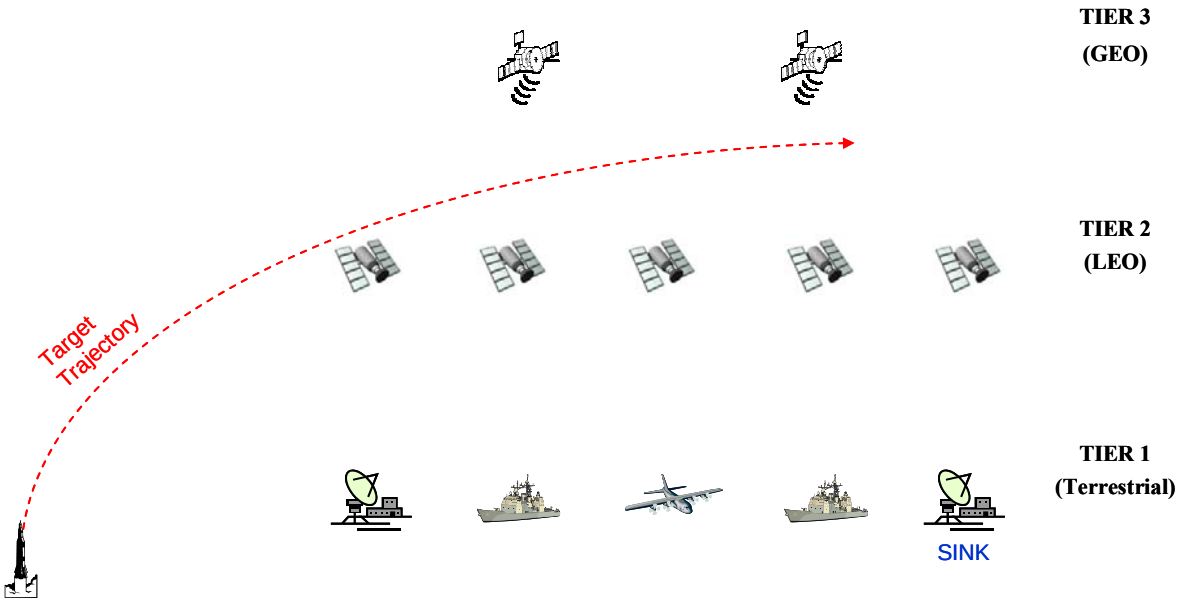

Figure 2. The architecture of the proposed hybrid, large-scale wireless sensor network, designed to support a ballistic missile defense system

The proposed WSN focuses on the detection and tracking of the ICBM during its early stages of flight: boost and post-boost phase, where the target maintains low maneuverability and has not yet deployed its countermeasure decoys. However, space-based IR sensor systems must compete with background factors, such as solar reflection/radiation and earth radiation (earthshine). Additionally, their large footprints require high sensitivity and resolution characteristics, and the nature of the target-background combination, which is not constant throughout the target trajectory, necessitates the medium wavelength IR (MWIR) and very-LWIR spectral coverage.

Furthermore, the sensor must have capabilities for target discrimination from decoys and debris, for booster classification and target identification. To address these issues, current IR sensor technologies are examined including a multi-color quantum-well IR photodetector (QWIP) step-stare focal plane array (FPA).

The hybrid nature of the WSN, which incorporates terrestrial and space-based platforms, fixed and mobile nodes, and RF as well as IR sensors, presents a great challenge in the data dissemination. Additionally, the necessity for real-time target tracking generates a set of requirements that must be fulfilled. These include maximization of the network data throughput and minimization of the network end-to-end time-delay.

Although the proposed hybrid, large-scale WSN does not share many of the characteristics of a traditional WSN, it nevertheless is a wireless network of sensors. Therefore, this study leverages the extensive research in the field of WSN. A clustering mechanism, called the "Area of Interest" (AOI), is introduced which combines the concept of *data centric* routing with in-network data aggregation. Based on this mechanism, a data dissemination algorithm suitable for a hybrid large-scale WSN and designed to meet the real-time and accuracy operational requirements imposed by the nature of the WSN is proposed. In the process, the issues of topology, coverage, clustering, in-network data aggregation, medium access control, and routing are analyzed through performance analysis as well as simulation.

Although this thesis is immediately applicable to an IBMDS, the results of this study may be extended to tactical missile defense systems as well as "traditional" wireless sensor networks intended for real-time object detection and tracking in military as well as civilian applications.

A. RELATED WORK

Levine [2] has laid out a detailed description of the operating principles of Quantum-Well IR Photodetectors (QWIP) and has conducted extensive analysis on the performance of multi-color QWIP. The term multi-color refers to the capability of a

single IR photodetector to sense multiple areas of the IR spectrum, from short-wavelength IR (SWIR) to mid-wavelength IR (MWIR) and very long-wavelength IR (VLWIR) radiation.

Gunapala [3] has performed extensive research on the integration of multi-color QWIP with large format Focal Plane Arrays (FPA). Current work at JPL involves the development of MWIR and LWIR 1024×1024 pixel QWIP FPAs, which have been demonstrated with excellent imaging performance. This research at JPL is funded by the MDA Advanced Systems (MDA/AS) since these sensors are ideal candidates for boost phase target detection due to their excellent uniformity that allows rejection of the high background and the narrow band of QWIP, which facilitates a two-color detection without much crosstalk [4].

As mentioned in the previous section, the proposed data dissemination mechanism is built upon a clustering mechanism that incorporates a *data centric* approach and in-network data aggregation. Gavalas [5] and Yu [6] have explored the benefits of the implementation of a clustering scheme in a MANET network. Krishnamachari [7] has modeled a *data centric* approach for data dissemination in WSN, which has been shown to have significant performance gains. Several data centric routing protocols for WSN, such as Sensor Protocol for Information via Negotiation (SPIN) [8] and Directed Diffusion [9], have been proposed. A technique that complements and is often integral to data centric routing in WSN is that of in-network data aggregation, which has proven to significantly reduce the offered load in "traditional" wireless sensor networks [10].

The performance analysis of the contention based medium access control scheme for the proposed hybrid, large-scale WSN is based on the on the work done by Klein [11], who focuses on the throughput and time delay performance of the slotted, non persistent Carrier Sense Multiple Access (CSMA) medium access control algorithm. Additionally, Lam's [12] analysis for the delay performance of a Time Division Multiple Access (TDMA) scheme in which a node utilizing TDMA is modeled as a single-server M/G/1 queue with unlimited buffer capacity is utilized in the performance analysis of the contention free medium access control scheme for the proposed WSN.

B. THESIS OBJECTIVE

This thesis has two main objectives. First, the examination of the IR signatures presented by the target-background combination and the investigation of modern IR sensor technologies in search of a suitable IR sensor for the proposed hybrid, large-scale WSN that will meet the requirements associated with the early warning, detection and tracking of multiple ballistic threats. Second, the development of an efficient data dissemination mechanism as well as a suitable medium access control scheme for the proposed hybrid large-scale WSN, designed to meet the real-time and accuracy operational requirements imposed by the nature and mission of the WSN, without introducing excessive data overhead and increased time-delays.

C. THESIS ORGANIZATION

This thesis is organized as follows. Chapter II investigates the IR signatures of the target-background combination. Multi-color IR sensors are examined, and the operating principles of a QWIP FPA are presented. The proposed IR sensor is evaluated through performance analysis and the considered RF sensors are briefly discussed. Chapter III describes the hierarchical architecture of the hybrid, large-scale wireless sensor network (WSN). A data dissemination algorithm suitable for the proposed WSN is presented, and a clustering mechanism, called the "Area of Interest" (AOI), is introduced. Chapter IV models the proposed hybrid, large-scale WSN using the OPNET Modeler© simulation platform. The performance of the proposed AOI mechanism and its accompanying data dissemination algorithm is evaluated. Two medium access control schemes, a contention-based and a contention-free scheme, are examined. Chapter V summarizes the work done, highlights its contributions and identifies potential follow-on research.

Appendix A includes the Matlab codes used for simulation and graphing of results throughout the thesis. A procedure for creating and analyzing wireless networks with OPNET Modeler© is outlined in Appendix B. Appendix C highlights the modifications implemented in OPNET Modeler© to perform data aggregation within the AOI. Graphs for the atmospheric transmittance and the solar irradiance are provided in Appendix D.

II. SENSOR SYSTEMS

The proposed hybrid, large-scale sensor network incorporates IR as well as RF sensors in order to provide adequate spectral coverage. This chapter explicitly examines the performance of the IR sensors under the prism of the operational requirements. Specifically, the operational advantages provided by the multi-color operation will be highlighted, and the operating principles of a QWIP will be presented. Moreover, performance analysis will be conducted in order to evaluate the proposed IR sensor for the LEO satellite platform, which is involved in tracking and, therefore, imposes a greater design challenge. Additionally, the RF sensors are briefly addressed individually since the data traffic generated by them is dissimilar to that of the IR sensors, a fact that should not be neglected in the data dissemination.

A. IR SENSORS

The major concern in an IR sensor is the discrimination of the IR signal produced by the target of interest from the signals produced by the background. Inability to do so usually leads to degradation in target detection / tracking and occurrence of false alarms. Background factors, such as solar reflection/radiation, earth radiation (earthshine), rain, clouds, fog, terrain types and luminance (day-night), must be taken into account.

The designer of a strategic defense system, where space-based systems are involved, faces different challenges than the designer of a tactical warning system. The situation is more complicated since the sensors must contend with sources of clutter on the surface of the Earth and in the intervening atmosphere. Additionally, the sensors have large footprints covering large areas, and since they are “looking down” to the Earth the effects of earthshine and clutter can be detrimental. In ballistic missile defense, medium wavelength IR (MWIR), long wavelength IR (LWIR) and very-LWIR sensors are required due to the nature of the target-background combination, which is not constant throughout the target trajectory. Specifically, very-LWIR is important due to the colder environment in space applications [13].

These requirements create the necessity for IR multi-color operational capabilities. The term IR multi-color means that a single sensor has the ability to detect and track IR targets of interest in different areas of the IR spectrum. The multi-color operational feature is an important factor in the selection of the material for the design of the IR sensor. The most common materials used in these systems are HgCdTe (MCT) and Quantum Well infrared photodetectors (QWIP) [4].

Furthermore, the large detection ranges associated with the proposed WSN generate the requirements of high sensitivity and resolution, characteristics that are inherent in modern large-format IR focal plane arrays (FPAs). The development of FPAs has led to the consideration of staring IR sensor FPAs for ICBM defense. Such systems have enough detectors to cover the entire sensor field of view (footprint) simultaneously, without the need for scanning format implementations. This approach results in longer integration times, improved sensitivity and higher signal-to-noise ratio when compared to a traditional scanned system. The trade-off is design complexity due to the requirement for large number of detectors on the FPA. [14].

Further increase in the performance of the staring IR sensor in terms of resolution and reduction of the background noise associated with the large footprint area is accomplished by considering a step-stare IR sensor FPA. Such a system divides the total field of view into smaller fields (step) and periodically alternates among them.

1. Multi-color IR Sensors - Operational Advantages

As mentioned previously, a single IR sensor utilizing multi-color operation has the capability, with the same hardware, to monitor targets in multiple areas of the IR spectrum. Such a sensor presents superior performance in surveillance and target detection/tracking, especially in cases where the target and/or background are uncertain or may be altered in the process of an engagement. In the case of ballistic missile defense, an ICBM presents different IR signatures in each phase of its trajectory, where the corresponding target background is different as well [13].

Generally, a multi-color operation exhibits significant advantages in the discrimination of targets from background decoys and debris, which may be present

during the early stages of flight, minimizing the effects of earthshine and background clutter. Additionally, it enhances the capability for booster classification and target identification, which are of great importance to the command and control center and strongly determine the procedure for the interception of the target [15].

Furthermore, a method proposed by Evans [16] uses target data from a single sensor with multi-color capability in order to obtain target range and altitude estimates. The statistic used in this method is the target intensity ratio from two different wavelengths. This measured statistic, in combination with an a priori knowledge of the difference in absorption for the two wavelengths, allows for the estimation of the sensor to target range.

As already highlighted, the proposed WSN focuses on the detection and tracking of the ICBM during its early stages of flight, where the target maintains low maneuverability and has not yet deployed its countermeasure decoys. Initially, in the boost phase, the ICBM maintains high levels of IR radiation due to the presence of the missile exhaust plume. However, when the booster "burn-out" occurs, the IR signature of the target changes dramatically. In order to maintain target tracking during this transition state and achieve an effective missile plume-to-hardbody handover, the presence of a multi-color IR sensor is a necessity.

2. Quantum-Well IR Photodetector (QWIP)

Conventional photodetectors involve photo-excitation of carriers from the material valence band to its conduction band. However, such a promotion is possible if the energy of the incident radiation ($E_p = hv$) is greater than the energy difference between the valence and conduction bands, referred to as energy band-gap (E_g). Moreover, in order to detect a specific wavelength radiation, the energy of the incident radiation must exceed the value of the band-gap (E_g). This process is illustrated in Figure 3. The energy band-gap (E_g) of a semiconductor is related to the wavelength of the detected incident radiation by the relationship [17]:

$$E_g(\text{eV}) = \frac{1.238}{\lambda} \qquad \text{where } \lambda \text{ is in } \mu\text{m.} \tag{2.1}$$

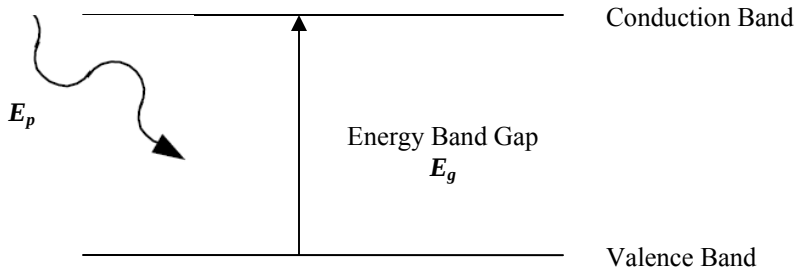

Figure 3. Photodetection process via interband transition

As the requirements for imaging applications evolved, these types of detectors introduced two fundamental limitations:

- The detection of long wavelength IR radiation ($\lambda \geq 10\mu m$) requires materials with energy band gaps on the order of $E_g \approx 0.1eV$. Such materials are known to present difficulties in the fabrication and processing [2].
- The selection of a certain semiconductor material limits the performance of the photodetector to the detection of single specific wavelength, with no capabilities of multiple wavelength detection (multi-color).

These difficulties motivated the study of "band-gap engineering," which led to the development of the QWIPs. Such detectors are characterized by "artificial" band-gap materials that are fabricated by using quantum wells in larger band-gap semiconductors ($E_g > 1eV$) [2], [18]. In this case, apart from the usual interband absorption mechanism described earlier (see Figure 3), which occurs between the valence and the conduction bands, inter-sub-band (or intraband) absorption is possible, which involves transitions (photo-excitations) within the same band. The inter-sub-band absorption mechanism is presented in Figure 4, where electrons and holes are transiting between energy levels E_1-E_2 in the conduction band and H_1-H_2 in the valence band, respectively. This development allows for the tailoring of the detector peak response wavelength, which varies according to the quantum well width L_w. Thus, the inter-sub-band transitions provide the capability for spectral coverage from the short wavelength IR (SWIR: $\lambda \sim 2\mu m$) to the very long wavelength IR (VLWIR: $\lambda > 14\mu m$) region.

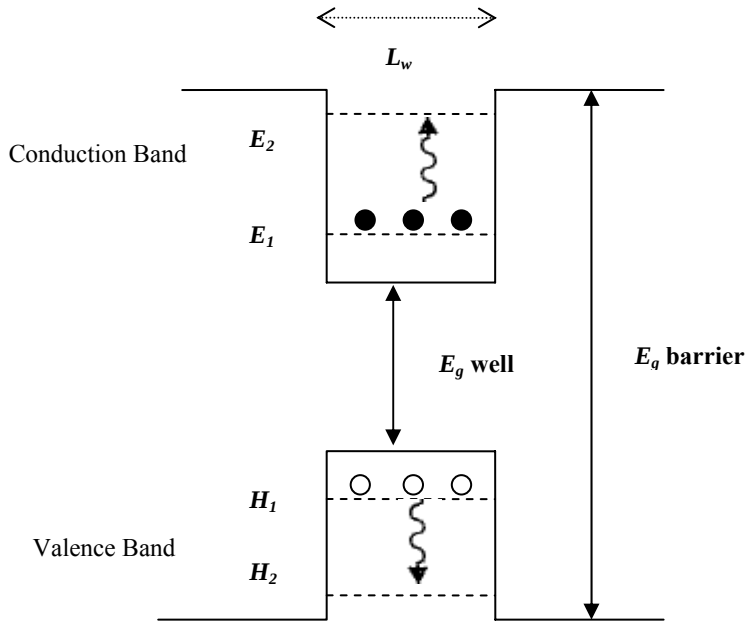

Figure 4. Inter-sub-band Absorption Mechanism in a Quantum well

Furthermore, in QWIP, a multi-spectral response is achieved by stacking several lattice-matched QWIP structures during the fabrication process. As a result, the detector has the capability to independently measure each spectral component (wavelength) [2]. Recent developments at Jet Propulsion Laboratory (JPL) involve the fabrication of a four-band QWIP FPA by stacking different quantum well structures, which is tuned for detection in the IR bands of 4-5.5 μm, 8.5-10 μm, 10-12 μm and 13-15.5μm, as illustrated in Figure 5 [19].

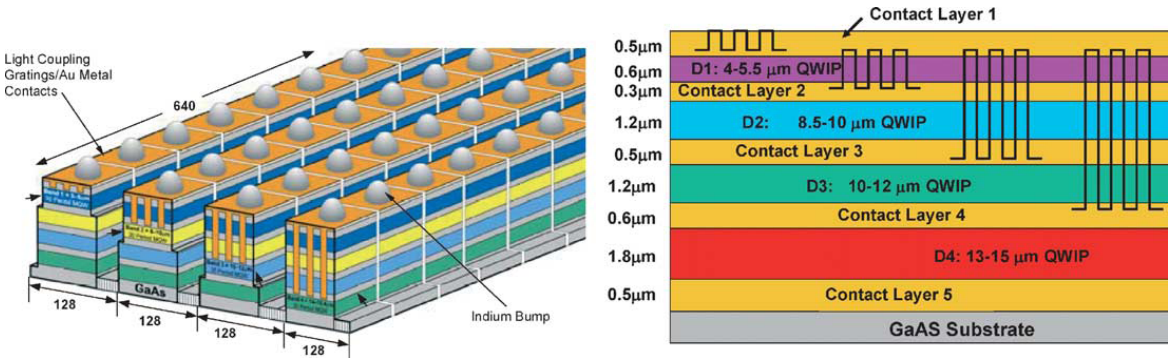

Figure 5. Schematic pixel and device layer diagram of a 4-band QWIP FPA

Major advantages of the QWIPs is their excellent uniformity, which allows for rejection of elevated backgrounds (suitable for boost-phase ICBM detection), low cost, low power dissipation, low *1/f* noise and their narrow-band spectrum, which results in low spectral crosstalk in multi-color operation. However, one major disadvantage is their relatively low quantum efficiency [4]. In Figure 6, an image of a Delta-II launch taken with a QWIP camera is shown [20].

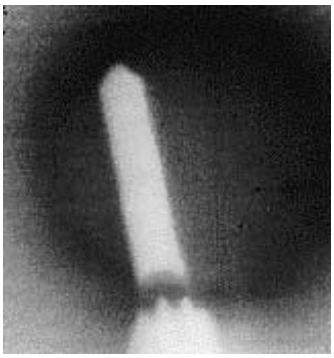

Figure 6. Delta-II launch viewed with a QWIP camera

For the IR sensor of the proposed WSN, as stated in the previous section, a two-color detector is required in order to effectively track the ICBM before and after the booster burn-out. The following analysis will reveal that such a sensor must have detection capabilities in the mid-IR region (λ = 3-5μm) as well as in the very-long-IR region (λ > 14μm). These peak response wavelengths, their corresponding required energy band gaps (E_g < 1eV), and the requirement for multi-spectral capabilities clearly call for the utilization of a multicolor QWIP. Moreover, the resulting energy band gap values from these spectral response requirements dictate the necessity for inter-sub-band transitions.

A prominent candidate for the development of such a detector is the GaAs/$Al_xGa_{1-x}As$ material system, which exhibits superior bond strength, material and thermal stability. Variation of the molar ratio x changes the band gap of the $Al_xGa_{1-x}As$ material, and therefore changes the height of the quantum well. Consequently, the inter-sub-band transition energy may be varied over a wide spectral range, which allows for the tuning of the QWIP FPA from SWIR to VLWIR regions [20].

3. IR Spectroscopy – Photodetection

In this section, the IR signature of the target will be examined for two different phases of its trajectory: in the boost phase and in the post-boost phase after the booster has "burned out". Next, the specifications of the focal plane array will be determined according to the operational requirements of the mission, and evaluation of the proposed QWIP will be conducted based on performance analysis involving the figures of merit for IR sensors.

a. Target Signatures - Background Characteristics

(1) Boost Phase IR signature: Initially, the boost phase of the ICBM is examined, where the altitude of the target is approximately below 250 km. In this phase, the missile exhaust plume is the principal contributor to the IR signature of the ICBM. The exhaust plume of an ICBM, which usually contains water vapor, carbon dioxide gas and solid particulates, at low altitudes has an average temperature of approximately 1400°K and an emissivity of about 0.9 [21]. At these temperatures, water vapor strongly radiates in IR bands centered at 2.7 and 6.3 μm and carbon dioxide in an IR band centered at 4.3 μm, thus nominating these bands as leading candidates for the IR sensor bandwidth [14].

Application of Planck's blackbody radiation formula, provided as (2.1), will allow the determination of the plume's maximum radiant exitance as well as the accurate wavelength value where this occurs:

$$M(\lambda,T)=\varepsilon(\lambda)\cdot\frac{2\pi hc^2}{\lambda^5\left(e^{\frac{hc}{\lambda kT}}-1\right)}\quad\left[\frac{\text{Watt}}{\text{cm}^2\times\mu\text{m}}\right] \tag{2.2}$$

where: M is the radiant exitance, ε is the emissivity, λ is the radiation wavelength, T (K) is the source temperature, h is Planck's constant ($6.626\cdot10^{-34}$ J·sec), k is Boltzmann's constant ($1.38\cdot10^{-23}$ J/K), and c is the speed of light [17].

The radiant exitance of the exhaust plume is plotted in Figure 7 as a function of the wavelength. On the same plot, the radiant exitance of an ideal blackbody with the same source temperature of 1400˚K is presented.

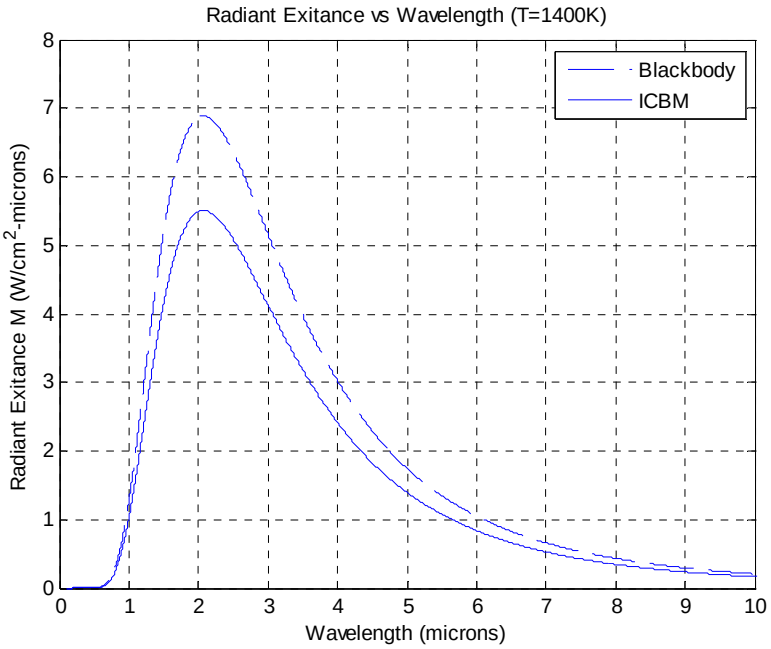

Figure 7. ICBM Boost Phase (Plume) Radiant Exitance

The maximum radiant exitance of the plume is calculated to be 5.512 W/cm^2 μm and the corresponding wavelength, referred to as peak wavelength, is 2.073 μm. Therefore, one may argue that the sensor bandwidth should be centered on this value of the peak wavelength in order to receive the maximum signal power from the target.

However, a design directly based on the peak wavelength would be incomplete without seriously examining the background. In this case, for wavelength values below 3 μm, the reflection from solar radiation is dominant (available in Appendix D), a fact that would generate enormous clutter for an IR sensor during daylight [22]. Further, the radiation originating from earthshine is significant for wavelengths greater than 5 μm [22]. To visualize these, the Earth and Sun are modeled as blackbodies with source temperatures of T = 300˚K and T = 5500˚K respectively [23] (assuming a

reflectivity of 0.5 for the Solar reflection), and their radiant exitances are illustrated in Figure 8 as a function of wavelength.

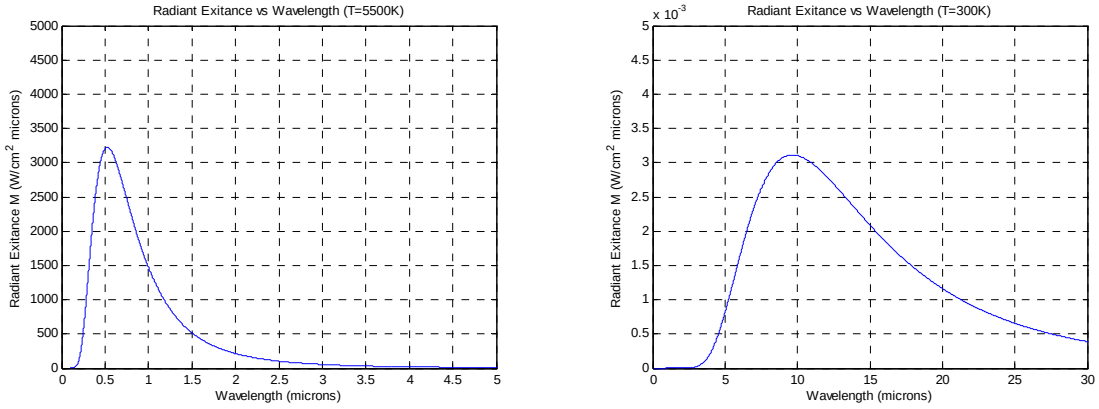

Figure 8. Solar and Earth Radiation (Blackbody models)

Considering the above background limitations in combination with the atmospheric transmittance in this region of the IR spectrum (available in Appendix D), a rational selection for the sensor bandwidth would be the mid-wavelength IR window between 3 to 5 μm. Furthermore, since the IR sensor under consideration is a narrowband QWIP, the precise sensor bandwidth will be from 3 to 4 μm.

(2) Post-boost Phase IR signature: When the missile booster "burns-out", which occurs at an approximate altitude of 250 km, the IR signature presented by the target changes significantly. At these altitudes, known as exosphere, gas molecules have no impact on the target trajectory and the temperature of the missile's surface is strictly governed by its surface configuration, solar radiation intensity and whether the missile is of the rotating type [21]. A typical temperature for the missile's surface is approximately 200˚K, depending on its emissivity coefficient and its thermal design. In the same manner as before, in order to determine the maximum radiant exitance as well as the peak wavelength, the target is modeled by application of Planck's blackbody radiation formula, provided as equation (2.1). The radiant exitance of the target for an emissivity of about 0.9 is plotted in Figure 9 as a function of the wavelength. On the same plot, the radiant exitance of an ideal blackbody with the same source temperature of 200˚K is presented.

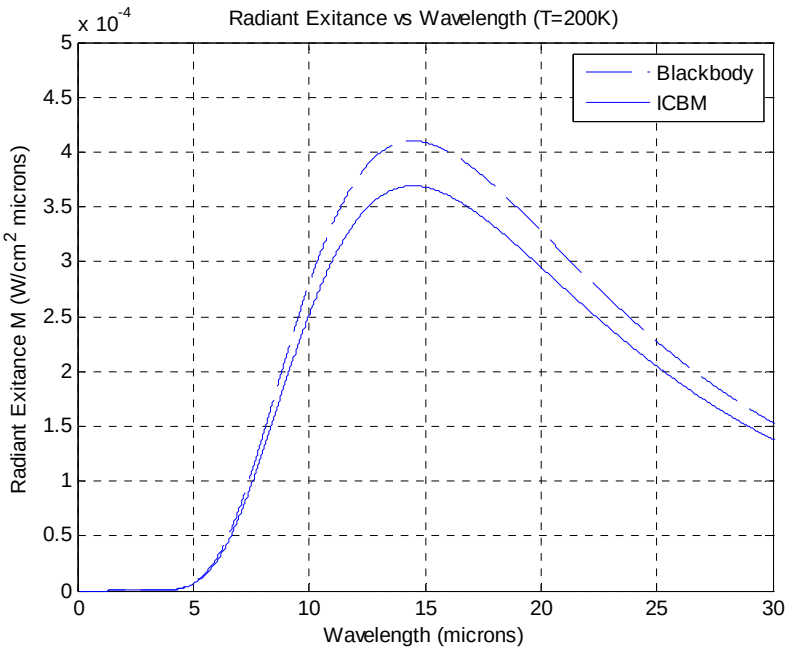

Figure 9. ICBM Post-Boost Phase Radiant Exitance

From the previous figure, the maximum radiant exitance of the plume is calculated to be $3.6895 \cdot 10^{-4}$ W/cm^2 μm and the peak wavelength is 14.507 μm. In this case, the background characteristics work in favor of the target signature. Specifically, measured exoatmospheric data indicates that the Earth's atmosphere totally blocks the earthshine in the carbon dioxide band between 14 and 16 μm [13]. On the other hand, the radiation of the target does not have to encounter the atmospheric transmittance effects due to the high altitude of the missile (250 km). As a result, the bandwidth considered for the narrowband QWIP will be from 14 to 15 μm.

b. Focal Plane Arrays (FPA)

The large detection ranges associated with the proposed WSN generate the requirements of high sensitivity and resolution for the IR sensors. These requirements can only be met with the utilization of large-format IR focal plane arrays (FPAs) [14]. Current developments include cryogenically cooled FPAs with large format, high sensitivity, low *1/f* noise, good uniformity and high operability [13], [3], [24].

The dominant factor in configuring the specifications of an IR focal plane array is the azimuthal resolution. To determine a value suitable for the proposed WSN, the dimensions of the target IR signature in combination with the detection range must be taken into account. The exhaust plume of an ICBM has an approximate length of 50 m [14]. On the other hand, once the ICBM enters the post-boost phase, the dimensions of the target IR signature are comparable to the physical dimensions of the missile, which has a typical length of 20 m. Therefore, selecting the worst case scenario, it would be safe to conclude that the sensor must be able to discriminate IR targets spaced 20 m apart at distances of 1000 km. These values lead to an azimuthal resolution of 20 μrad. This means that the horizontal and vertical instantaneous field of view (HIFOV, VIFOV) of each detector on the FPA must be 20 μrad.

Each IR sensor node in the WSN is required to cover a total footprint on the earth terrain of approximately 100,000 km^2. Considering a step-stare IR sensor FPA of 20 steps, each FPA step must cover a footprint of 5000 km^2. Therefore, as illustrated in Figure 10, the horizontal and vertical field of view (HFOV, VFOV) of the FPA is calculated to be $\theta = 0.07$ rad.

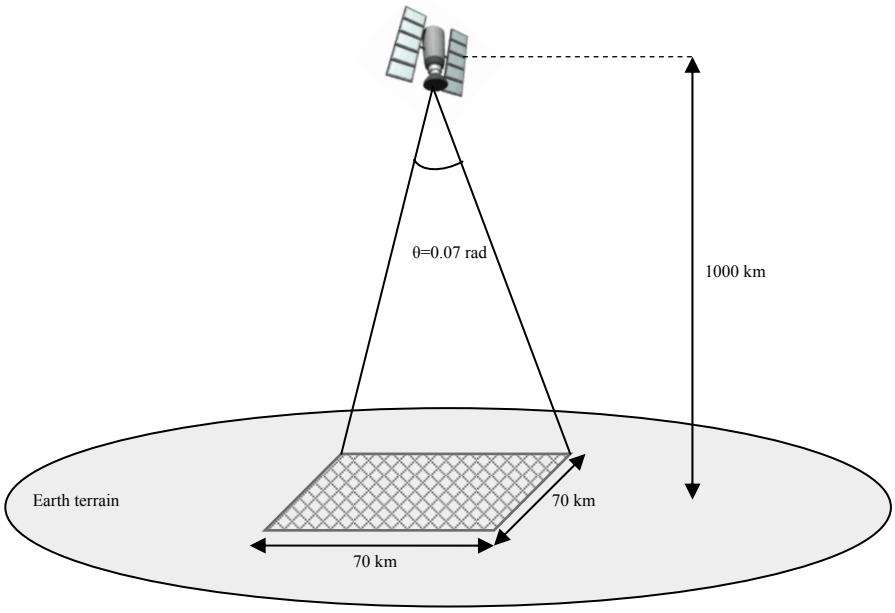

Figure 10. Focal Plane Array Field of View

Taking into account that the HIFOV and VIFOV of each detector on the FPA must be 20 μrad, in order to meet the azimuthal resolution requirements, the total number of detectors on the FPA must be equal to 12.25 million, as calculated below:

$$N = \left(\frac{HFOV}{HIFOV}\right)\cdot\left(\frac{\text{VFOV}}{\text{VIFOV}}\right) = \left(\frac{0.07\,\text{rad}}{20\,\mu\text{rad}}\right)\times\left(\frac{0.07\,\text{rad}}{20\,\mu\text{rad}}\right) = 3500\times 3500 = 12.25\times 10^{6} \qquad (2.3)$$

Mid-IR and long-IR QWIP focal plane arrays, incorporating 1024 × 1024 elements, have been developed in the Jet Propulsion Laboratory [3]. The development of a focal plane array with a number of elements exceeding this value requires the union of more than one array, as illustrated in Figure 11. Such a design involves a higher degree of complexity in order to eliminate the spatial alignment and temporal registration problems that arise when separate arrays are used. This, of course, constitutes a trade off between high azimuthal resolution and design complexity.

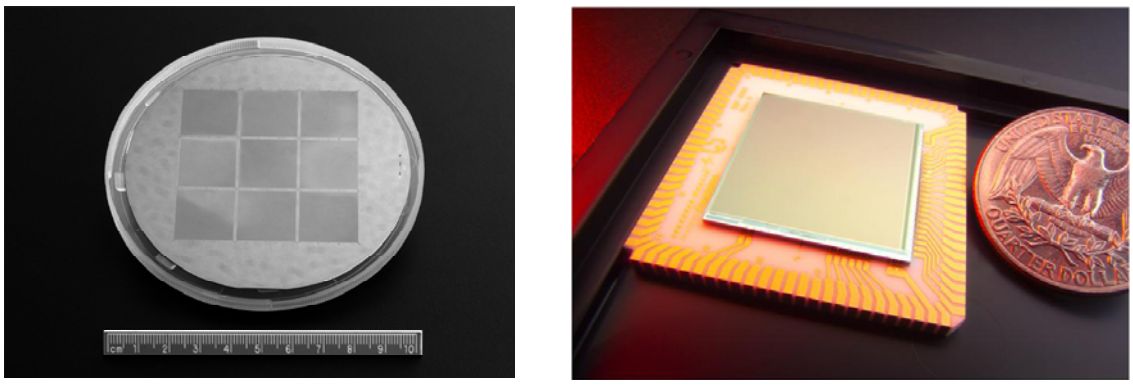

Figure 11. Nine 1024×1024 pixel QWIP FPAs on a GaAs wafer (left) and a 1024×1024 pixel QWIP FPA mounted on a 84-pin chip carrier (right) (JPL)

To determine the data rate at which such an IR sensor would generate target data and inject it into the proposed WSN, it is considered that the image resolution has a nominal value of 8-bits per pixel and the frame rate R_{frame} is 100 Hz. These specifications produce a raw data rate, R_b, of 9.8 Gbps as given by:

$$R_b = \left[3500\times 3500\,\frac{\text{pixels}}{\text{frame}}\right]\times\left[100\,\frac{\text{frames}}{\text{sec}}\right]\times\left[8\,\frac{\text{bits}}{\text{pixel}}\right] = 9.8\ \text{Gbps} \qquad (2.4)$$

It should be noted that this raw data rate may be significantly reduced if it is assumed that there exists a capability for onboard image processing (e.g., image compression).

c. IR Sensor Figures of Merit (FOM)

The performance analysis is conducted under the assumption that the IR sensor is operating under "Background Limited Infrared Photodetection" (BLIP) conditions. This means that the dominant noise source is the background photon flux, and all other internal noise associated with the detector itself, such as Johnson noise, Generation-Recombination noise, and *1/f* (one-over-f) noise, are considered negligible. BLIP operation is common in IR scanning and staring systems [17].

(1) Normalized detectivity: The figure of merit D^* (pronounced "dee-star"), known as "normalized detectivity," is examined. This quantity is the sensor sensitivity normalized to a 1 cm^2 area and 1 Hz noise equivalent bandwidth and may interpreted as a signal-to-noise ratio (SNR) out of a detector when radiant power of 1 W is incident on the detector, given an area of 1 cm^2 and noise equivalent bandwidth of 1 Hz. By definition, the D^* of an IR sensor is generally given by [17]:

$$D^* = \frac{\sqrt{A_d \cdot \Delta f}}{NEP} \tag{2.5}$$

where A_d is the detector area, Δf is the noise-equivalent bandwidth, and *NEP* is the noise-equivalent power, which represents the amount of incident radiant power on the detector that yields a signal-to-noise (SNR) ratio of unity.

Specifically, D^* for a cooled photodetector, operating under BLIP conditions, is provided by the following formula [17]:

$$D^*_{BLIP}(\lambda, f) = \frac{\lambda}{2hc}\sqrt{\frac{\eta}{E_{background}}} \tag{2.6}$$

where λ is the background radiation wavelength, η is the detector quantum efficiency, h is Planck's constant, and $E_{background}$ is the total background photon irradiance.

In order to obtain $E_{background}$, the background photon irradiance $M_{background}$ must be integrated over the IR sensor band under consideration. The $M_{background}$ is given by [17].

$$M_{background}(\lambda,T)=\frac{2\pi c}{\lambda^4\left(e^{\frac{hc}{\lambda kT}}-1\right)}\quad\left[\frac{\text{photon}}{\text{s}\times\text{cm}^2\times\mu\text{m}}\right] \tag{2.7}$$

where T is the temperature of the background noise source. At this point, the luminance has to be taken into account. Under day-time luminance conditions, both noise contributions, the earth radiation (earthshine) and the reflection from the solar radiation, must be considered, and (2.7) must be evaluated and summed for both T = 300 and 5500 ˚K. However, in night-time luminance conditions, the dominant background noise is the earth radiation, and T = 300˚K in (2.7).

The figure of merit D^* should be calculated for each band of the multi-color IR sensor in question separately since the integration of the background photon irradiance in the 3-4 μm and the 14-15 μm IR bands produces different results. Additionally, due to the fact that the IR sensor is considered to be a QWIP, which are characterized by low values of quantum efficiency, a typical selection would be approximately η = 5%.

Under these conditions, the normalized detectivities for the two spectral areas of operation of the QWIP are calculated to be:

- Day-time luminance conditions

$$D^*_{BLIP-Day}(3.5\mu\text{m})=6.09\cdot10^7\left[\frac{\text{cm}\sqrt{\text{Hz}}}{\text{Watt}}\right]\qquad D^*_{BLIP-Day}(14.5\mu\text{m})=1.75\cdot10^{10}\left[\frac{\text{cm}\sqrt{\text{Hz}}}{\text{Watt}}\right]$$

- Night-time luminance conditions

$$D^*_{BLIP-Night}(3.5\mu\text{m})=5.01\cdot10^{10}\left[\frac{\text{cm}\sqrt{\text{Hz}}}{\text{Watt}}\right]\qquad D^*_{BLIP-Night}(14.5\mu\text{m})=2.03\cdot10^{11}\left[\frac{\text{cm}\sqrt{\text{Hz}}}{\text{Watt}}\right]$$

(2) IR Range Equation: The range equation for an IR sensor will be derived from the definition of the SNR, which is given by [17]:

$$SNR = \underbrace{\left(\frac{D^*}{\sqrt{A_d \cdot \Delta f}} \right)}_{1/\mathrm{NEP}} \cdot \underbrace{\left(\frac{I \cdot A_{enp}}{r^2} \right)}_{\text{signal flux}} \tag{2.8}$$

where I (W/sr) is the radiant intensity of the target source, A_{enp} is the area of the collection aperture (entrance pupil) of the detector optics, and r is the detector to target range. In (2.8), the first term is recognized as the reciprocal of the NEP and the second term as the radiant flux of the source reaching the detector since A_{enp}/r^2 is actually the solid angle subtended by the entrance pupil of the detector.

In the expression for the SNR, the only terms that have not yet been determined are the noise-equivalent bandwidth Δf, which is also the detector signal bandwidth, and the area of the entrance pupil A_{enp}. The detector bandwidth Δf is directly related to the frame rate of the sensor FPA. Specifically, the frame rate was considered in the previous section as 100 Hz, which means that the frame time is $\tau_f = 0.01$ sec. For a staring IR sensor, Δf and τ_f are related according to the formula [17]:

$$\Delta f \cong \frac{1}{2\tau_d} \tag{2.9}$$

This yields a value for the detector signal bandwidth equal to $\Delta f = 50$ Hz.

To determine the area of the detector entrance pupil, the Fraunhofer diffraction theory must be taken into account. Specifically, the criterion for resolvable images, known as Rayleigh's criterion requires that the centers of an image pattern are no nearer than the angular radius of the Airy disk [23]. Thus, the limit of resolution is given by:

$$\Delta\theta = \frac{2.44\lambda}{D_{lens}} \tag{2.10}$$

where $\Delta\theta$ is the required angular resolution, calculated in the previous section to be 20 μrad, λ is the signal wavelength, and D_{lens} is the diameter of the detector lens.

Substituting for the two wavelengths under consideration, λ = 3.5μm and λ = 14.5μm, we obtain two values for the lens diameter: 0.427 m and 1.8 m. Between these values, the larger is chosen in order not to degrade the performance of the detector in the VLIR region. Assuming that the entrance pupil has the same dimensions as the optics lens, we obtain the area of the entrance pupil from the equation $A_{enp} = \pi D^2/4 = 2.55\ \text{m}^2$.

Although not required for the solution of the IR range equation, determining a value for the focal length of the detector lens would complete the optics analysis of the detector. The focal length F is calculated as 1 m from the following relation [17]:

$$\text{HIFOV} = \text{VIFOV} = \frac{\sqrt{A_d}}{F} \tag{2.11}$$

All the parameters in the IR range equation have now been determined and are summarized in Table 1 for convenience.

Parameter	**λ=3-4 μm**	**λ=14-15 μm**
D^*	$5.01\cdot10^{10}$ cm√Hz/W	$2.03\cdot10^{11}$ cm√Hz/W
I	$1.38\cdot10^{6}$ W/sr	15.84 W/sr
r	1000 km	750 km
A_d	$4\cdot10^{-10}$ m^2 (20 μm × 20 μm)	
Δf	50 Hz	
A_{enp}	2.55 m^2	

Table 1. IR Equation Parameters

According to the parameters appearing in Table 1, the SNR for day and night-time luminance conditions, for both bands in the IR spectrum, is calculated according to (2.8) as:

$$\begin{aligned} &\text{Day-time:} \quad SNR(3\text{-}4\mu\text{m}) \simeq 36.7\,\text{dB}, \quad SNR(14\text{-}15\mu\text{m}) \simeq 14.4\,\text{dB} \\ &\text{Night-time:} \quad SNR(3\text{-}4\mu\text{m}) \simeq 65.8\,\text{dB}, \quad SNR(14\text{-}15\mu\text{m}) \simeq 25\,\text{dB} \end{aligned} \tag{2.12}$$

In a typical missile surveillance receiver, an SNR value of at least 14 dB ensures a detection probability of 99.9% with ultra low false alarm rate [21].

Therefore, the achieved SNR values are considered satisfactory. However, one must not neglect the fact that the performance analysis was conducted under the assumption of BLIP operational conditions neglecting other sources of noise, which would undoubtedly degrade the performance of the detector. In Table 2, the specifications of the proposed tracking IR sensor for the LEO satellites, which were derived throughout this section, are summarized. The Matlab codes involved in the target IR signature and performance analysis calculations are available in Appendix A.

Parameter	Value
Type	FPA Step Stare
Format	3500 × 3500 pixels
Detector	Two-color QWIP
Response wavelengths	3-4 μm and 14-15 μm
Material	GaAs/$Al_xGa_{1-x}As$ Alloy
IHFOV-IVFOV	20 μrad
HFOV-VFOV	0.07 rad
Detector area (A_d)	20 μm x 20 μm
Lens Diameter (D_{lens})	1.8 m
Entrance Pupil (A_{enp})	2.55 m^2
Focal Length (F)	1 m
Frame Rate (R_{frame})	100 Hz

Table 2. IR Sensor Specifications

4. Future Considerations

Currently, for military applications, the materials utilized are: InSb for MWIR and HgCdTe (MCT) for LWIR with sensitivity and acceptable operating temperatures. These materials present a mature technology and affordable cost. However, HgCdTe detectors have started to present many deficiencies in operability and FPA uniformity, especially at the VLWIR region for space and low background applications. This, along with the requirements for multi-color operation, wide-band spectral coverage, very large format FPAs and affordable cost, has become a challenge for the IR detection community.

Extensive research is performed by the Advanced Systems (AS) office of the Missile Defense Agency (MDA) in the field of passive EO/IR sensors for future ballistic missile defense capabilities. The objective is the investigation of potential materials that will accomplish coverage of the whole IR spectrum, including VLWIR large-format FPAs of high uniformity, with simultaneous multi-color capabilities [4].

Potential candidate materials that are under investigation include:

- Sb-based strained-layer superlattice (type-II SLS) photodetectors that combine the advantages of both HgCdTe (high quantum efficiency) and QWIP (high uniformity), especially at LWIR and VLWIR.
- Multi-color, large format QWIP FPAs that will present a quantum efficiency / gain product larger than 30%. Such a development would cover almost all the requirements of a BDMS. Research is conducted at JPL, where as mentioned previously 1024x1024 QWIP FPAs are currently being developed.

B. RF SENSORS

The RF sensors employed by the proposed WSN will be briefly addressed in order to determine the data traffic that they will generate and consequently inject into the network. Specifically, the RF sensors under consideration are divided into two main categories based on their host operational platform: fixed and mobile. These sensors must have capabilities for target detection / tracking, kill-assessment as well as background and countermeasure discrimination throughout the trajectory of the ICBM. Additionally, forward deployable sensors are necessary that will enhance the probability of early warning by obtaining data from the boost-phase of the trajectory.

This RF sensor configuration is similar to that employed by the MDA in the IBMDS. In detail, these include the forward deployable, X-band transportable radar (FDR) and the S-band phased array radars onboard Aegis warships that mainly contribute to the initial phase of the target trajectory. Additionally, the mobile sea-based X-band radar (SBX) that is capable of moving throughout ocean areas provides coverage for the midcourse phase of the target trajectory.

If we assume that an RF sensor engaged in tracking transmits the target range, bearing and altitude in double precision floating-point format, the total number of data bits per track data point is 192 bits. Moreover, we consider that the sensor, while tracking, maintains a nominal pulse rate frequency (PRF) of 1,000 pulse repetitions per second. Combining these, we calculate the raw data rate to be 192 kbps as given by:

$$R_b = \left(192 \frac{\text{bits}}{\text{packet}}\right) \cdot \left(10^3 \frac{\text{packets}}{\text{sec}}\right) = 192\,\text{kbps} \tag{2.13}$$

It should be noted that this raw data rate may be significantly reduced if the capability of onboard data processing is assumed (e.g., data compression).

C. SUMMARY - DISCUSSION

This Chapter initially examined the IR sensors of the proposed WSN, under the prism of the operational constraints and requirements. In ballistic missile defense, the operational advantages provided by the multi-color operation of the sensor are necessary due to the nature of the target-background combination, which is not constant throughout the target trajectory. Specifically, by modeling the target IR signatures, it has been shown that medium wavelength IR (MWIR) and very-LWIR spectral coverage is mandatory. Extensive research in the area has proven that QWIP are most suitable detectors for such application due to their high uniformity and multi-color capabilities.

Large-format, staring IR FPAs are considered that provide high sensitivity, high resolution, and cover the entire sensor field of view. Further increase in the performance of the FPA is accomplished by considering a step-stare type FPA, which leads to reduction of the background noise associated with the large footprint area. The raw data traffic generated by the IR sensor FPA was calculated. Moreover, the proposed IR sensor was evaluated based on performance analysis, assuming BLIP operating conditions, where the resulting values for the D^* and the SNR were considered satisfactory. Additionally, the types, characteristics, and deployment of the RF sensors incorporated in the WSN were briefly addressed and the raw data traffic generated by them was calculated.

THIS PAGE INTENTIONALLY LEFT BLANK

III. HYBRID, LARGE-SCALE WIRELESS SENSOR NETWORK

A network designed to support a missile defense system can be thought of as a hybrid, large-scale wireless sensor network (WSN). The term hybrid is derived from the fact that the network incorporates terrestrial and space-based nodes, IR and RF sensors, fixed as well as mobile platforms. The network is considered large-scale because of the increased propagation delays associated with the large distances between the network components, which can be in excess of 8000 km. Although our proposed network is not considered a wireless sensor network in the conventional sense, it is, nevertheless, a wireless network of sensors. The work presented will adopt and leverage the wide spectrum of advancements in the field of "traditional" wireless sensor networks.

A. SENSOR NETWORK ARCHITECTURE

A ballistic missile defense system should be capable of providing a layered defense against multiple ballistic threats of all ranges and in all phases of flight. This implies that the network architecture of such a system plays an important role in its successful operation. In designing the architecture of the network, the critical factors that must be accounted for are: coverage, target trajectory, network topology, operational requirements, and physical constraints.

1. Coverage and Topology of the Wireless Sensor Network

Crucial factors in the design of the network architecture and the deployment of the sensor nodes are those of sensor coverage and communication connectivity. This is important, first, for the early warning/detection and continuous tracking of the threat and, second, for the successful inter-communication among the sensor node platforms. In the case of the IBMDS, where the major threat is Inter-continental Ballistic Missiles (ICBM), wide area coverage is required to maintain target tracking throughout the whole trajectory of the target to include boost, mid-course and terminal guidance phases. A typical ICBM has a maximum range of 8000 km and a peak trajectory altitude of 1500 km [25].

To achieve these objectives, a hierarchical network topology, composed of three different tiers, defined by altitude above the earth, and incorporating both terrestrial and satellite nodes, is proposed. The terrestrial nodes, which are both mobile and fixed RF and IR sensor platforms, reside in the lower tier. The second tier is formed by the LEO satellites carrying search and track IR sensors with overlapping global coverage. The top tier consists of GEO satellites carrying search IR sensors that provide wider fields-of-view and redundancy in the sensor network. An illustration of this architecture is presented in Figure 12.

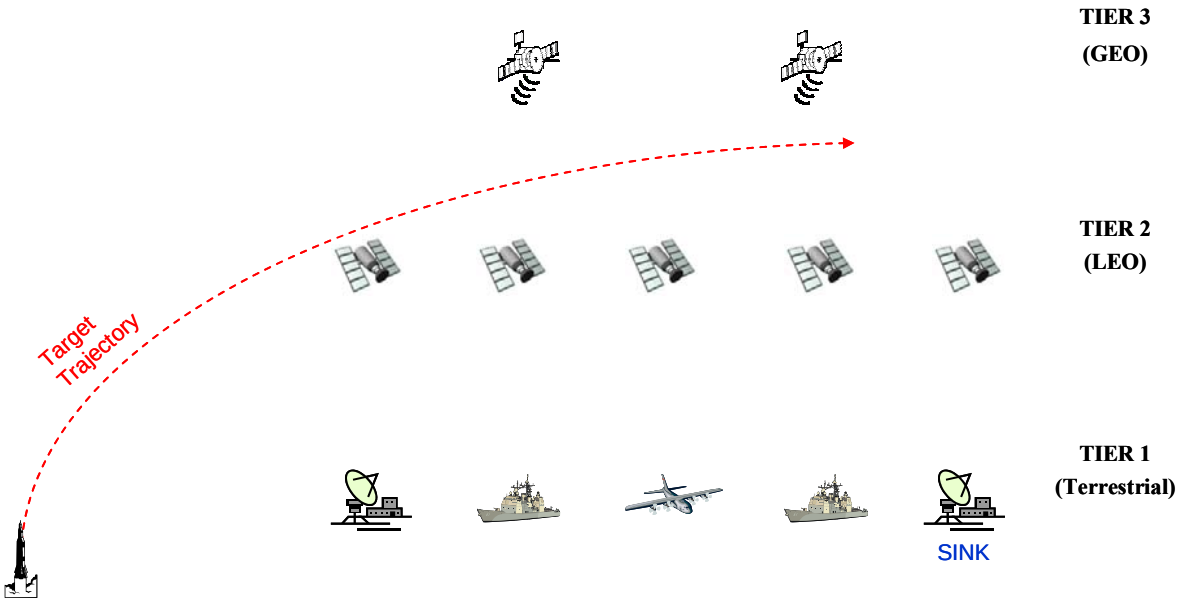

Figure 12. Hybrid, large-scale wireless sensor network architecture

2. Requirements and Constraints

The necessity for real-time target tracking with a hybrid, large-scale WSN generates a set of requirements that must be fulfilled. These include maximization of the network data throughput and minimization of the network end-to-end time delay. As stated in Chapter I, the considered BMDS focuses on intercepting the target while it is in the boost phase. This of course implies that specific latency bounds must be guaranteed for the data dissemination within the WSN utilized by the BMDS. A typical ICBM has a

boost phase duration of approximately 3 min, which means that within this period of time the target of interest must be acquired, validated (target discrimination, identification), reported to the C^2 center and effectively intercepted. Additionally, while in the boost phase, the ICBM maintains a maximum and average velocity of 3 and 7 km/sec, respectively. Therefore, an end-to-end time delay of 1 sec for data dissemination in the WSN results in an uncertainty of 3 to 7 km in the position of the target reported to the C^2 center. Any end-to-end time delay value greater than this would lead to unacceptable accuracies in the target position jeopardizing the effective and timely interception of the target while in the boost phase.

However, these requirements must be met under certain imposed constraints in the dissemination of the data. The hybrid nature of the WSN, which incorporates terrestrial and space based platforms, fixed and mobile nodes, and RF as well as IR sensors, presents a great challenge in the data dissemination. Furthermore, the availability and reliability of the network links is critical to the communication between the node components and consequently to the performance of the WSN.

B. DATA DISSEMINATION

To effectively accommodate the data traffic described in Chapter II, we need to efficiently resolve the issues of routing and route discovery. The problem of routing in wireless sensor networks is challenging due to the limited energy, processing and storage capacity, the ad-hoc, random deployment of the sensor nodes, and the need for multiple sources to route their traffic to a single destination. Recently, much research in WSN routing has focused on a Data Centric approach, which has been shown to have significant performance gains [7]. Although the proposed hybrid, large-scale WSN does not share many of the constraints imposed on traditional WSN, particularly in terms of energy and on-board node processing, it still exhibits one of their basic characteristics, in the sense that the data traffic is based on the sensed phenomena. To leverage these recent advancements in WSN, a data dissemination mechanism is proposed that combines the "content based" feature of the *Data Centric* routing approach with the principles of data aggregation and clustering.

1. Data Centric Routing and Data Aggregation

In the *Data Centric* approach, a packet is routed based on its content. This implies that the data dissemination is application/data specific and is not performed based on node identity as in the *Node Centric* approach. In the latter, multiple, individual paths must be discovered and maintained between source nodes (sensors) and sinks (destinations) that are interested in similar sensed data [26]. Data dissemination may be either event driven or query driven. In other words, data are either pushed from the sensor to the destination once they are sensed or a sink issues queries and sources generate data in response to these queries [27]. Routes can be thought of as "query gradients" and routing tables maintain entries for active queries only, which leads to a significant reduction in the overhead. Several data centric routing protocols for WSN, such as Sensor Protocol for Information via Negotiation (SPIN) [8] and Directed Diffusion [9], have been proposed.

In-network data aggregation complements and is often integral to data centric routing in WSN. The concept is to consolidate the information acquired by different sensors at specific nodes within the network, instead of having each sensor node route its traffic individually back to the sink. Due to the nature of the WSN, which incorporates node platforms carrying similar sensor types and monitoring the same target simultaneously, the data generated by these sensors will often be highly correlated in both time and space. This will result in the presence of redundant information, a fact that allows for data aggregation. Different degrees of aggregation may be considered, from simple data consolidation, which merely reduces the excess overhead by collecting the data from multiple packets and re-encapsulating them with a single header and trailer, to advanced data fusion techniques, which involve a substantial computational load. In-network data aggregation has proven to significantly reduce the offered load in "traditional" wireless sensor networks [10].

In designing in-network aggregation, one must take into account the source-sink separation, the density of the network, the degree of aggregation, the physical location where the aggregation will occur, and the time-delay trade-off associated with each of

these factors. Improper design may lead to significant time-delays since the data from sources nearer to the destination may have to be held at an intermediate node where aggregation will occur with the data originating from sources that are farther away from the destination [10]. This is shown in Figure 13, where node F routes its traffic to the sink through the aggregation node G, with a path cost of a+b, instead of routing its traffic directly the sink with a smaller path cost c.

Therefore, it is expected that the combination of a data centric routing approach with in-network aggregation in a WSN will lead to a significant reduction in the overhead and the offered load.

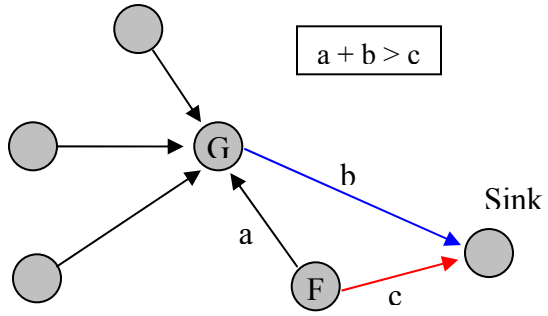

Figure 13. Improper design of data aggregation

2. Area of Interest (AOI) - A Data Centric Clustering Mechanism

Based on the concept of data centric routing in combination with in-network data aggregation described above, a clustering mechanism, called the "Area of Interest" (AOI), is now introduced. Clustering is the process where hierarchies are built among the network nodes so that the topology can be abstracted [5]. In a clustering scheme, geographically adjacent nodes are organized into forming a virtual group referred to as the "cluster". A member within each cluster is assigned the duty of being the "clusterhead" and normally serves as the cluster coordinator performing intra-cluster transmission arrangements, and forwarding data traffic to inter-cluster links. The implementation of a clustering mechanism offers two important benefits: first, it limits the inter-cluster transmissions thus reducing the traffic load and, second, it reduces the routing overhead by restricting the set-up and maintenance of routing information to the clusterheads [6].

The AOI is defined as a cluster within the hybrid, large-scale WSN that is comprised of the sensor nodes that are actively engaged in tracking the target of interest, as illustrated in Figure 14. Data aggregation occurs within each AOI so formed prior to routing the target data back to the destination (sink). The degree of aggregation in this work involves merely data consolidation, as described in the previous section, and no data fusion. The formation of each AOI as well as the selection of the aggregation node within an AOI will be addressed in the proposed data dissemination algorithm of the next section.

The concept of the AOI allows us to model two separate major data flows within the WSN: intra-AOI flow among the nodes currently forming the AOI in which the sensor nodes will route their traffic to the selected aggregation node and backflow from the AOI aggregation node to the destination (sink).

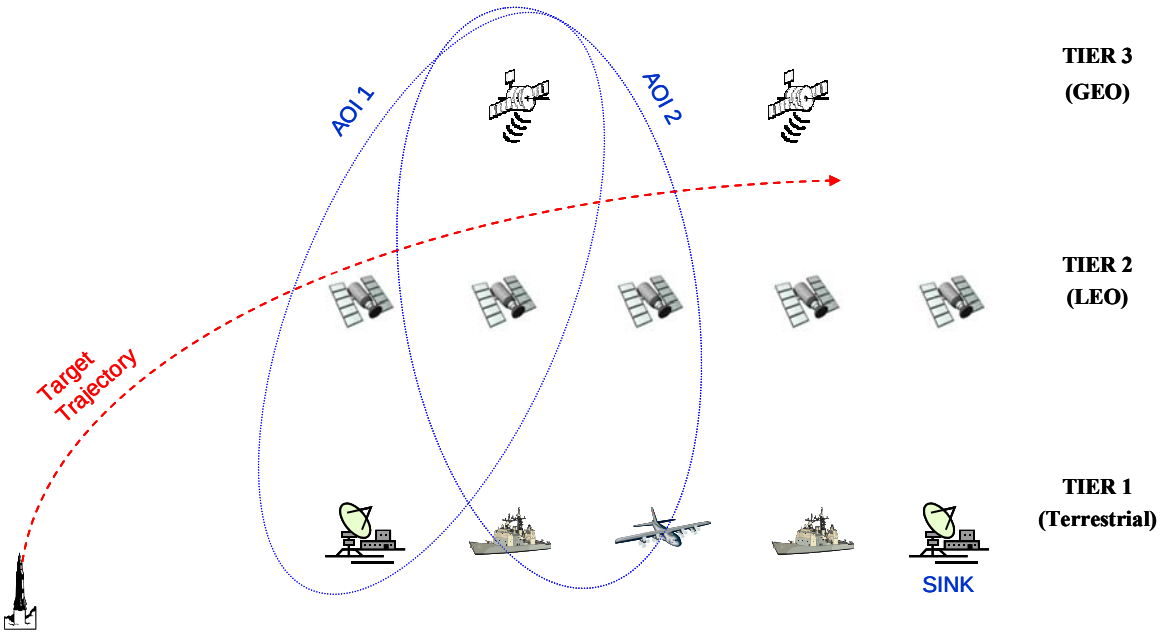

Figure 14. "Area of Interest" (AOI)

As the target moves along its trajectory through the sensor field, the composition of the AOI will change as different sensors actively track the target. Two consecutive AOIs are presented in Figure 14. This AOI composition update constitutes a concept described as the AOI "virtual motion".

3. Proposed Data Dissemination Algorithm

Building upon the clustering mechanism of the AOI and incorporating the concept of in-network data aggregation within the AOI, a data dissemination mechanism consisting of five separate phases is introduced. This algorithm defines the operation of the proposed hybrid, large-scale WSN from the detection of the target of interest to the delivery of the information to the destination (sink). A flowchart of the proposed algorithm, as implemented in the entire WSN, is provided in Figure 15.

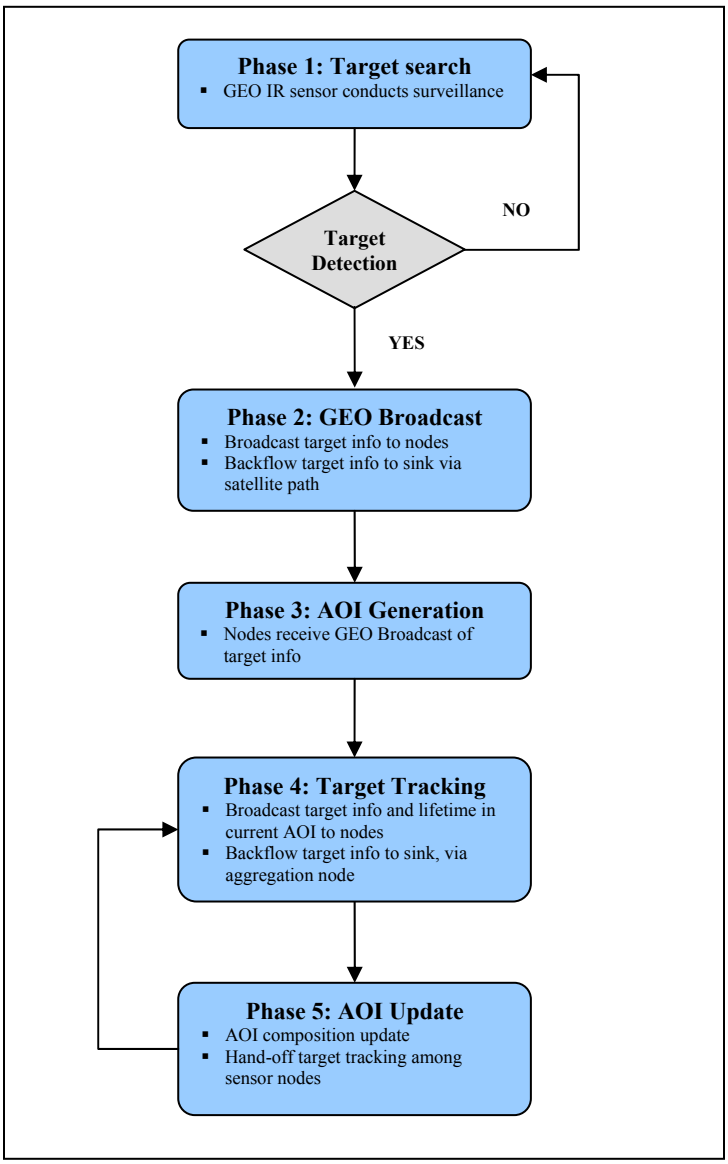

Figure 15. Flow chart of the proposed data dissemination algorithm in the WSN (network level)

Additionally, a flowchart of the proposed algorithm as facilitated by a candidate AOI member node is presented in Figure 16.

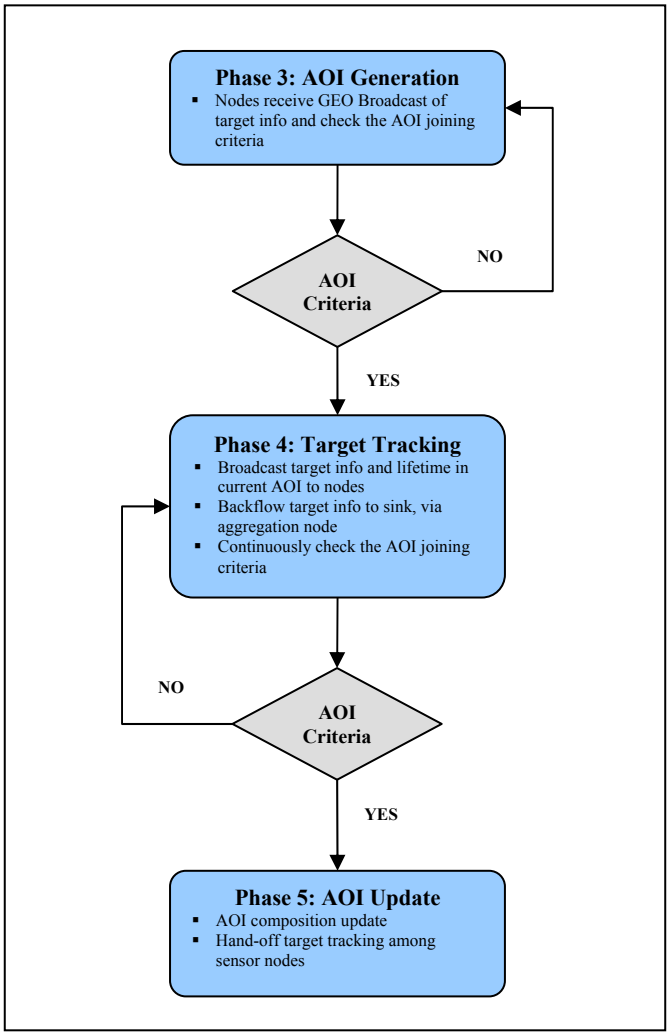

Figure 16. Flow chart of the proposed data dissemination algorithm at the node level

In the following, we examine in detail each phase of the data dissemination algorithm.

a. Phase 1: Target Detection

This is the initialization phase of the algorithm in which the IR search sensors onboard the GEO satellites achieve initial detection of the target. This implies that the functions of target discrimination, classification and potentially identification have already been conducted, and the target is considered valid. Moreover, the possibility

of initial detection by a LEO satellite or a terrestrial node should not be ruled out. However, this case will not be investigated in this work.

b. Phase 2: GEO Target Broadcast

The GEO satellite that has initially detected the target is unaware of the identity or network address of the closest sensor nodes. Therefore, in order to forward the target data to the node platforms carrying the tracking sensors, the GEO satellite merely broadcasts the information to all nodes within its communication range. Since the initial AOI has not yet been established, it is assumed that the backflow of the initial target data to the sink is routed through the GEO satellite path. This, however, implies the existence of a fixed traffic route through the GEO satellite nodes that has been set-up ahead of time. This is commonly referred to as a proactive routing approach. The increased end-to-end delays in the GEO satellite path associated with the large propagation delays due to the GEO satellite altitude is the reason why this routing solution is not implemented in the following algorithm phases for the backflow to the sink.

c. Phase 3: AOI Formation

All sensor nodes within communication range of the GEO satellite will receive its target information broadcast. These sensor nodes will make a local decision on whether or not to join the initial AOI and initiate target tracking. For the LEO satellites, this decision will be based on a range threshold from the individual sensor to the target and a determination whether the target is inbound or outbound. The terrestrial nodes share the same criteria with the modification that the threshold distance will be measured from their own position to the projection of the target trajectory on the Earth's surface.

d. Phase 4: Target Tracking

During the tracking phase, sensor nodes in the AOI continuously check the joining criteria to verify their membership in the AOI. Additionally, they broadcast the target information as well as the amount of time they have been members of the current AOI, referred to as lifetime in the AOI. This broadcast serves four purposes:

(1) The data will be collected by the aggregation node in the current AOI and forwarded in the backflow to the destination (sink).

(2) The broadcast serves as a "heartbeat" status message that will be utilized by the node components of each AOI to verify the proper operation of the remaining AOI members. The significance of the "heartbeat" status message should be highlighted. Although the failure of a sensor or node platform other than the aggregation node degrades the performance of the tracking system, it is not of critical importance to the operation of the WSN. However, if the aggregation node fails, AOI members must be urgently informed and action must be taken to prevent a disruption in the backflow to the sink. This will involve immediate reelection of a new aggregation node based of the lifetime in the AOI criterion mentioned above.

(3) The sensor nodes outside the AOI, but within radio transmission range, overhear the broadcast and monitor the target position. This allows these nodes to continuously check the AOI joining criteria and locally decide whether they should join the current AOI.

(4) The broadcast message serves as the criterion for the selection of the aggregation node within the AOI. When the current aggregation node exits the AOI, the node with the lowest lifetime in the AOI will be selected as the next aggregation node. This aggregation node selection criterion resembles the principle of a selection scheme known as "Center at Nearest Source (CNS)" [10]. According to this, all sources forward their data directly to the node nearest to the destination, where after being aggregated the data are sent to the sink. However, this approach requires that the geographical position of the sink is known beforehand. Utilizing this scheme in the selection of the AOI aggregation node, it is assumed that the target is in-bound to the sink, which is the most likely scenario.

e. Phase 5: AOI Composition Update

As the target position progresses within the network, nodes will enter and exit the AOI. Therefore, the AOI composition will be updated accordingly. Exit criteria could include both range and closest point of approach (CPA) considerations.

4. Simulation Results - AOI "Virtual Motion"

In this section, we model a sample missile defense network in MATLAB and provide simulation results to evaluate the composition update of consecutive AOIs as well as to verify that it is consistent with the data dissemination algorithm described previously. Specifically, by applying the AOI joining criteria described in the data dissemination algorithm of the previous section, it can be observed that the AOI "follows" the target as it moves along its trajectory through the sensor field. This movement of the AOI constitutes the AOI "virtual motion" mentioned earlier. The AOI composition as a function of time and target trajectory for two different time instants is presented in Figure 17.

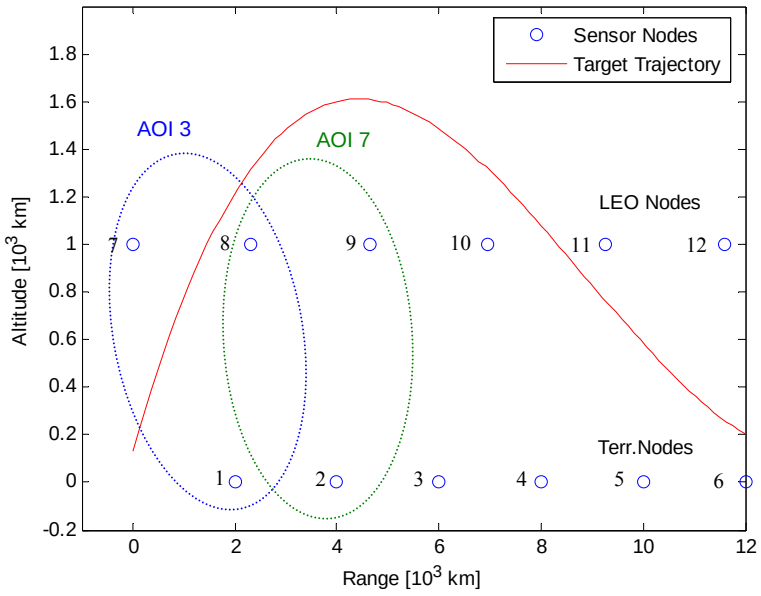

Figure 17. AOI composition and target trajectory.

In Table 3, the composition of the AOIs at one hundred time instants, which equivalently represent one hundred target positions throughout the simulation, is included. We observe that, during the simulation, nodes enter and exit the AOI, forming a total number of eighteen different AOIs (in terms of node composition). The MATLAB code for this simulation is included in Appendix A.

AOI	Terrestrial Nodes	LEO Nodes
1	1	7, 8
2	1, 2	8
3	1, 2	8, 9
4	2	8, 9
5	2	9
6	2, 3	9
7	2, 3	9, 10
8	3	9, 10
9	3, 4	10
10	3, 4	10, 11
11	4	10, 11
12	4, 5	10, 11
13	4, 5	11
14	4, 5	11, 12
15	5	11, 12
16	5, 6	11, 12
17	5, 6	12
18	6	12

Table 3. AOI composition at 100 time instants for the simulation of Figure 17

C. SUMMARY

In this chapter, a hierarchical network architecture for a hybrid, large-scale wireless sensor network (WSN) designed to support an integrated missile defense system has been proposed. This WSN is composed of three tiers, incorporating both terrestrial and satellite nodes, carrying IR and RF sensors.

A clustering mechanism, called the "Area of Interest" (AOI) was introduced, which combines the concept of data centric routing with in-network data aggregation. Building upon this AOI mechanism, a data dissemination algorithm suitable for a hybrid large-scale WSN was presented. The algorithm is designed to meet the real-time and accuracy operational requirements imposed by the nature and mission of the WSN without introducing excessive data overhead and increased time-delays. Simulation results verified that the AOI "virtual motion," which is the adaptation of the AOI composition to the position of the target of interest as it moves through the sensor field, is consistent with the proposed algorithm.

IV. DATA DISSEMINATION PERFORMANCE

The proposed hybrid, large-scale WSN is modeled using the OPNET Modeler© simulation platform. In the first section, the performance of the proposed AOI mechanism and the accompanying data dissemination algorithm is evaluated, and simulation results are provided for throughput and delay. The next two sections address the issue of medium access control among the sensor nodes. A contention based scheme, Carrier Sense Multiple Access Medium Access Control (CSMA MAC), and a contention free approach, Time Division Multiple Access Medium Access Control (TDMA MAC), are considered. Performance analysis as well as simulation results are included for both approaches, and a comparison is made to identify potential tradeoffs.

A. AOI AGGREGATION PERFORMANCE

The performance of the proposed AOI mechanism and the effectiveness of the in-network data aggregation occurring within the AOI are evaluated by monitoring the dissemination of the data traffic generated by the sensor nodes throughout the network. The evaluation is based on the metrics of overall end-to-end time delay and network data throughput.

1. Opnet Modeler© Network Topology and Node Configuration

The network topology for the hybrid, large-scale WSN, as shown in Figure 18, is comprised of the Tier 1 terrestrial nodes and the Tier 2 LEO satellites. It is assumed that the proposed data dissemination algorithm has entered Phase 3, which means that the initial AOI has been formed and target tracking has commenced. Accordingly, the GEO satellites of Tier 3 have been omitted from the simulation since they do not contribute to the data traffic once the data dissemination algorithm has reached this tracking phase. Tier 1, which includes the terrestrial platforms, consists of the RF Sensor, the intermediate nodes 6, 7, and 8 and the Sink. Tier 2 is comprised of four LEO satellites labeled IR Sat 1, 2, 3, and 4.

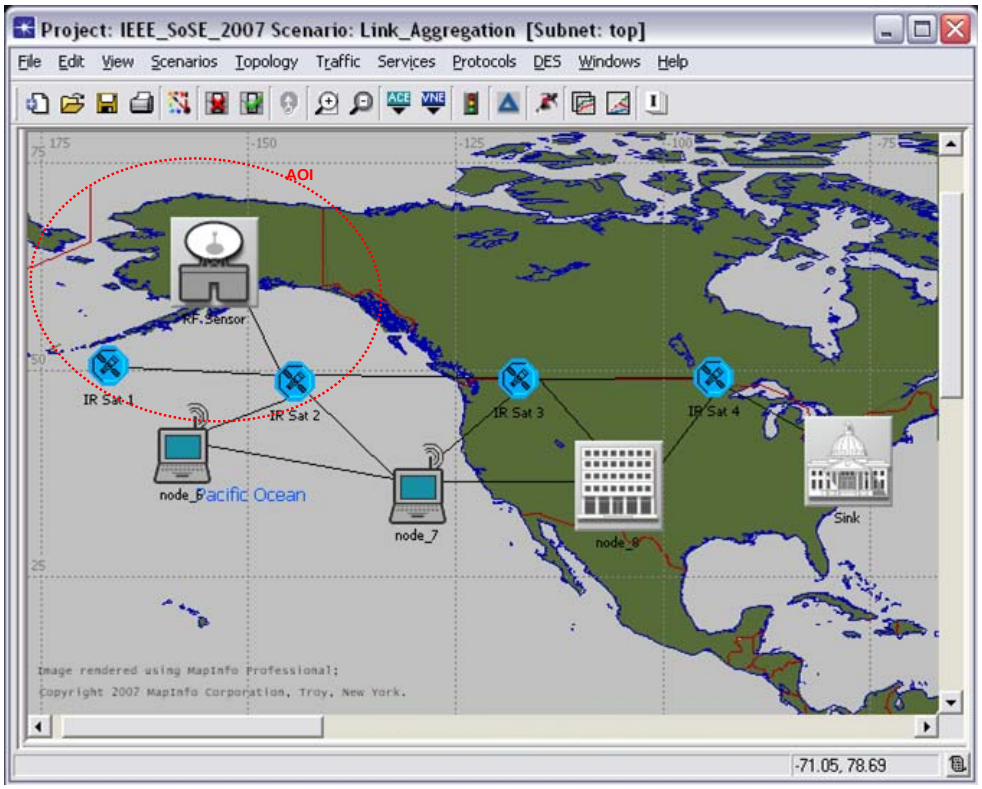

Figure 18. Hybrid, large-scale WSN modeled in OPNET Modeler

The OPNET modeling environment is characterized by a hierarchical network design structure. Three levels of hierarchy are considered: (1) the *Network Model* describing the network topology, (2) the *Node Model* specifying the characteristics of each component node, and (3) the *Process Model* implementing the function of each node. These OPNET hierarchical design levels are further addressed in Appendix B.

In OPNET, the transmission channel characteristics are configured by a multi-stage mechanism called the *Transceiver Pipeline*. Each stage of this mechanism, which is performed on a per-receiver basis each time a transmission occurs, is responsible for determining a specific attribute of the communication link, such as antenna gain, link closure, channel match, transmission delay, propagation delay, channel data rate, received signal power, background noise, interference noise, signal-to-noise ratio, probability of bit error (BER), and error correction. Default procedures are provided for each pipeline stage which may, however, be replaced by user defined procedures.

For the initial simulation, in the network model, the inter-node communication paths have been modeled as point-to-point, duplex, packet switched links that have been configured according to the characteristics of a typical wireless channel. The attributes used for the point-to-point links are provided in Table 4.

Attribute	Value
Propagation speed	Speed of light ($3 \cdot 10^8$ m/sec)
Propagation delay	Distanced based
Data Rate	1 Mbps
Probability of Bit Errors (BER)	10^{-4}

Table 4. OPNET point-to-point link attributes used to simulate a typical wireless channel

The procedure in OPNET for the configuration of a *Node Model* to support data aggregation is presented in Appendix C.

2. Simulation Results - Comparison

As stated previously, it is assumed that the initial AOI has been formed and target tracking has been established. Specifically, two sensors (represented as IR Sat 1 and RF Sensor in Figure 18) have initiated target tracking and periodically inject sensor data traffic into the network at a rate that defines the offered data load on the network. As reflected in Table 3 and shown in Figure 18, the initial AOI is comprised of the following nodes: RF Sensor, IR Sat 1and IR Sat 2. In accordance with the lifetime in AOI criterion of the proposed algorithm (described in Chapter III), the elected AOI aggregation node is IR Sat 2.

The simulation is performed under two different scenarios: one in which data aggregation is performed within the AOI and the other where no aggregation takes place and each sensor individually routes its traffic to the sink. The data throughput (bits/sec) at the sink is plotted in Figure 19 as a function of sensor load for the two different scenarios. This sensor load represents the repetition frequency at which the sensors acquire target data and inject them into the network (PRF and frame rate of the RF and IR sensors, respectively). It can be clearly seen that aggregation within the AOI improves the data throughput across the full range of network load.

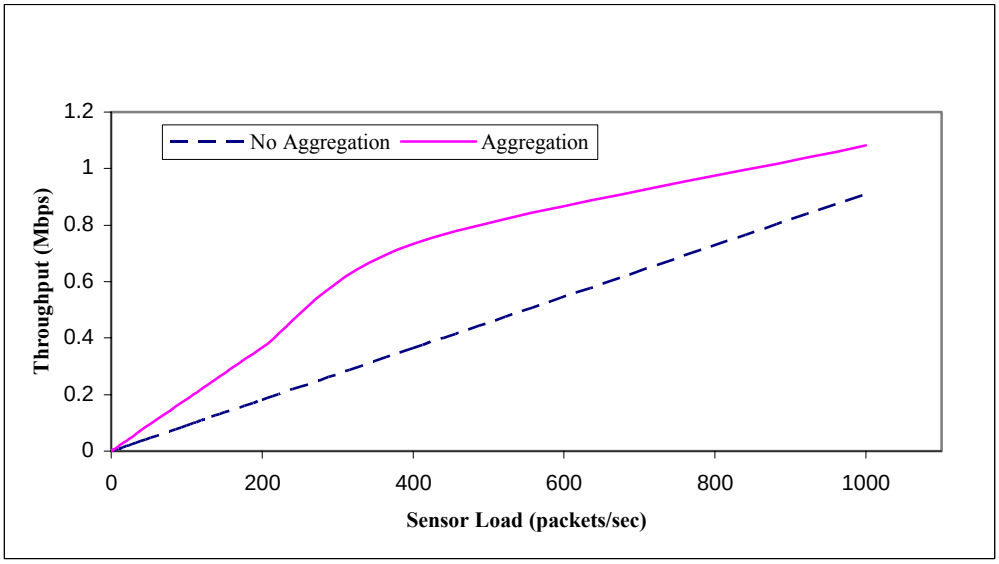

Figure 19. Network Data Throughput for the simulation of Figure 18

This improvement in throughput comes with the tradeoff of increased end-to-end delay as can be seen in Table 5. However, this increase in delay is small when compared to the overall end-to-end delay (less than 15% for this example). It should be re-emphasized that, for this analysis, the data aggregation node does not perform any data fusion or duplicate suppression. It can be expected that data fusion or duplicate suppression at the aggregation node will further improve throughput at the expense of additional delay.

Scenario	Delay (msec)
No Aggregation	31
Aggregation	36

Table 5. Overall end-to-end time delay for the simulation of Figure 18.

3. Routing Considerations

In the simulation of the previous section, the inter-node communication paths were modeled as point-to-point, duplex, packet switched links, and routing was performed based on the Open Shortest Path First (OSPF) routing protocol. OSPF is a *link-state* protocol in which each node checks the status of all of its links periodically by sending *hello* messages and broadcasts this information to its neighbors. The neighbors in

turn disseminate this link status information throughout the entire network [28]. Based on this information, each node constructs a complete routing table with global knowledge. The primary advantage of a link-state protocol is the fact that it provides faster convergence than a distance-vector routing protocol, i.e., each node updates its routing table by exchanging distance information with its neighbors. By faster convergence, it is meant that data dissemination and routing stabilize faster after a link or node failure occurs in the network [29].

However, OSPF is also a proactive protocol, i.e., valid routes must be discovered and complete routing tables must be built before actual data dissemination takes place. This introduces a significant initialization time delay. In the proposed simulation, the initial set-up time delay is found to be approximately 30 sec as shown in Figure 20 where it is observed that until the initial set-up is complete no data dissemination occurs.

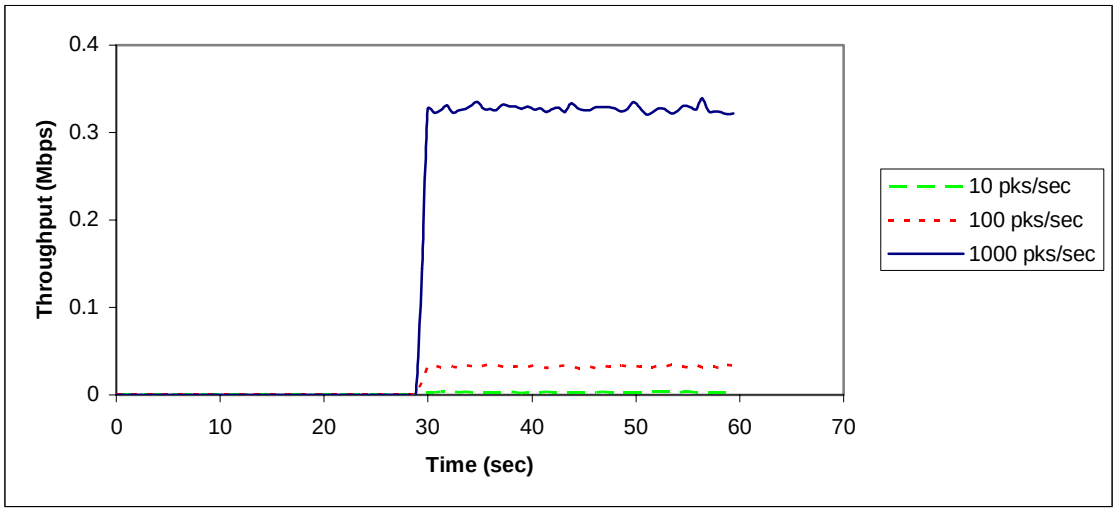

Figure 20. Network Data Throughput versus Time for three different sensor loads

The objective of this simulation is to evaluate the performance of the AOI mechanism and not the performance of the implemented routing protocol. Accordingly, the simulation models the network after the completion of the initialization phase, and it is assumed that routes have been discovered and routing tables throughout the network have already been constructed.

B. MEDIUM ACCESS CONTROL (MAC) ISSUES

Earlier in this chapter, the inter-node communication paths were modeled as point-to-point, duplex, packet switched links. This approach is a common practice in commercial satellite links where the communication among terrestrial stations is facilitated through a communications satellite. In this case, the satellite, which usually employs high-gain directional antennas, merely acts as a relay point between the terrestrial stations. This constitutes a one-hop distance network, where a dedicated communication path is assigned to each communication interface.

However, the nature of the proposed hybrid, large-scale WSN presents the following singularities. (1) The network topology requires the establishment of multi-hop satellite-to-satellite communication links. (2) Within each formed AOI, multiple sensor nodes must simultaneously forward their traffic to the aggregation node. This implies that each AOI member sensor node should maintain multiple active communication link interfaces. (3) The majority of the sensor nodes constituting the WSN are considered trusted nodes (organic to the WSN); however, it is possible that non trusted nodes may become members of the WSN as opportunistic sensor platforms supporting the WSN mission. This fact assigns an ad-hoc feature to the proposed WSN and necessitates for automatic network reconfiguration and self organization giving rise to the issues of link availability and reliability.

Consequently, the approach of dedicated point-to-point communication links among the network nodes for proposed hybrid, large-scale WSN would not be very realistic. On the contrary, it would be rational to consider the transmission medium as a shared medium among the sensor nodes constituting the network and treat the data dissemination accordingly, instead of assuming that each sensor node has an available dedicated point-to-point channel to propagate its traffic. This implies the necessity for the implementation of a medium access control mechanism among the sensor nodes. In this section, a contention-based scheme, Carrier Sense Multiple Access (CSMA), and a contention-free approach, Time Division Multiple Access (TDMA), are investigated for implementation in the hybrid, large-scale WSN.

1. Carrier Sense Multiple Access (CSMA)

In this section, the "slotted, non persistent CSMA medium access algorithm is considered in the context of our hybrid, large-scale WSN. With CSMA, a node that wishes to transmit senses the medium/channel to determine whether a transmission from another node is in progress (carrier sense). This allows the medium to be shared among multiple nodes (multiple access). The specific algorithm for non persistent CSMA functions as follows upon the arrival of a packet for transmission [30]:

- If the medium is sensed idle, the node proceeds with transmission of the packet.
- If the medium is sensed busy, the node reschedules the transmission of the packet for a later time according to a retransmission delay distribution.

In a slotted version of this scheme, time is divided into slots of size equal to the maximum propagation delay. The nodes, which must maintain a global synchronization, are allowed to commence transmission only at the beginning of a time slot. Thus, if a packet arrives for transmission during a slot, then the node will sense the medium at the beginning of the next slot and operate according to the rules of the non persistent CSMA algorithm given above [11].

a. Performance Analysis

The following analysis focuses on the throughput and time delay performance of the slotted, non persistent CSMA. The analysis as well as the derivation of the throughput equation can be found in [11]. There, it is assumed that the packets have a constant length and that the packet interarrival times are exponentially distributed. The normalized throughput is given by

$$U = \frac{\alpha F e^{-\alpha F}}{\left(1 - e^{-\alpha F}\right) + \alpha} \tag{4.1}$$

where F is the offered load and α is the ratio of the maximum propagation delay to the packet transmission time.

The normalized data throughput is plotted as a function of offered load in Figure 21.

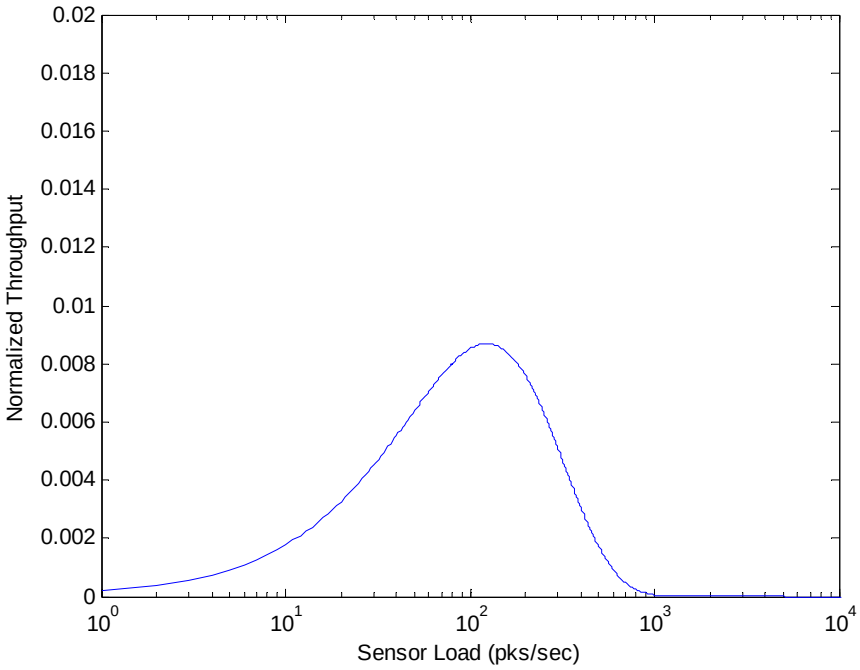

Figure 21. Normalized Throughput of slotted, non persistent CSMA as a function of Sensor Load for a hybrid, large-scale WSN (maximum propagation distance is 2400 km, packet length 192 bits and channel data rate 1 Mbps).

The analysis for the calculation of the mean time delay can also be found in [11]. In this work, a positive acknowledgement scheme is assumed, i.e., the acknowledgement packets are correctly received with a probability of one. The equation for the time delay is then given by

$$D = \left(\frac{F}{U} - 1\right)\left(T + T_{ack} + 2\tau + X\right) + T + \tau \tag{4.2}$$

where, the ratio of the offered load to the normalized throughput $\frac{F}{U}$ is obtained from (4.1), T is the packet transmission time, T_{ack} is the acknowledgement packet transmission time, τ is the maximum propagation delay and X is the mean value of the retransmission delay distribution. The time delay as a function of offered (sensor) load is plotted in Figure 22.

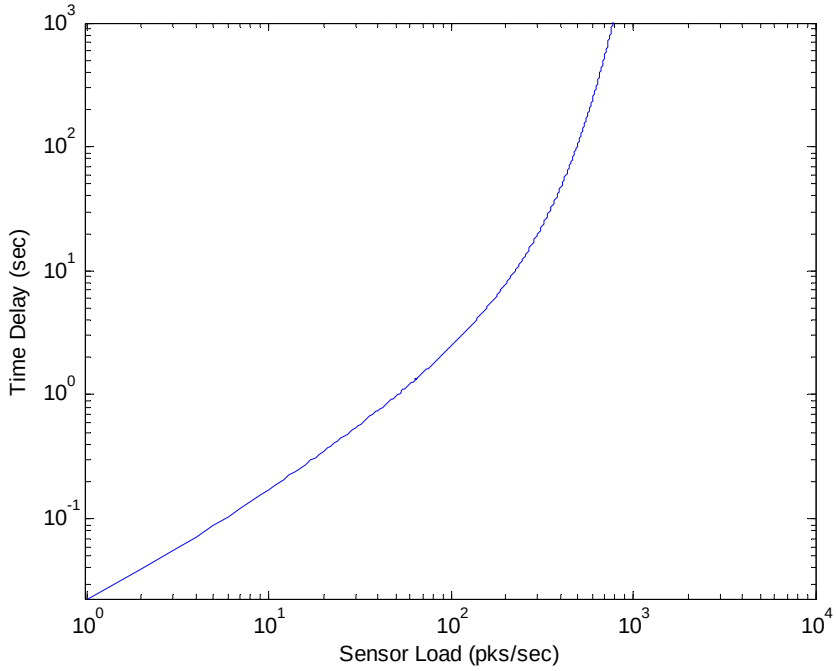

Figure 22. Mean Delay for slotted, non persistent CSMA as a function of Sensor Load for a hybrid, large-scale WSN (maximum propagation distance is 2400 km, packet length 192 bits and channel data rate 1 Mbps).

From Figures 21 and 22, it is observed that the CSMA approach has poor performance in terms of data throughput and introduces large time delays across the whole range of sensor loads for a hybrid, large-scale WSN. These results are not surprising considering the large propagation delays associated with the proposed WSN topology lead to extensive traffic collisions among the nodes contending for the medium.

b. OPNET Network Topology and Node Configuration

In principle, the *Network Model* considered for the hybrid, large-scale WSN is the same as that described in the previous section for the point-to-point communication links. Again, it is assumed that the initial AOI has been formed and target tracking has commenced. However, in this case, the *Node Models* have been configured in a different way and include a whole different set of *Process Models*, in order for them to support the OPNET *WLAN Model*. This *WLAN model* is an implementation of the IEEE 802.11 standard, which is based on the slotted, non persistent CSMA algorithm.

The network topology appears in Figure 23. The transmission channel characteristics are modeled in the *WLAN Model* suite by a set of stages collectively referred to as the *WLAN Pipeline*. An illustrated procedure for creating a WLAN based network in OPNET Modeler© is available in Appendix B where the *Network Model* construction, the *Node Model* configuration and the *WLAN Pipeline* stages are explicitly presented.

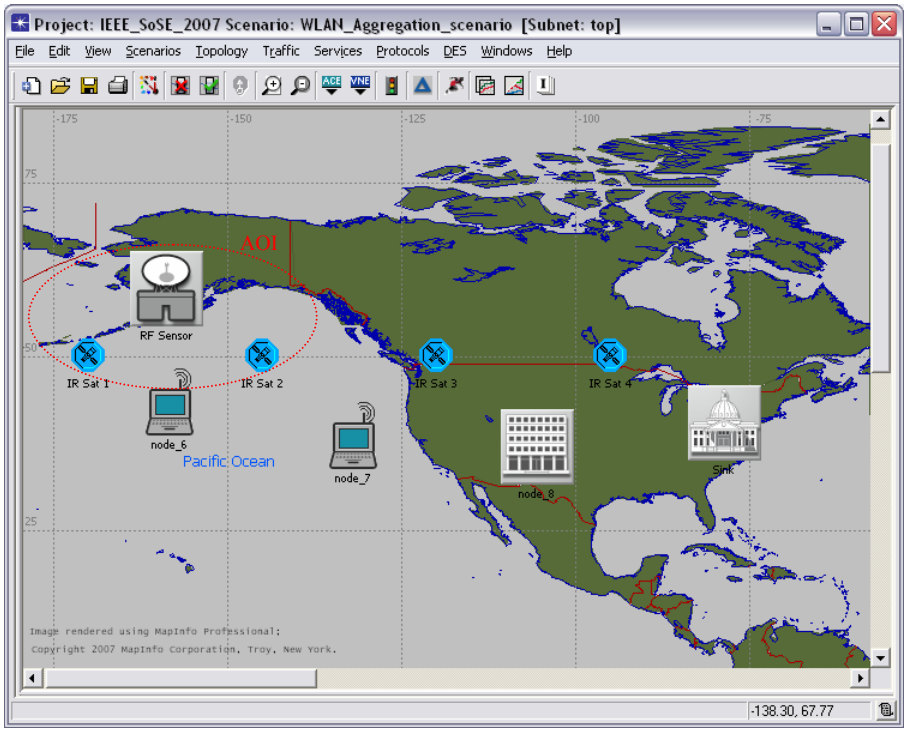

Figure 23. WLAN-based hybrid, large-scale WSN modeled in OPNET

c. Simulation Results - Comparison

The scenario used for the *WLAN Model* simulation is identical to the one used for the point-to-point links. In summary, sensors IR Sat 1 and RF Sensor inject sensor data traffic into the network, and the elected AOI aggregation node is IR Sat 2. The results for the CSMA/CA scheme (*WLAN Model*) are compared to the results of the point-to-point links form the previous section.

The data throughput (bits/sec) at the sink, for the two different approaches, is plotted in Figures 24 and 25 as a function of the sensor load. It can be clearly observed that the point-to-point links always outperform the CSMA/CA in terms of data

throughput. Specifically, when the sensor load exceeds an approximate value of 10 packets/sec, the performance of the CSMA/CA reaches a peak value and levels off.

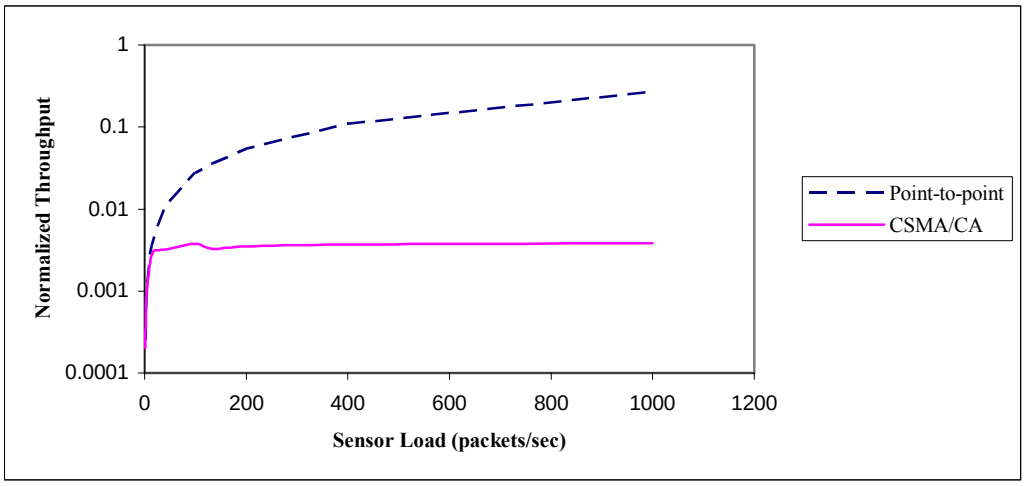

Figure 24. Normalized Network Data Throughput of CSMA/CA versus Point-to-point link as a function of Sensor Load

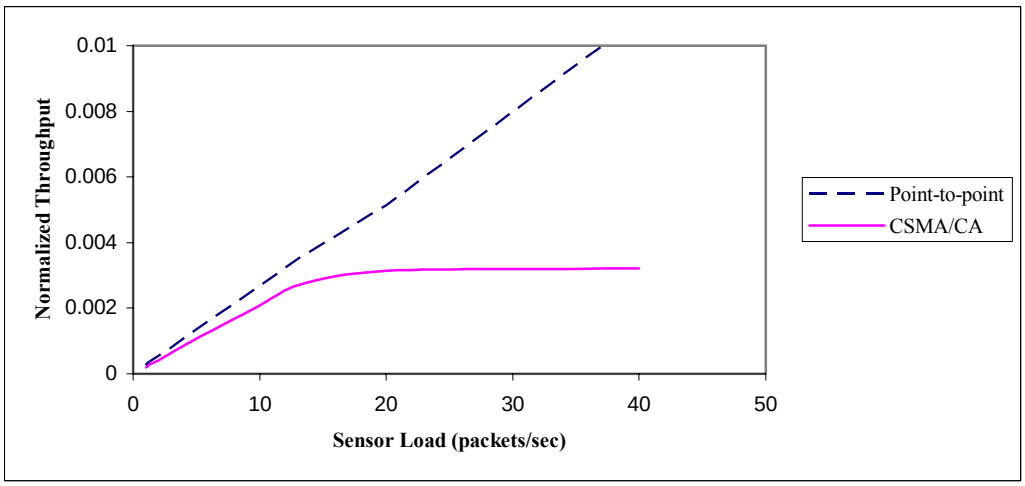

Figure 25. Normalized Network Data Throughput of CSMA/CA versus Point-to-point link for sensor load values below 40 packets/sec.

The overall end-to-end time delay (sec) for the two different approaches is plotted in Figures 26 and 27 as a function of sensor load. The same observations regarding the limited performance of the CSMA/CA scheme at high sensor load values are applicable here as well.

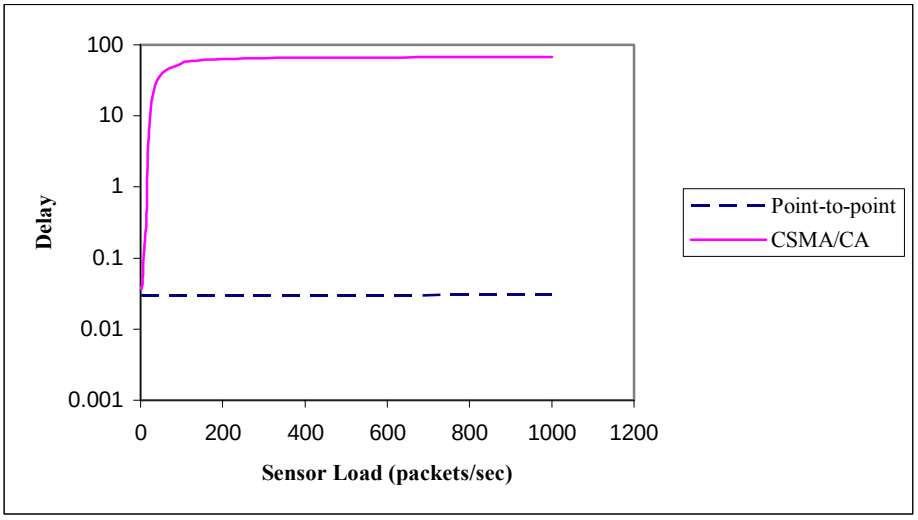

Figure 26. Overall end-to-end time delay of CSMA/CA versus Point-to-point link as a function of Sensor Load

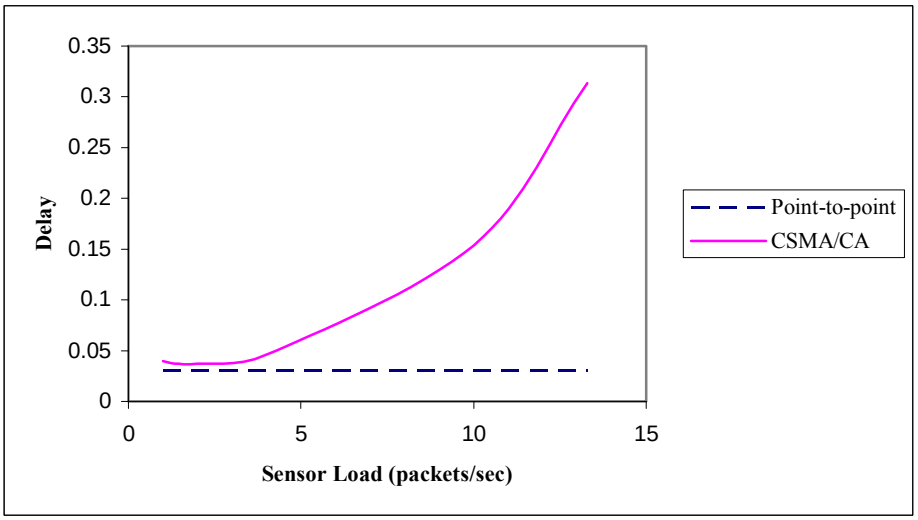

Figure 27. Overall end-to-end time delay of CSMA/CA versus Point-to-point link for sensor load values below 15 packets/sec.

As stated in Chapter III, two separate traffic flows are considered in the proposed network: the intra-AOI flow among the sensor (source) nodes and the current AOI aggregation node, and the backflow from the AOI aggregation node to the sink. To locate where in the network this time delay occurs in the CSMA/CA scheme, we analyze these two traffic flows separately and plot the end-to-end time delay experienced in each flow in Figures 28 and 29.

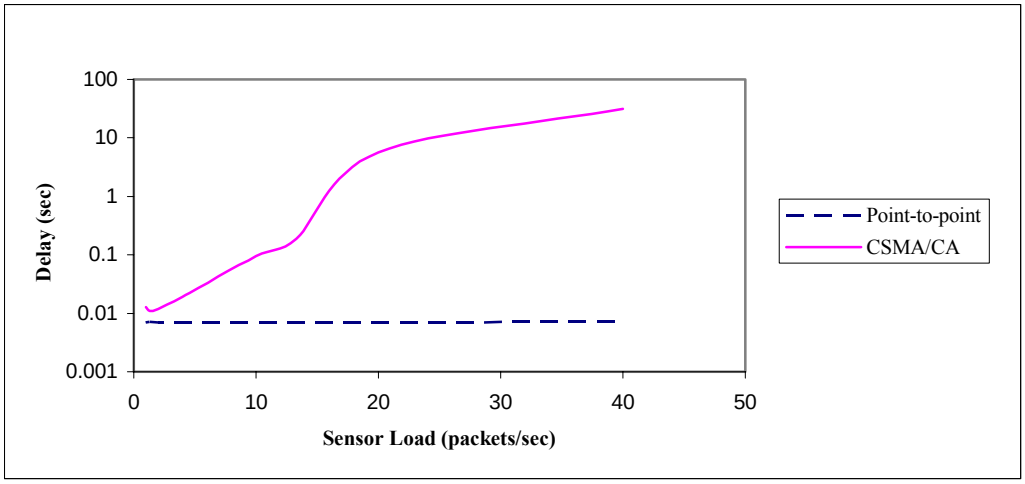

Figure 28. End-to-end time delay in the intra-AOI flow as a function of Sensor Load

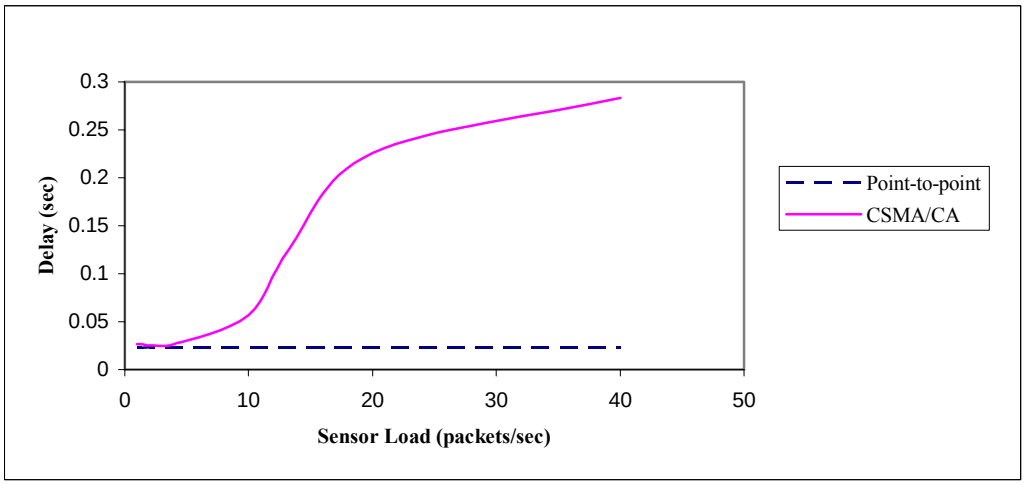

Figure 29. End-to-end time delay in the backflow to the sink as a function of Sensor Load

It is clearly observed that the greater proportion of the excessive time delay is experienced within the AOI, in the flow from the sensor nodes to the aggregation node (note that the scale in Figure 28 is logarithmic).

Before comparing the results obtained by the simulation with those derived in the performance analysis, two major points should be highlighted. First, the analysis equations for the "slotted, non-persistent CSMA" protocol (4.1, 4.2) assume a one-hop network and, therefore, a comparison between analysis and simulation is only possible within the limits of the AOI. Second, the performance analysis was based on the

slotted, non-persistent CSMA algorithm whereas the simulation was conducted with the OPNET *WLAN Model,* which is an implementation of the IEEE 802.11 wireless standard and incorporates the Carrier Sense Multiple Access / Collision Avoidance (CSMA/CA) algorithm. The basic difference between them is the utilization of a four-frame exchange scheme by the IEEE 802.11 standard. According to this scheme, a source first issues a request to send frame (RTS) to the destination, and the destination in turn responds with a clear to send frame (CTS). Upon receiving the CTS frame, the source transmits the data frame, and the destination responds with an acknowledgement (ACK). The RTS frame alerts all the nodes within reception range of the source that a frame exchange is under way, and these nodes refrain from transmitting in order to avoid a collision. In the same manner, the CTS frame alerts all the nodes within reception range of the destination [30].

This four-frame exchange enhances the reliability of the IEEE 802.11 standard by reducing collisions and minimizing the effects of the *Hidden Node* problem [31]. In the *Hidden Node* problem, the packets originating from two nodes that are out of transmission range of each other and, therefore, cannot sense each other's transmissions, thus collide in the vicinity of an intermediate node as shown in Figure 30.

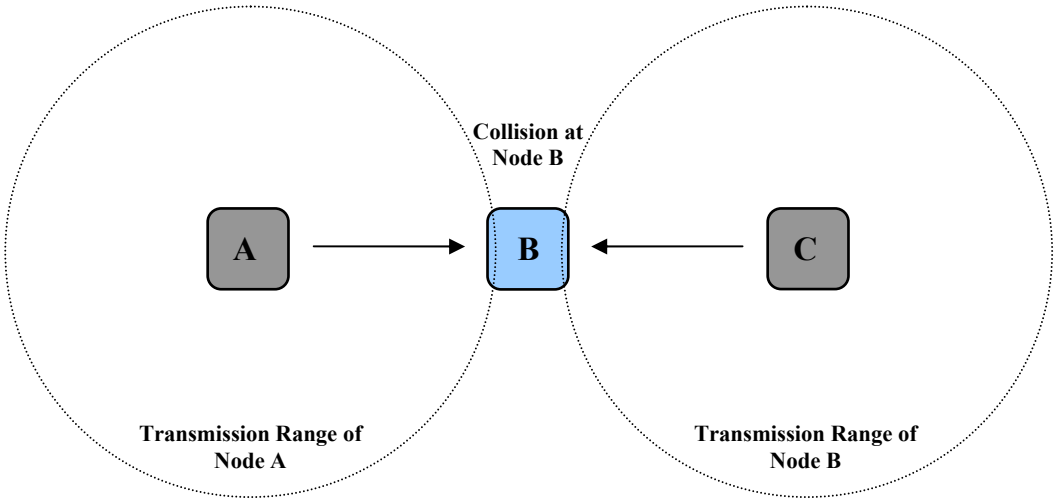

Figure 30. The Hidden Node Problem: packets originating form nodes A and C that are out of transmission range of each other, collide at destination node B.

The network data throughput and the end-to-end time within the AOI, for the whole range of sensor loads, are presented in Figures 31 and 32, respectively.

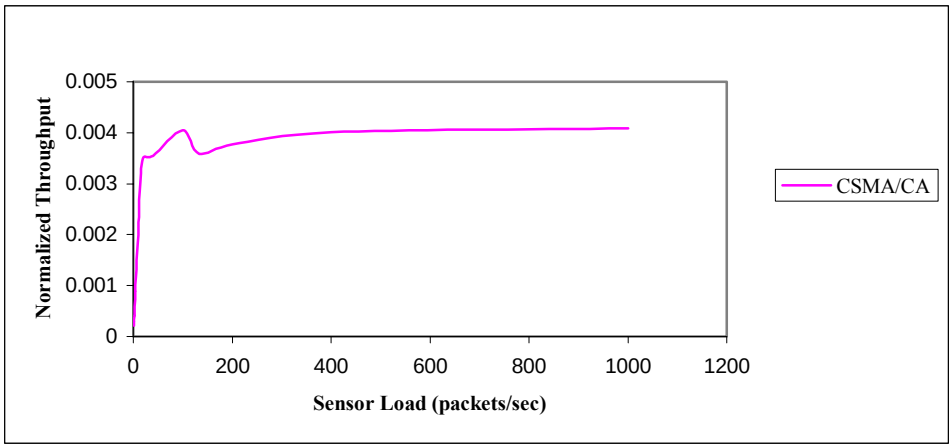

Figure 31. Normalized Network Data Throughput in the intra-AOI flow

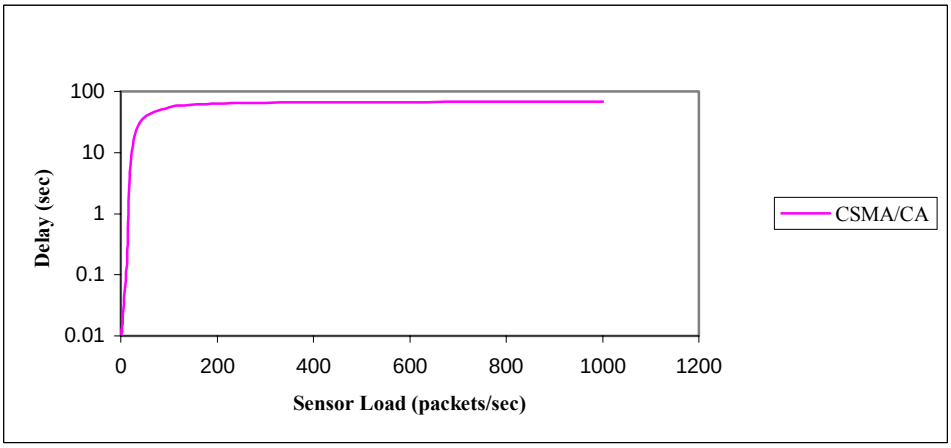

Figure 32. End-to-end time delay in the intra-AOI flow

The analysis and simulation results from the implementation of the CSMA/CA scheme clearly show a poor throughput performance and excessive time delay in the intra-AOI flow, especially for sensor load values greater than 10 packets/sec. The contention for the medium among the sensor nodes, in their attempt to forward their traffic to the aggregation node, in combination with the large propagation delays associated with the proposed WSN architecture, lead to extensive traffic collisions that are detrimental to the performance of the WSN. Therefore, it would be reasonable to investigate a contention free medium access control approach.

d. Routing Considerations

In the previous simulation, routing was performed based on the Ad Hoc on Demand Distance Vector (AODV) routing protocol [32]. AODV is designed for mobile nodes in an ad hoc network. It provides for self-organizing, dynamic, multihop routing among wireless nodes, offering reduced processing and memory overhead as well as fast convergence in the case of a link failure or a network topology change. In AODV, routes are only built when necessary and only maintained if they remain active. A route is considered active as long as data dissemination occurs along its path.

Three types of messages are utilized by AODV: Route Requests (RREQs), Route Replies (RREPs), and Route Errors (RERRs). Specifically, when a source node desires to send data to a destination for which there is no existing route, it issues a RREQ broadcast across the network. Intermediate nodes that receive this request message set-up backward pointers to this source by updating their routing tables. A RREP message is sent back to the originating source node, either from the destination or from any intermediate node aware of an active route to the destination. If a link failure occurs while a route is maintained active, the node upstream of the failure location issues a RERR message to the source node declaring the destination unreachable. In this case, the source node performs a new route discovery by issuing a new RREQ message. This "on demand" route setup is directly responsible for the initialization delay seen in the results.

Again, the simulation objective here is the performance of the medium access control scheme and not the performance of the implemented routing protocol. As mentioned earlier, it is assumed that the proposed data dissemination mechanism has entered Phase 3, which indicates that the initial AOI has been formed and target tracking has commenced. Therefore, the simulation models the network after the completion of the route discovery process, i.e., active routes have already been established between the two sensor node sources and the destination. This has the desired effect of bypassing the impact of the AODV setup process. As illustrated in Figure 33, throughout the whole simulation only one route request on average was issued by each source and only two route replies were sent from the destination (one for each sensor source). This

observation verifies that the route discovery process only occurs once and no other delay associated with a new route discovery process of AODV was introduced.

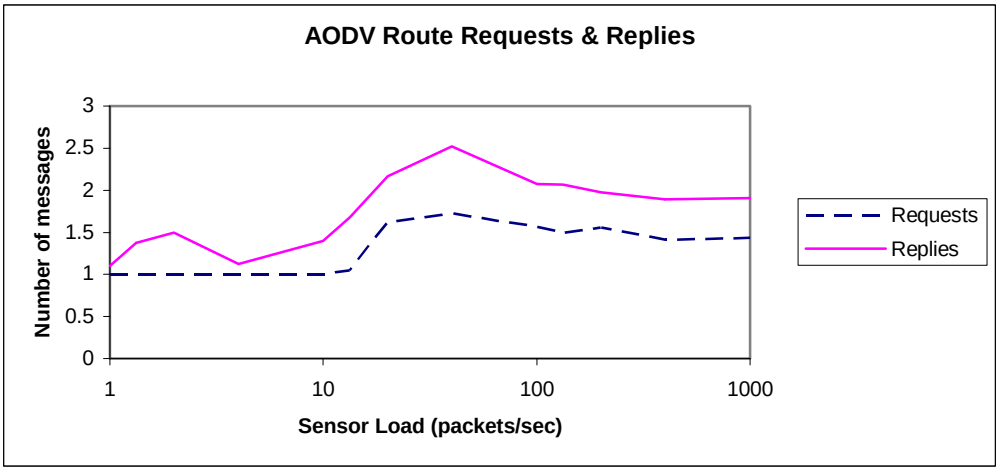

Figure 33. AODV Route Request and Route Reply messages

2. Time Division Multiple Access MAC (TDMA MAC)

The simulation results in the previous section suggest the need for an alternate approach for data dissemination within the AOI since it is there that the excessive time delays occur. As highlighted earlier, the transmission medium should be considered a shared medium among the nodes constituting the network. However, in the previous section, it was shown that a contention approach for access to the shared medium exhibits limited performance in terms of data throughput and latency. In this section, the implementation of a contention-free approach for access to the shared medium is investigated, using a Time Division Multiple Access Medium Access Control (TDMA MAC) scheme.

a. Performance Analysis

The analysis of this section is focused on the delay performance of a Time Division Multiple Access (TDMA) medium access control scheme. According to this scheme, the channel is shared among the nodes constituting the network by dividing it into time slots of fixed length. Each node is assigned a time slot or slots, and transmission is allowed only within this slot(s).

This analysis is based on the work of Lam [12]. A node utilizing TDMA is modeled as a single-server queue with unlimited buffer capacity. In addition, the data message arrival is assumed to be characterized by an independent Poisson process. It considers that M nodes are sharing the channel, each node is assigned a time slot t_{slot}, and these M time slots are organized to form a time frame T_{frame}, as illustrated in Figure 34. Therefore, any node will transmit a data message into a time slot of $t_{slot} = \frac{T_{frame}}{M}$ seconds, and then refrain from transmitting and become idle for a period of $\frac{(M-1)T_{frame}}{M}$ seconds before transmitting its next message.

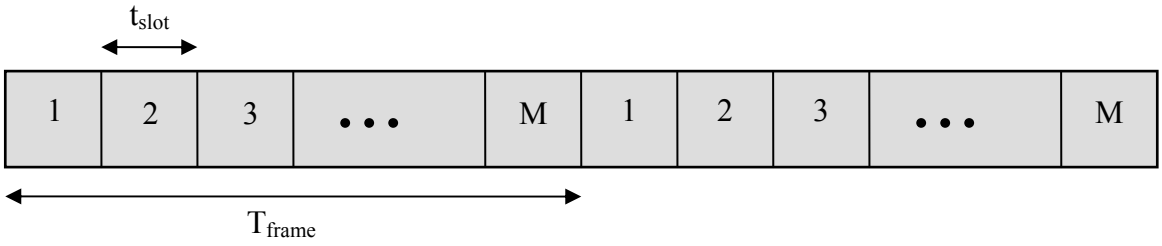

Figure 34. Frame format (T_{frame}) of the TDMA medium access control scheme

Based on an M/G/1 queue and the application of Little's formula [33] and by taking into account both the waiting time (in queue) as well as the service time (transmission), the mean delay is found to be:

$$D = \gamma_1 T_{frame} - \frac{T_{frame}}{2} + \frac{T_{frame}}{M} + \frac{\lambda \gamma_2 \left(T_{frame}\right)^2}{2\left(1 - \lambda \gamma_1 T_{frame}\right)} \tag{4.3}$$

where λ is the message arrival rate, and γ_1 and γ_2 are the first and second moments of the random variable characterizing the number of packets per message, respectively.

For the purposes of analysis, it is assumed that two sensor nodes share the medium (i.e., M is 2) and that the number of packets per message is a constant value of one. This is to ensure that the results in this section are consistent with those of sections A and B.1. The first and second moments γ_1 and γ_2 are then found to be equal to one, and (4.3) simplifies to:

$$D = 2t_{slot} + \frac{2\lambda\left(t_{slot}\right)^2}{1-2\lambda t_{slot}}, \text{ where } \frac{T_{frame}}{2} = t_{slot}\,. \tag{4.4}$$

The selection of an appropriate value for the slot time is critical in the performance of a TDMA medium access control scheme. To avoid collisions within the medium, the slot length must be at least equal to the packet transmission time plus the maximum propagation delay. Moreover, to minimize interference between successive time slots, a guard interval should be added at the end of each time slot. It is assumed that global time synchronization necessary for the utilization of a TDMA approach is provided by Global Positioning Satellite (GPS) receivers, which can achieve a clock accuracy of 100 ns. Thus, the guard time interval should be at least 200 ns [34]. A layout of the considered time slot is presented in Figure 35.

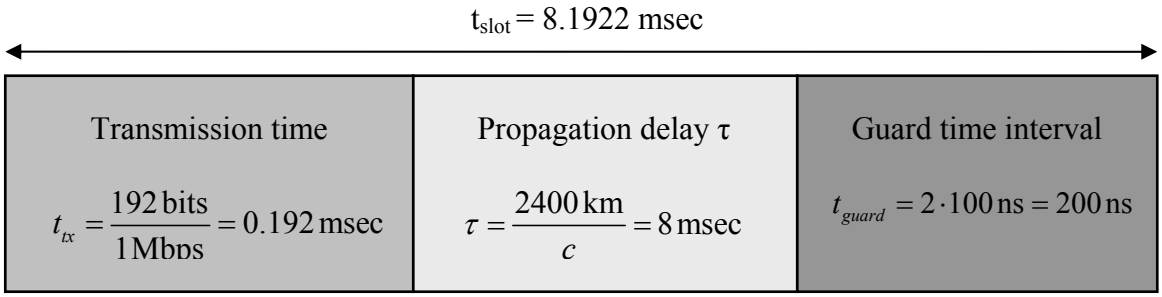

Figure 35. Layout of considered TDMA Time slot

The TDMA frame consists of two time slots; therefore, its length will be $T_{frame} \approx 16.4$ msec, which leads to a frame rate $R_{frame} \approx 60$ frames/sec. The frame rate is a limiting factor in the design since it may not be exceeded by the packet arrival rate (representing the sensor load); otherwise, the waiting time will become infinite and the scheme will collapse. This limitation for the packet arrival rate can also be seen in (4.4) where we observe that when the denominator of the second term approaches zero, the delay becomes infinite:

$$1-2\lambda t_{slot} \geq 0 \quad \Rightarrow \quad 2\lambda t_{slot} \leq 1 \quad \Rightarrow \quad \lambda \leq \frac{1}{2t_{slot}} = \frac{1}{T_{frame}} = R_{frame}\,. \tag{4.5}$$

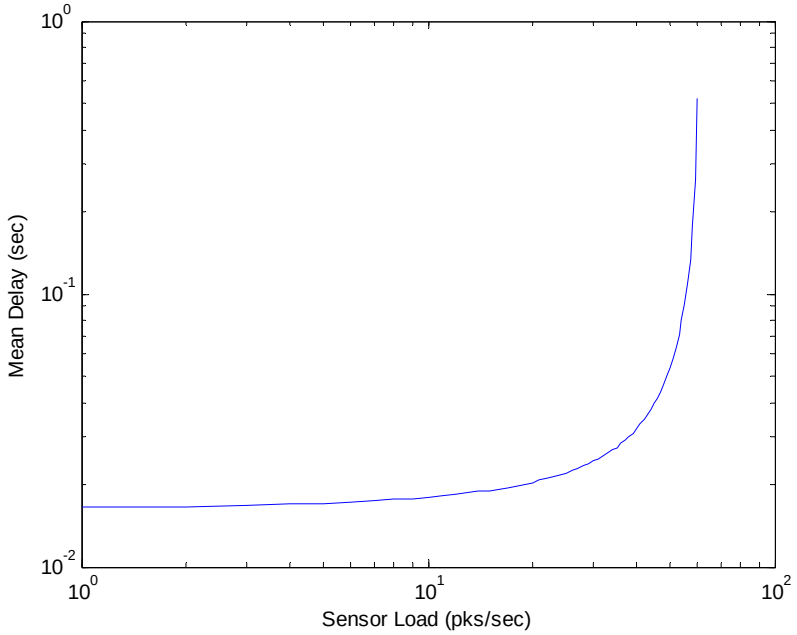

Figure 36. TDMA Mean Delay as a function of Sensor Load

From Figure 36, which plots mean delay as a function of sensor load, we observe that a TDMA scheme provides acceptable performance in our network only for sensor loads below 60 packets/sec. Additionally, an increase in the frame time, which is proportional to the propagation delay and the number of nodes sharing the medium, will result in a further reduction of the achievable sensor load.

b. OPNET Network Topology and Node Configuration

Unlike the simulations of the previous sections, the OPNET *Network Model* for the evaluation of the TDMA MAC scheme will not include all the nodes in the hybrid, large-scale WSN topology. As discussed earlier, the analysis focuses only on the data traffic within the limits of the AOI; therefore, it is only necessary to model the nodes constituting the initial AOI and the data dissemination within this AOI. Again, it is assumed that the initial AOI has been formed and target tracking has commenced. Additionally, the *Node Models* have been configured differently, incorporating a specific set of *Process Models*, to support the TDMA MAC scheme. The transmission channel

characteristics are configured according to the standard *Transceiver Pipeline* stages, using values identical to those of the previous simulations. The network topology is shown in Figure 37.

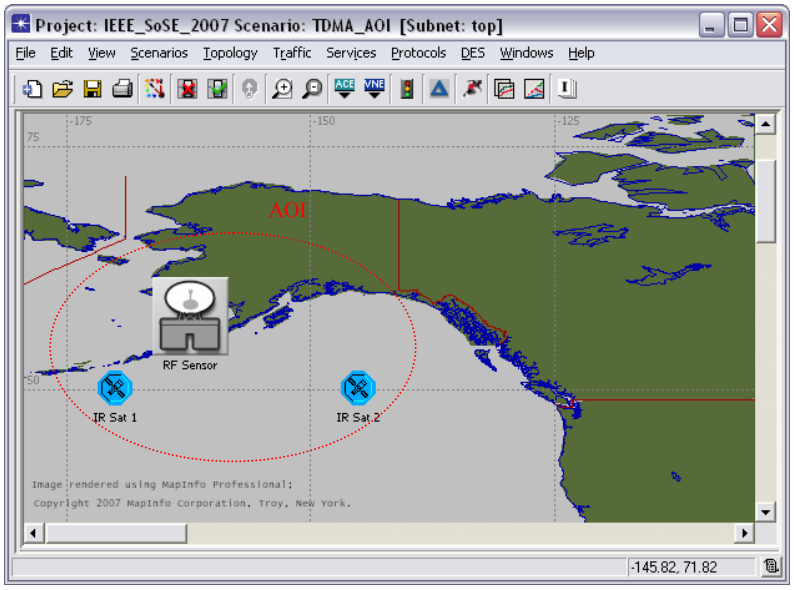

Figure 37. TDMA MAC Network Model in OPNET

c. Simulation Results

The scenario used for the simulation is identical to that used in the previous simulations. In summary, sensors IR Sat 1 and RF Sensor in Figure 37 inject sensor data traffic into the network and the elected AOI aggregation node is IR Sat 2. The end-to-end delay in the intra-AOI flow, from the sensor nodes (sources) to the AOI aggregation node, is plotted in Figures 38 and 39 as a function of sensor load. The simulation performance of the TDMA MAC scheme is consistent with the performance analysis. Specifically, when the sensor load reaches an approximate value of 60 packets/sec, the maximum allowed sensor load according to the performance analysis, the TDMA scheme saturates and begins to introduce extremely high mean delay values.

Comparing the results of the TDMA scheme to those of CSMA/CA approach and point-to-point links, we observe that the point-to-point scheme exhibits the lowest end-to-end delay within the AOI among the proposed solutions. For very low sensor load values (below 10 packets/sec), CSMA/CA experiences less delay than

TDMA. Between 10 and 60 packets/sec, TDMA outperforms CSMA/CA. For sensor loads above 60 packets/sec, the delays of both the CSMA/CA and TDMA approaches fail to meet the real time objectives.

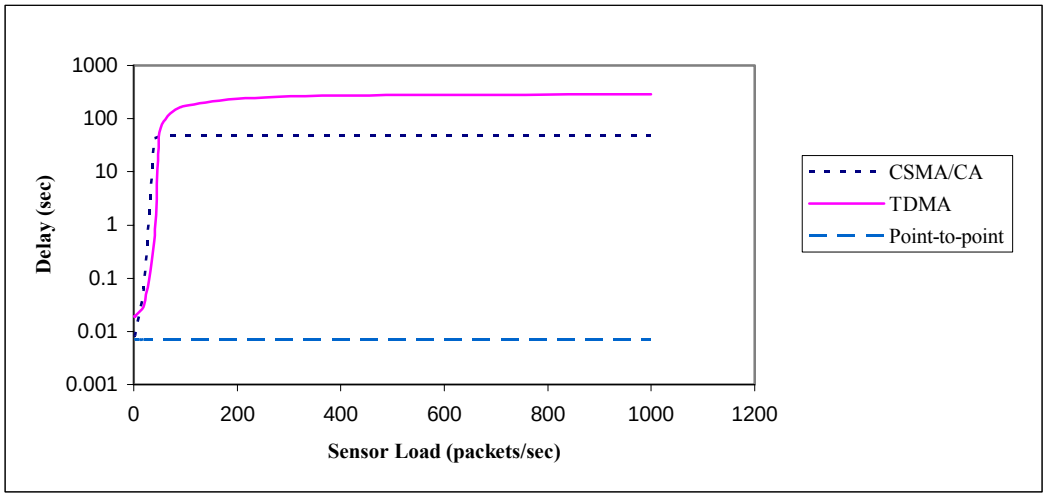

Figure 38. End-to-end delay in the intra-AOI flow for CSMA/CA, TDMA and point-to-point links as a function of sensor load

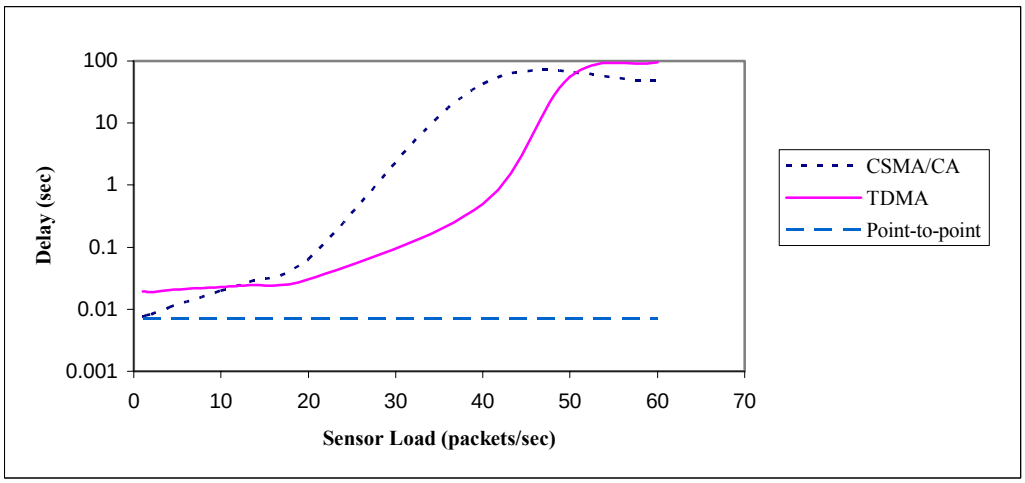

Figure 39. End-to-end delay in the intra-AOI flow for CSMA/CA, TDMA and point-to-point links for sensor load values below 60 packets/sec.

Although the sensor load (packets/sec) is proportional to the sensor PRF or frame rate, they do not necessarily have to be equal. This, however, implies that data processing is available on-board the sensor node that will allow a reduction in the offered sensor node load without degrading the performance of the actual sensor.

C. SUMMARY

In this chapter, we evaluated the performance of the proposed hybrid, large-scale WSN through analysis and simulation. OPNET Modeler© Simulation platform was used to model the dissemination of the data in the WSN.

The AOI clustering mechanism, in combination with in-network data aggregation within the AOI, was shown through simulation to present a clear advantage in terms of data throughput, by reducing the data overhead, without introducing excessive time delay and sacrificing the operational requirements of the network.

The unrealistic implementation of point-to-point links for the proposed WSN led to the consideration of a shared medium and the search for a suitable medium access control mechanism. Contention-based and contention-free approaches were considered. Through analysis as well as simulation, it was shown that the contention-based CSMA scheme performed poorly in terms of throughput and introduced significant time delays, especially at higher sensor loads. Moreover, a closer look at the simulation results revealed that the excessive time delay occurred within the AOI due to the heavy contention for medium access among the sensor nodes in combination with the large associated propagation delays. This observation suggested a contention-free data dissemination within the AOI mechanism, such as TDMA.

Through analysis and simulation of the TDMA scheme, it was shown that the frame rate of the TDMA system limits the achievable sensor load of the proposed hybrid, large-scale WSN to less than 60 packets/sec. Moreover, an increase in the number of sensors or the maximum propagation distance would increase the frame length and further reduce this achievable sensor load. However, the performance analysis and the simulation of the TDMA scheme allowed only one data packet to be transmitted within a time slot. The situation is expected to improve significantly if more (than one) data packets are transmitted per time slot.

Through simulation, it was demonstrated that for very low sensor loads (below 10 packets/sec) CSMA/CA introduces less delay than TDMA whereas between 10 and 60 packets/sec, TDMA outperforms CSMA/CA. For sensor loads greater than 60

packets/sec, both approaches fail to meet the real-time requirements. Once again, on-board data processing at sensor node would allow a reduction in the offered sensor load without degrading the performance of the sensor.

V. CONCLUSION

This thesis investigated how real-time target tracking in an integrated ballistic missile defense system (IBMDS) may be supported using a hybrid, large-scale wireless sensor network (WSN). In particular, a hierarchical network architecture composed of three different tiers, defined by altitude above the Earth, incorporating both terrestrial and satellite sensor nodes, carrying IR and RF sensors was proposed. Through IR spectroscopy, the target-background combination was examined for the boost and post-boost phase of the target trajectory. Current IR sensor technologies were investigated, including performance analysis for a multi-color quantum-well IR photodetector (QWIP) step-stare focal plane array (FPA). Future IR sensor technologies, candidates for implementation in the WSN, were briefly discussed. The study examined how the implementation of a data dissemination algorithm, incorporating a clustering mechanism called the AOI, may ensure a reliable and real-time cooperation between the nodes of the network. In the process, the constraints of a real-time wireless IR sensor network were highlighted and the issues of topology, coverage, clustering, in-network data aggregation, medium access control, and routing were analyzed through analysis as well as simulation.

A. CONTRIBUTIONS

Initially, the study examined the IR signatures of the target in combination with the competing background, which are not constant throughout the target trajectory. This, along with the resolution and sensitivity requirements associated with the large detection ranges in a BMDS, led to the employment of a multi-color quantum-well IR photodetector (QWIP) step-stare, large-format, focal plane array (FPA). The high performance of the proposed IR sensor was demonstrated through performance analysis by evaluation of the IR sensor figures of merit.

A clustering mechanism, called the “Area of Interest” (AOI) was introduced, which combines the concept of data centric routing with in-network data aggregation. Building upon this AOI mechanism, a data dissemination algorithm suitable for a hybrid large-scale WSN, designed to meet the real-time and accuracy operational requirements

imposed by the nature and mission of the WSN without introducing excessive data overhead and increased time-delays was presented. Simulation results verified that aggregation within the AOI improves the data throughput across the full range of network load [35].

Medium access control (MAC) issues were investigated since the nature of the proposed WSN dictated the necessity for a shared medium consideration, rather than providing for dedicated communication links as in the case of traditional satellite point-to-point communications. A contention-based scheme, CSMA MAC, and a contention-free approach, TDMA MAC, were considered. Performance analysis as well as simulation showed that a contention-free approach is more appropriate for implementation in wireless networks associated with large propagation delays and increased offered loads.

B. FUTURE WORK RECOMMENDATIONS

The research, performance analysis and simulations conducted in this thesis did not address all of the issues associated with the incorporated sensors and the data dissemination in a WSN designed for an IBMDS. Several areas are left for future investigation.

In this thesis, a two-color (MWIR-VLWIR) QWIP FPA was considered. Further investigation may include an IR detector with multi-color capabilities of more than two-colors, involving FPAs of larger and different format. Such a development would cover almost all the IR sensor requirements of a BDMS. Moreover, the examination of modern detector materials such as the Sb-based strained-layer superlattice (type-II SLS) photodetectors is highly recommended since they combine the advantages of both HgCdTe (high quantum efficiency) and QWIP (high uniformity).

Additionally, although in this thesis the RF sensors were briefly addressed, future work could consider the evaluation of specific RF sensors in terms of their capabilities for target detection / tracking, kill-assessment as well as background and countermeasure discrimination throughout the trajectory of the ICBM.

The data dissemination mechanism presented in this thesis modeled the traffic flow from the sensor nodes to the sink (command and control center), assuming that the AOI clustering mechanism had a limited number of sensor members, a low degree of in-network data aggregation was performed within the AOI, and the target trajectory was in bound toward the sink. Future work may consider modeling multiple traffic flows including weapon assignment flows, expanding the AOI to include more sensors, performing a higher degree of in-network data aggregation involving data fusion techniques and examining the case of multiple sinks. Additionally, although the objective of the performed simulations was the evaluation of the performance of the proposed data dissemination mechanism and the implemented medium access control schemes and not that of the implemented routing protocol, future research may examine the performance of specific routing protocols suitable for implementation in the WSN. Alternative MAC schemes may be investigated that support wireless sensor networks associated with large propagation delays and increased offered loads.

Although this thesis is immediately applicable to an IBMDS, the results of this study may be extended to tactical missile defense system as well as "small sensor" wireless sensor networks intended for real-time object detection and tracking in military as well as civilian applications.

THIS PAGE INTENTIONALLY LEFT BLANK

APPENDIX A: MATLAB CODES

Matlab codes used for plotting the IR spectroscopy graphs and for simulating the AOI "virtual motion" are included in this appendix.

1. Matlab Code for Ir Spectroscopy

This section presents the ir_signature.m and ir_detectivity.m codes developed to plot Figures 5, 6, and 7 regarding target and background IR signatures and to calculate the D^* values in the performance analysis of the IR sensors, according to equations (2.6) and (2.7), respectively.

a. **ir_signature.m:** Target and Background IR signatures

```
% Parameter Initialization
c=3e8;          % Speed of light
h=6.626e-34;    % Planck constant
k=1.38e-23;     % Boltzmann's constant


% PART I
% Calculation of Radiant Exitance Vs Wavelength Boost-Phase (T=1400K)
T=1400;  % Temperature in K
lamda=0.1e-6:0.001e-6:100e-6;
RadiantExitance1=(2*pi*h*c^2)./((lamda.^5).*(exp((h*c)./(lamda*k*T))-1))/1e10;

%Determine Max Radiant Exitance & Wavelength
[y,i]=max(RadiantExitance1);
Max_Radiant_Exitance_1=0.8*y %#ok<NOPRT>
Wavelength_1=i*0.001+0.1 %#ok<NOPRT>

%Plot Radiant Exitance (Blackbody)
figure(1)
plot(lamda*1e6,RadiantExitance1,'--');
title('Radiant Exitance vs Wavelength');
xlabel('Wavelength (microns)');
ylabel('Radiant Exitance M (W/cm^2-microns)');
AXIS([0 10 0 8]);
grid on
hold on
```

```
%Plot Radiant Exitance (Emissivity 0.9)
plot(lamda*1e6,0.8*RadiantExitance1);
title('Radiant Exitance vs Wavelength (T=1400K)');
xlabel('Wavelength (microns)');
ylabel('Radiant Exitance M (W/cm^2-microns)');
AXIS([0 10 0 8]);
grid on


% PART II
% Calculation of Radiant Exitance Vs Wavelength Post Boost Phase (T=200K)
T=200;  % Temperature in K
lamda=0.1e-6:0.001e-6:100e-6;
RadiantExitance2=(2*pi*h*c^2)./((lamda.^5).*(exp((h*c)./(lamda*k*T))-1))/1e10;

%Determine Max Radiant Exitance & Wavelength
[x,j]=max(RadiantExitance2);
Max_Radiant_Exitance_2=0.9*x %#ok<NOPRT>
Wavelength_2=j*0.001+0.1 %#ok<NOPRT>

%Plot Radiant Exitance
figure(2)
plot(lamda*1e6,RadiantExitance2,'--');
title('Radiant Exitance vs Wavelength');
xlabel('Wavelength (microns)');
ylabel('Radiant Exitance M (W/cm^2 microns)');
AXIS([0 30 0 0.0005]);
grid on
hold on

%Plot Radiant Exitance (Emissivity 0.9)
plot(lamda*1e6,0.9*RadiantExitance2);
title('Radiant Exitance vs Wavelength (T=200K)');
xlabel('Wavelength (microns)');
ylabel('Radiant Exitance M (W/cm^2 microns)');
AXIS([0 30 0 0.0005]);
grid on


% PART III
% Calculation of Radiant Exitance Vs Wavelength Earthshine (T=300K)
T=300;  % Temperature in K
lamda=0.1e-6:0.001e-6:100e-6;
RadiantExitance3=(2*pi*h*c^2)./((lamda.^5).*(exp((h*c)./(lamda*k*T))-1))/1e10;

%Determine Max Radiant Exitance & Wavelength
[z,w]=max(RadiantExitance3);
Max_Radiant_Exitance_3=z %#ok<NOPRT>
Wavelength_3=w*0.001+0.1 %#ok<NOPRT>
```

```
%Plot Radiant Exitance
figure(3)
plot(lamda*1e6,RadiantExitance3);
title('Radiant Exitance vs Wavelength (T=300K)');
xlabel('Wavelength (microns)');
ylabel('Radiant Exitance M (W/cm^2 microns)');
AXIS([0 30 0 0.005]);
grid on

% PART IV
% Calculation of Radiant Exitance Vs Wavelength Solar Reflection (T=5500K)
T=5500;  % Temperature in K
lamda=0.1e-6:0.001e-6:100e-6;
RadiantExitance4=(2*pi*h*c^2)./((lamda.^5).*(exp((h*c)./(lamda*k*T))-1))/1e10;

%Determine Max Radiant Exitance & Wavelength
[z,w]=max(RadiantExitance4);
Max_Radiant_Exitance_4=z %#ok<NOPRT>
Wavelength_4=w*0.001+0.1 %#ok<NOPRT>

%Plot Radiant Exitance (Reflectivity 0.5)
 figure(4)
 plot(lamda*1e6,0.5*RadiantExitance4);
 title('Radiant Exitance vs Wavelength (T=5500K)');
 xlabel('Wavelength (microns)');
 ylabel('Radiant Exitance M (W/cm^2 microns)');
 AXIS([0 5 0 7000]);
 grid on
```

b. **ir_detectivity.m:** IR sensor D^* calculations

```
% Parameter Initialization
c=3e8;          % Speed of light
h=6.626e-34;    % Planck constant
k=1.38e-23;     % Boltzmann's constant
T1=300;         % Temperature in K
T2=5500;        % Temperature in K
ita=0.05;       % Quantum efficiency

% PART I – Day-time Luminance
% Calculation of Peak D*Blip (Lamda=3 to 4 microns)
lamda=3e-6:0.001e-6:4e-6;
Photon_Flux1=(2*pi*c)./((lamda.^4).*(exp((h*c)./(lamda*k*T1))-1));
Photon_Flux2=(2*pi*c)./((lamda.^4).*(exp((h*c)./(lamda*k*T2))-1));
Photon_Flux= Photon_Flux1+ Photon_Flux2;
integral=trapz(lamda,0.9*Photon_Flux)/1e4;
Dblip_1=(3.5e-6/(2*h*c))*sqrt(ita/integral)
```

```
% Calculation of Peak D*Blip (Lamda=14 to 15 microns)
lamda=14e-6:0.001e-6:15e-6;
Photon_Flux1=(2*pi*c)./((lamda.^4).*(exp((h*c)./(lamda*k*T1))-1));
Photon_Flux2=(2*pi*c)./((lamda.^4).*(exp((h*c)./(lamda*k*T2))-1));
Photon_Flux= Photon_Flux1+ Photon_Flux2;
integral=trapz(lamda,0.01*Photon_Flux)/1e4;
Dblip_2=(14.5e-6/(2*h*c))*sqrt(ita/integral)


% PART II – Night-time Luminance
% Calculation of Peak D*Blip (Lamda=3 to 4 microns)
lamda=3e-6:0.001e-6:4e-6;
Photon_Flux=(2*pi*c)./((lamda.^4).*(exp((h*c)./(lamda*k*T1))-1));
integral=trapz(lamda,0.9*Photon_Flux)/1e4;
Dblip_1=(3.5e-6/(2*h*c))*sqrt(ita/integral)

% Calculation of Peak D*Blip (Lamda=14 to 15 microns)
lamda=14e-6:0.001e-6:15e-6;
Photon_Flux=(2*pi*c)./((lamda.^4).*(exp((h*c)./(lamda*k*T1))-1));
integral=trapz(lamda,0.01*Photon_Flux)/1e4;
Dblip_2=(14.5e-6/(2*h*c))*sqrt(ita/integral)
```

2. Matlab Code for AOI Virtual Motion

This section presents the AOI.m code developed to plot the formation as well as the composition of subsequent AOIs during the target motion through the sensor field, as presented in Figure # and Table # respectively.

```
% Initial parameters
RadarFieldHorizSize=12;
RadarFieldVertSize = 2;
NumDataPts=100;

% Definition of target trajectory positions
Target = [0 0;1 1;4 1.4;6 1.6;8.3 1;12 0.2];
TgtCoeff = polyfit(Target(:,1),Target(:,2),3);
x_coord = linspace(0,RadarFieldHorizSize,NumDataPts);
y_coord = TgtCoeff(1)*x_coord.^3 + TgtCoeff(2)*x_coord.^2 + TgtCoeff(3)*x_coord.^1
          + TgtCoeff(4)*ones(size(x_coord));
Target_Position = [x_coord' y_coord'];

% 2-D Sensor Node Grid / Origin target launch (bottom left corner)
% Dimensions in km*10^3
 Sensor_nodes=[2,0 ; 4,0 ; 6,0 ; 8,0 ; 10,0; 12,0
               0,1; 2.318,1 ; 4.636,1 ; 6.954,1 ; 9.272,1 ; 11.59,1];
```

```
% Distance from current target position to all sensors
Target_Distance = [];
for i=1:length(Sensor_nodes)
   for j=1:length(Target_Position)
      Target_Distance_Node(j)= sqrt((Target_Position(j,1)-Sensor_nodes(i,1))^2
                                    +(Target_Position(j,2)-Sensor_nodes(i,2))^2);
   end
   Target_Distance = [Target_Distance;Target_Distance_Node];
end
% Calculation of AOI Criteria/threshold
Threshold=2;
for j=1:length(Target_Position)
   for i=1:length(Sensor_nodes)
      [k,m]=find(Target_Distance<Threshold);
   end
end

A=[k,m];

% Plots
figure (1)
plot (Sensor_nodes(:,1), Sensor_nodes(:,2),'ob',Target_Position(:,1),Target_Position(:,2),'r')
axis([0 12 0 2]);
```

THIS PAGE INTENTIONALLY LEFT BLANK

APPENDIX B: WIRELESS NETWORKS IN OPNET MODELER

In OPNET Modeler, the workflow, which refers to the creation and analysis of a network, involves a four-step procedure as illustrated in Figure 40. In this appendix, each stage in the procedure will be briefly addressed and important points critical to the proper operation of a wireless network will be highlighted.

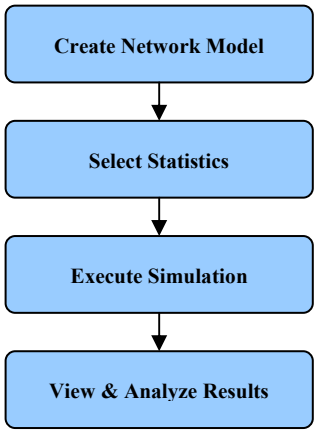

Figure 40. OPNET Modeler Workflow

1. Network Model Creation

OPNET Modeler© is characterized by a hierarchical network design structure. The highest level in the hierarchy is referred to as the "Network model", which describes the network topology. The next level of hierarchy is the "Node Model", which describes a specific component node in the network. The "Node Model" is comprised of individual modules that characterize the operation and capabilities of the parent node. The lowest level in the hierarchy is the "Process Model" which contains the code to implement the functions performed in each module of a node. This hierarchy is illustrated in Figure 41. The main staging area, where network models are built, either from the model library or by custom configuration, statistics about the network are chosen, simulations are run and results are viewed, is called the Project Editor and is depicted as the top icon in Figure 41.

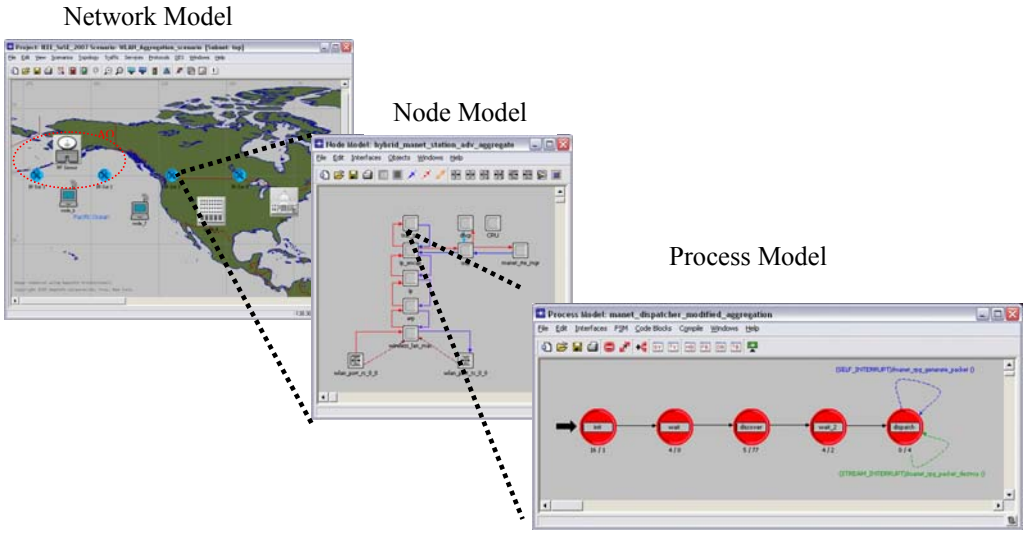

Figure 41. OPNET Modeler Hierarchical Design

a. Network Topology

Initially, the geographic size of the wireless network must be determined among the selections of office, campus, enterprise or world. Next, the selected network nodes from the object palette should be placed on the workspace of the Project Editor as shown in Figure 42. These may be default node models from the WLAN and the MANET model library or user custom built nodes.

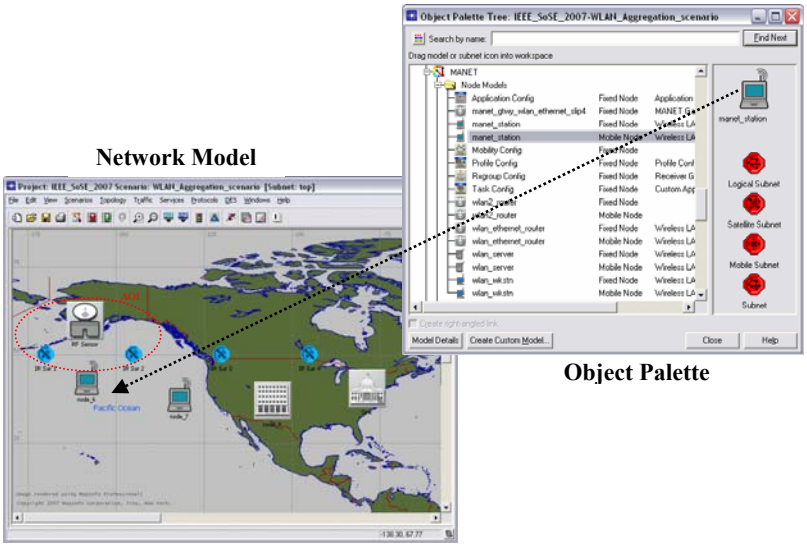

Figure 42. Node selection from Object Palette

b. Node Configuration

A node model from the MANET model library in OPNET Modeler is considered for emulating the sensor nodes of the WSN. Specifically, the mobile "manet_station" node model is adopted and modified in order to support satellite and fixed node characteristics. The user has the ability to configure a large number of attributes associated with the node model. This section will focus on the configuration of specific attributes that are critical to the performance of the wireless network.

(1) Routing Protocol: The chosen routing protocol must be declared in the attributes of each node component of the network. The user may select among several MANET routing protocols, namely OLSR, DSR, AODV and TORA, as shown in Figure 43.

(2) Traffic Generation: The "manet_station" node model incorporates a raw packet generator the attributes of which may be configured as presented in Figure 43. The packet inter-arrival time attribute is used to realize the offered sensor load into the network. The IP address of the destination (sink) is determined here as well. The addressing scheme is examined in the next section.

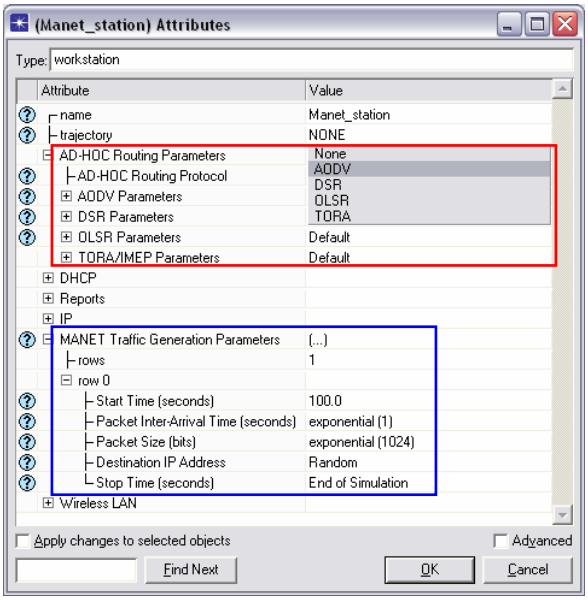

Figure 43. MANET node model attributes (Routing protocol, Packet generator)

(3) IP addressing: It is recommended that the assignment of IP addresses to the node components is selected to be performed automatically by OPNET Modeler as illustrated in Figure 44. Otherwise, improper manual address assignment may lead to the inability of the MANET routing protocol to locate the destination node.

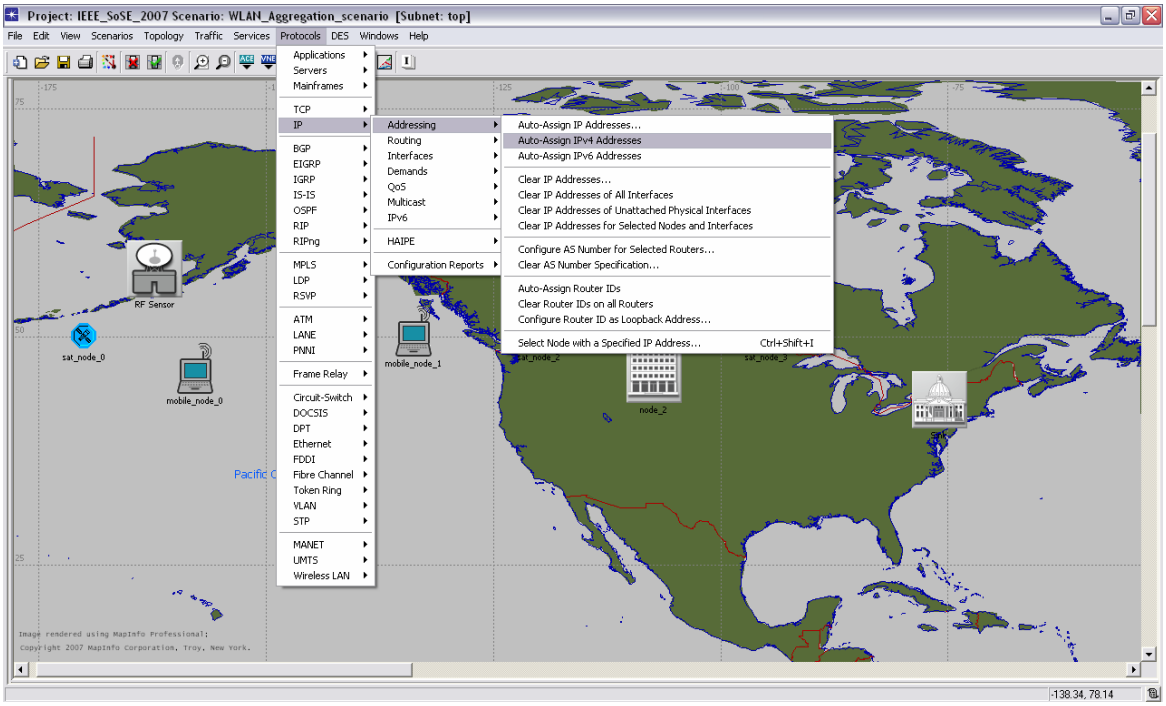

Figure 44. Automatic IP address assignment

(5) Transceiver Pipeline: As mentioned in Chapter III, the transmission channel characteristics are configured by a multi-stage mechanism called "Transceiver Pipeline". Each stage of this mechanism is responsible for handling or calculating a specific attribute of the communication link, such as antenna gain, link closure, transmission delay, propagation delay, channel data rate, received signal power, background noise, signal-to-noise ratio and probability of bit error (BER).

The WLAN Model suite uses a different set of pipeline stages than the standard radio transceiver pipeline, and it is important that they should not be mixed-and-matched. Although an explicit description of each pipeline stage is beyond the scope of this study, several key factors will be highlighted:

- Line-of-sight conditions between a transmitter and a receiver is a prerequisite in a communication link. Therefore, if the altitude of the nodes relative to the Earth's surface does not provide a line-of-sight communication, the link computation is discontinued by the link closure pipeline stage and the nodes are said to be occluded, as illustrated in Figure 45. The maximum distance that allows two stations of specific antenna heights to be within optical line-of-sight of each other is given by [36]:

$$d_{\max} = 3.57(\sqrt{h_1} + \sqrt{h_2}) \tag{B-1}$$

where d_{max} is the maximum optical line-of-sight distance in km, and h_1 and h_2 are the antenna heights of the two stations in meters.

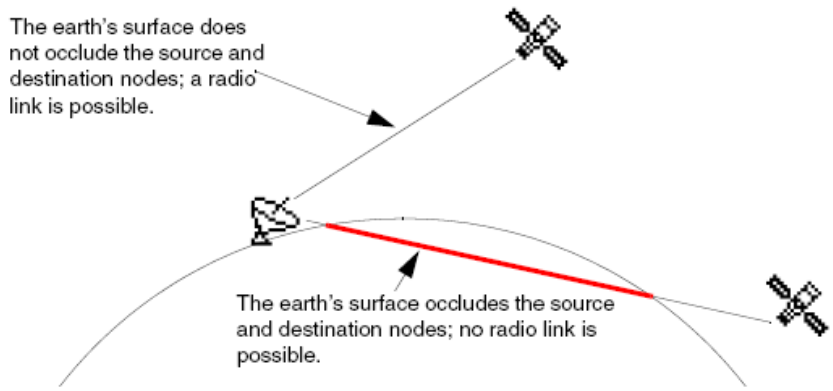

Figure 45. Link Closure Pipeline Stage (OPNET Modeler© 12.0 Documentation)

- Data packets arriving at the receiver are classified as valid if their power exceeds a predetermined power threshold. The calculation of the power of the received packets is based on link budget analysis and Friis' formula for free space path loss [37]:

$$P_R = \frac{P_T G_T G_R}{\left(\frac{4\pi d}{\lambda}\right)^2} \tag{B-2}$$

where, P_T and P_R are the transmitted and received power respectively, G_T and G_R are the antenna gains of the transmitter and receiver, d is the link distance,

and λ is the transmission frequency. Therefore, an appropriate combination of these values is required. The transmitted power and the received power threshold are determined in the attributes of the node model in the parameters for the WLAN, as presented in Figure 46. The antenna gains are indirectly determined by configuring the antenna pattern (directivity) with the aid of the antenna pattern editor.

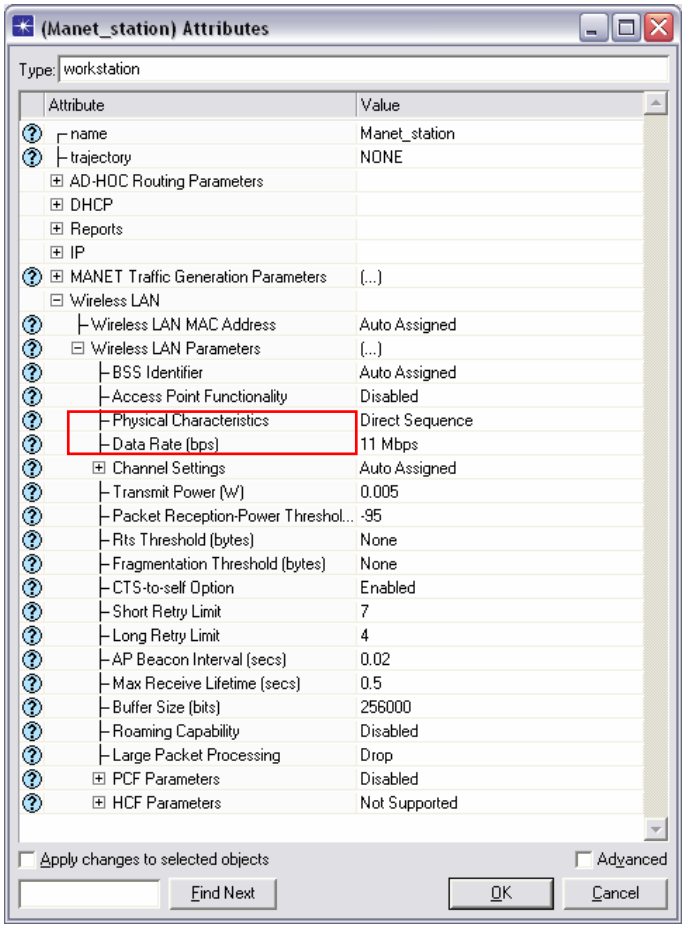

Figure 46. MANET node model attributes (WLAN parameters)

Most of the node attributes regarding the WLAN parameters may also be found and configured in the attributes of the transmitter and receiver modules of the corresponding nodes. However, the attribute value declared in the fields of the WLAN parameters has priority and dominates in case an inconsistency occurs.

2. Selection of Network Statistics

Prior to executing a simulation, the user must determine the system variables and metrics he wishes to collect. A simulation can generate a significantly large number of either built-in or user defined local as well as global statistics. These statistics are associated with the protocols implemented throughout the network and are available at the network level (global) as well as in the node and module level (local). In most cases, a small portion of the available data are of interest to the user. Therefore, the collection of unnecessary information may degrade the simulation speed and exceeds the storage space.

The mechanism that specifies which information is to be collected during a simulation is called *Probe Object*. Probe objects are not part of the network model, instead they serve the role of a passive data collection mechanism that is "attached" to a node or module in the network model that is capable of generating information during a simulation. Of the different types of the existing probes, the interest here is placed on the statistic probes. These may be selected for each node and its modules individually through the "Chose individual DES statistics" option by right-clicking on the node in the Project Editor, as shown in Figure 47.

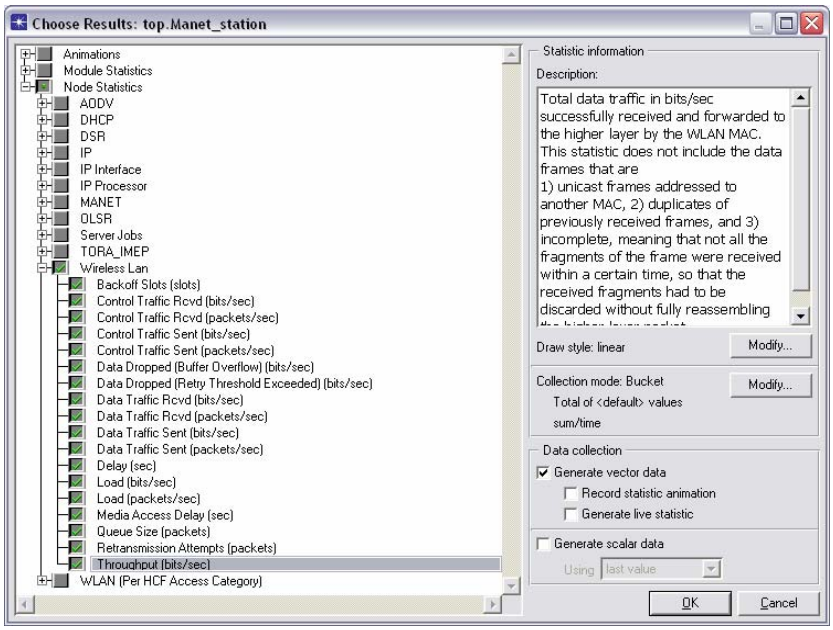

Figure 47. Selection of Individual WLAN Node Statistics

3. Simulation Execution

In OPNET Modeler, the mechanism responsible for executing a simulation run is called the *Discrete Event Simulator (DES)*. The user has the ability to configure certain attributes of the simulation run, such as duration, update interval and values per statistic. Additionally, the DES has the capability of executing parametric simulations runs. The parameter may be selected to be any attribute of the network's node models. To declare a node attribute as a simulation parameter its value field in the attributes of the corresponding node has to be set to "promote attribute to higher level". This parameter then appears in the "object attribute" field of the DES, where the user has the capability of assigning to it multiple values, as illustrated in Figure 48.

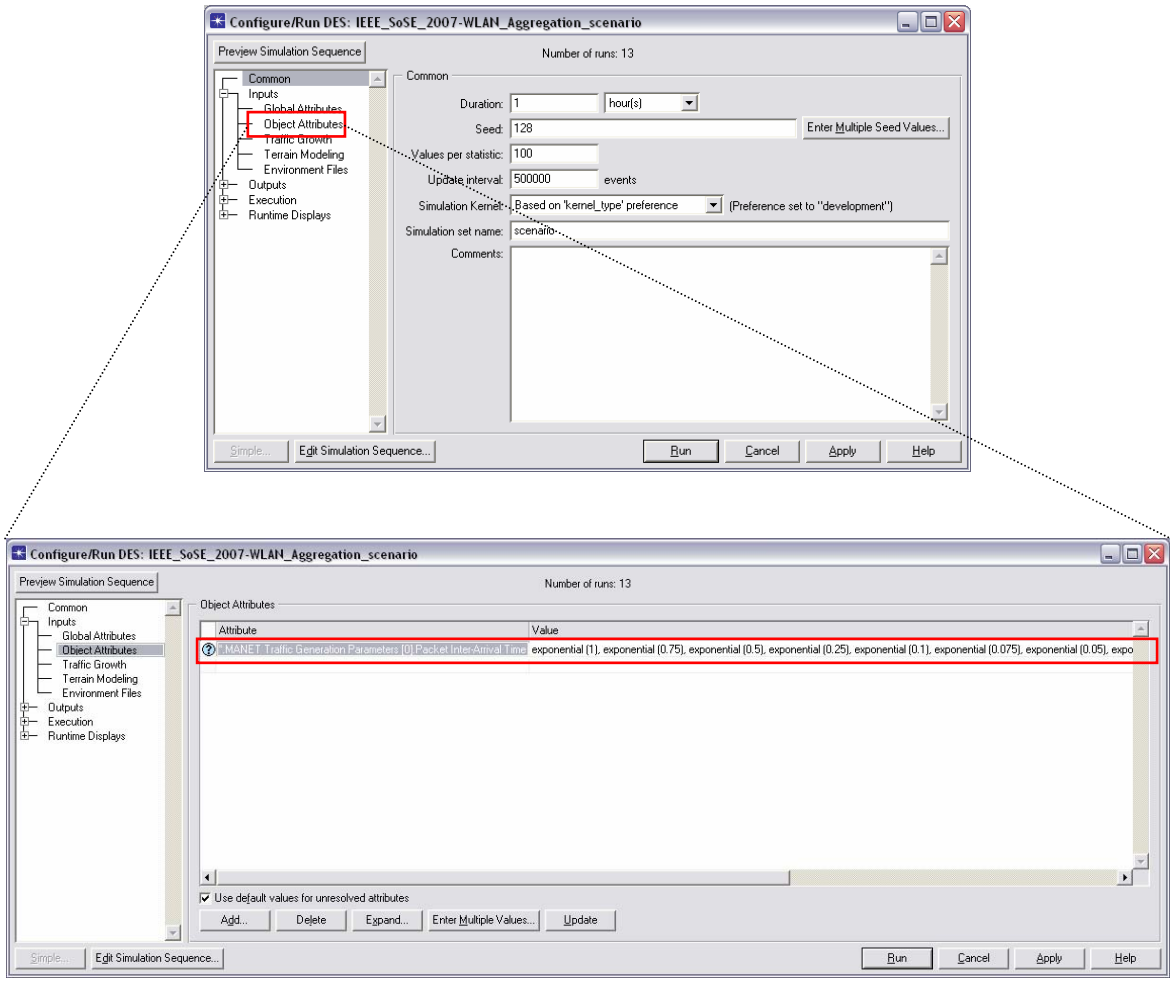

Figure 48. Declaration of multiple simulation parametric values in the DES

4. Presentation and Analysis of Results

Upon successful completion of the simulation run, the results may be viewed by selecting the "view results" button in the project editor. The user has the ability to observe the simulation results in two different ways as described below.

a. DES Graphs

In the "DES Graphs" window, the collected statistics may be presented as a function of time. Additionally, if a parameter was set for the simulation run, then the results obtained from each parametric simulation may be viewed either stacked or overlaid. In Figure 49, the results collected from several parametric simulations for the WLAN throughput are presented overlaid as a function of time.

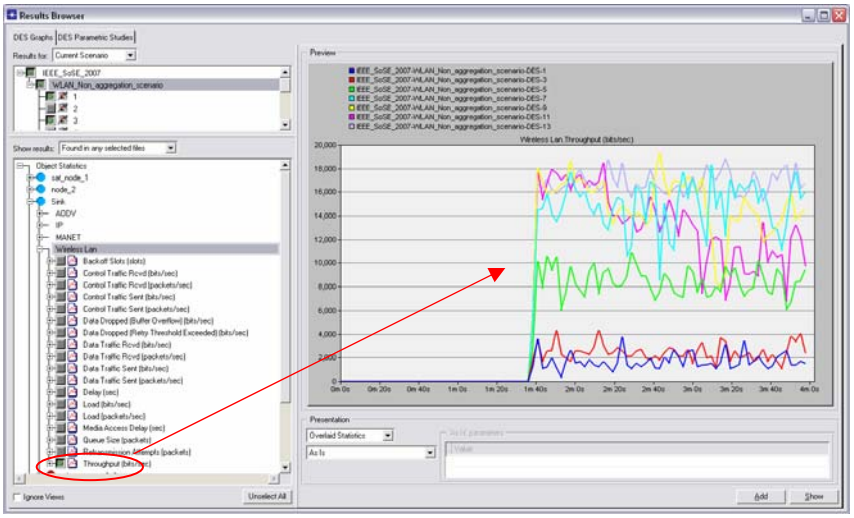

Figure 49. Overlaid results from parametric simulation runs as a function of time

b. DES Parametric Studies

In the "DES Parametric Studies" window, the collected statistics may be presented as a function of the selected parameter for the simulation. In Figure 50, the results obtained for the WLAN throughput are presented as a function of the source packet inter-arrival time.

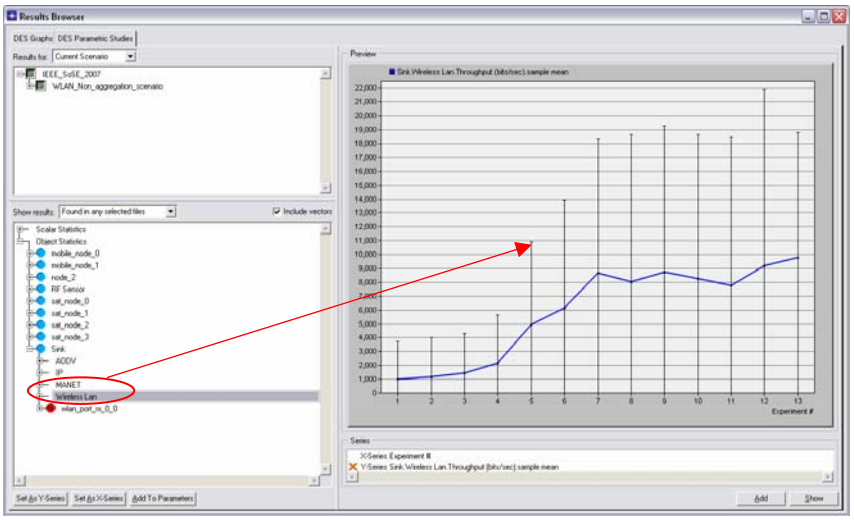

Figure 50. Results from parametric simulation runs as a function of the parameter

Furthermore, in both the "DES Graphs" and the "DES Parametric Studies", the user has the capability to export the collected statistics to a Microsoft Excel spreadsheet for further analysis, as illustrated in Figure 51.

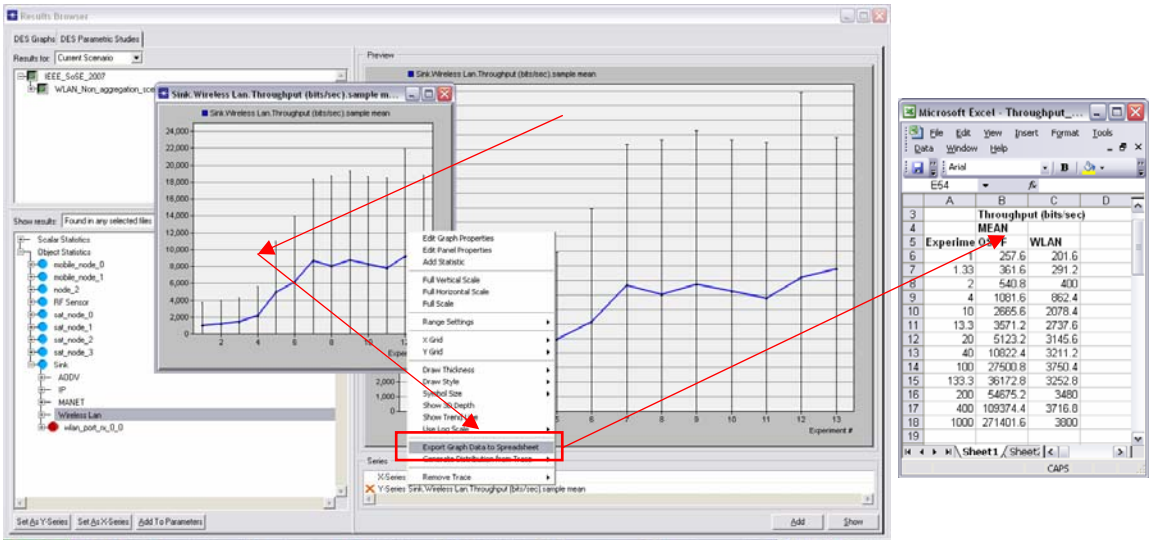

Figure 51. Export of collected statistics to a Microsoft Excel spreadsheet

APPENDIX C: DATA AGGREGATION IN OPNET MODELER

This appendix presents, through illustrations, the procedure in OPNET Modeler for the configuration of a "Node Model" to support data aggregation. As explained in Chapter III, the term aggregation does not imply any kind of sensor data fusion, merely consolidation of the received data.

Initially, from the network model, the node required to support data aggregation is identified and expanded. Next, within the node model, the process model for the traffic source module is expanded as well. This is illustrated in Figure 52.

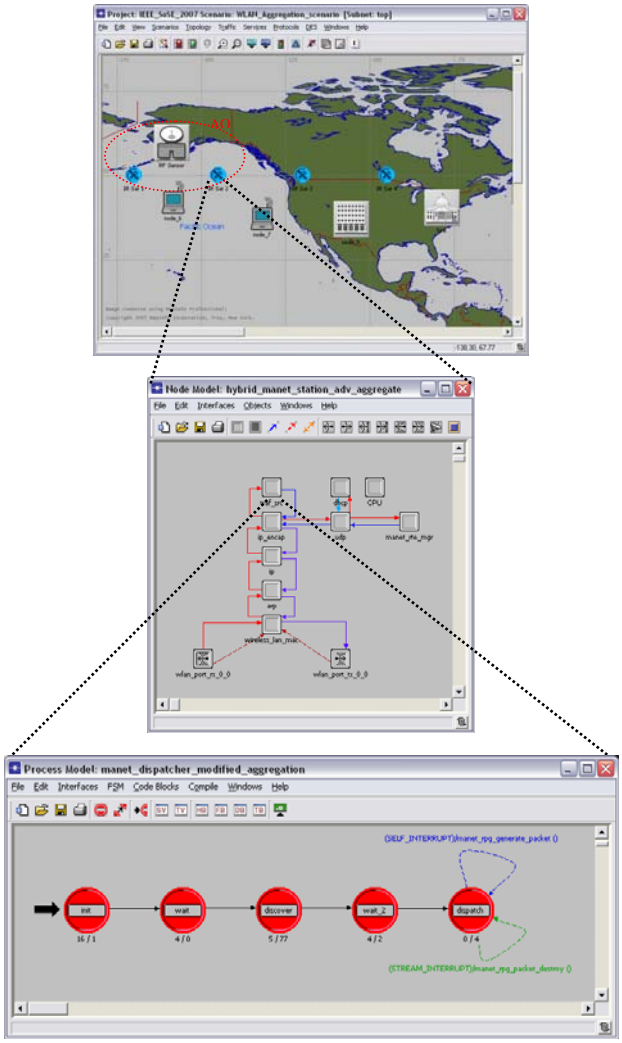

Figure 52. Network-Node-Process Model expansion

The objective is to implement a counter in the aggregation node that will be incremented each time a data packet arrives at the node. Until this counter reaches a predetermined threshold value, no packets are generated and forwarded by the aggregation node. When the threshold value is obtained, a new packet that has data length equal to the sum of the data of the received packets is generated and forwarded on the backflow to the destination.

1. Global Variable: aggr_threshold

First, the value of the threshold for the aggregation counter must be declared as a global variable. In OPNET Modeler, global variables provide a means for multiple processes in different modules to store information in a common location. The declaration of a global variable should be entered into the header block of the process model with which it is most closely associated, as shown in Figure 53 [38]. In this case, the threshold value is set to two since the data originating from two sensor nodes is being aggregated.

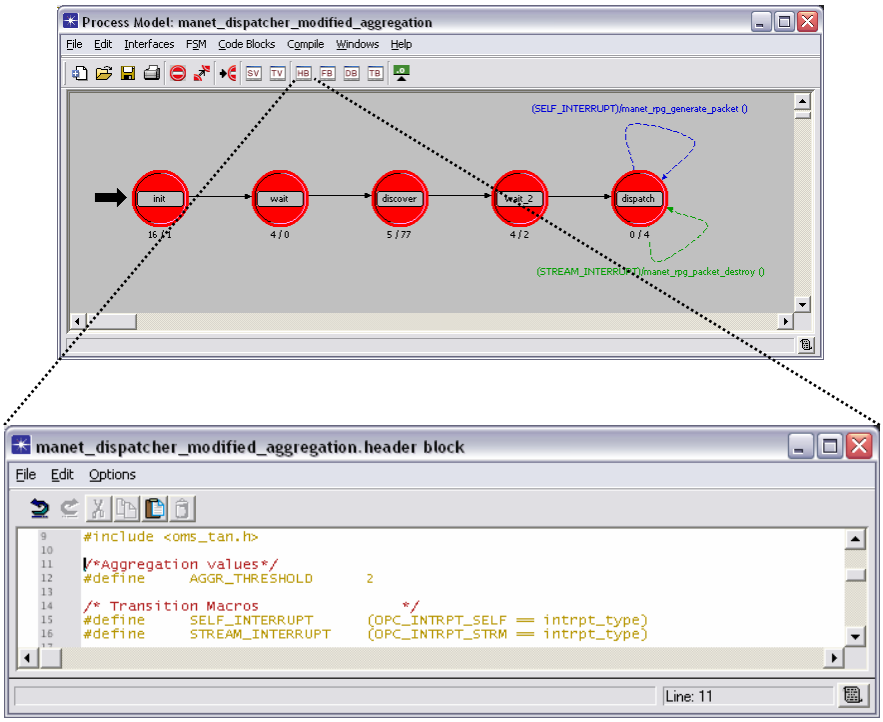

Figure 53. Global Variable Declaration

2. State Variable: aggr_counter

The counter implemented in the aggregation node must be declared as a state variable. In OPNET Modeler, state variables are used to represent the information accumulated and retained by a process. This name is due to the fact that these variables, together with the current position of a process within its state transition diagram, represent the complete state of a process at any time. State variables are declared in a dedicated area of a Proto-C model, referred to as the *state variable block*, as shown in Figure 54 [38].

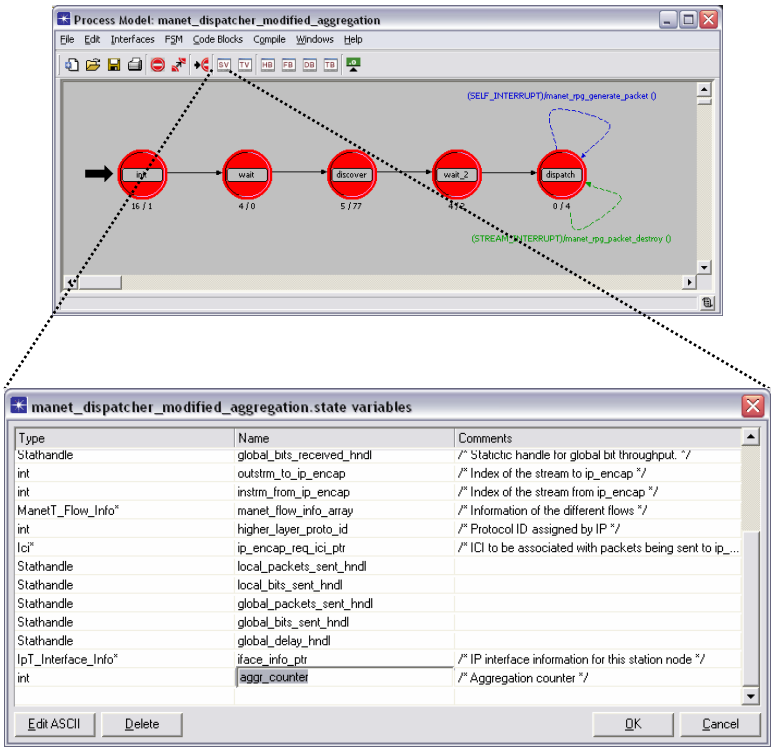

Figure 54. State Variable Declaration

3. Function Block

The function block is the section where the functions associated with a specific process model are specified. All normal syntactic rules of the C/C++ programming language apply within this section of the model. Functions defined within the function block have access to global variables as well as state variables. The contents of the function block can be edited as shown in Figure 55.

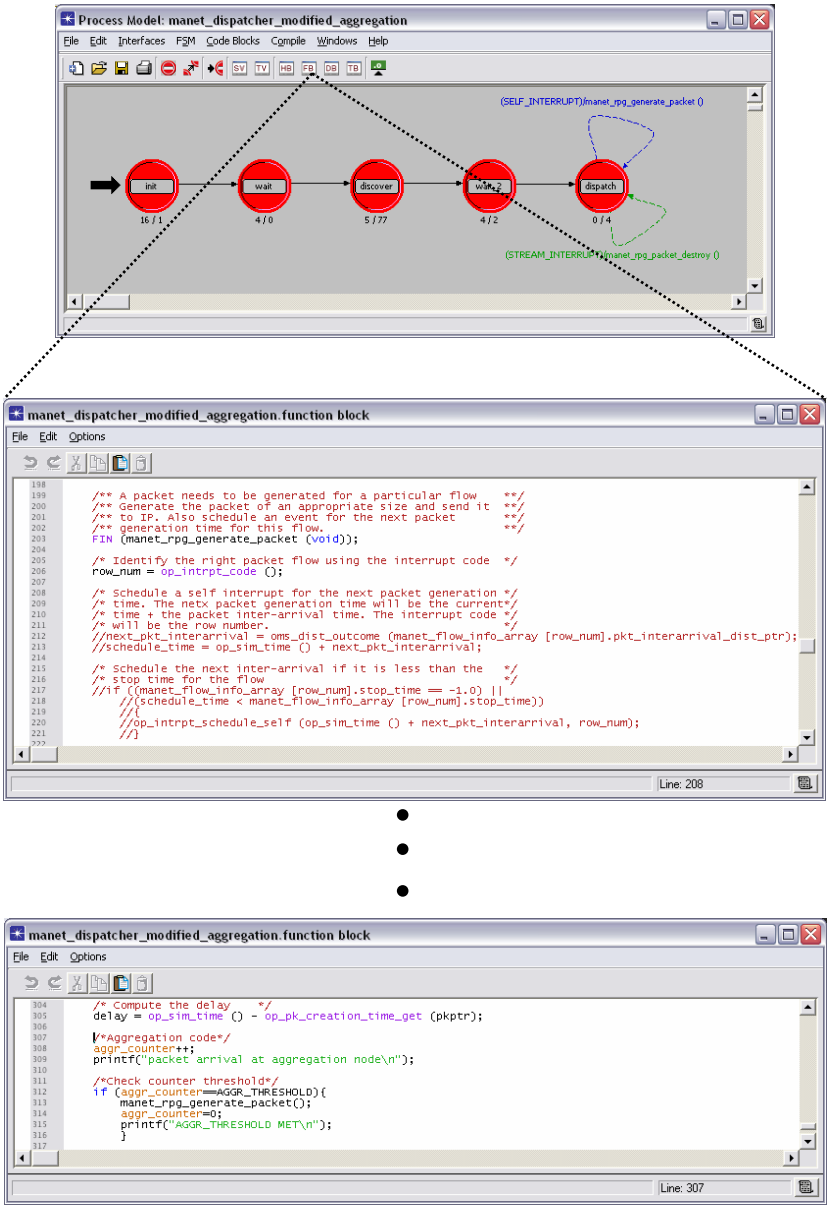

Figure 55. Process Function Block

In this case, the default content of the traffic source process function block has been modified in order to perform the task described previously. Specifically, the part of the function block, which triggers the traffic source to generate data automatically, has been omitted (lines 208-221 in Figure 55), and new commands have been added that implement the aggregation counter and the associated data packet generation (lines 307-316 in Figure 55).

APPENDIX D.

This appendix includes the graphs for the atmospheric transmittance and the solar spectral irradiance.

1. Atmospheric Transmittance for Wavelengths: 0.5 to 24 µm

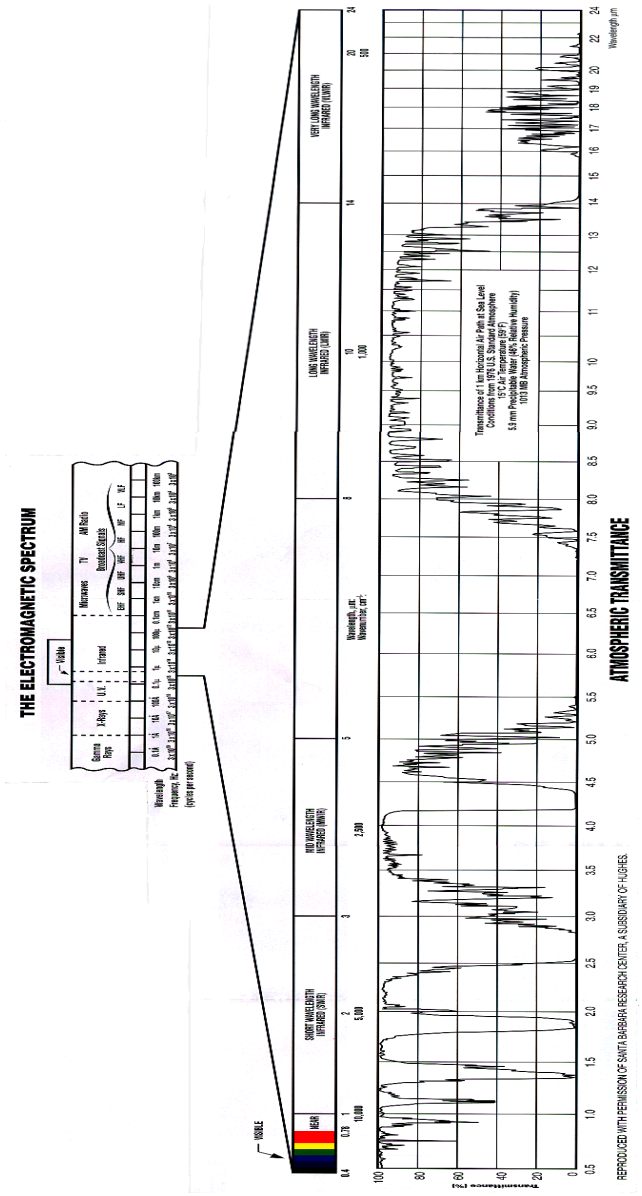

Figure 56. Atmospheric transmittance for wavelengths: 0.5 to 24 µm. (Santa Barbara Research Center, subsidiary of Hughes

2. Solar Spectral Irradiance

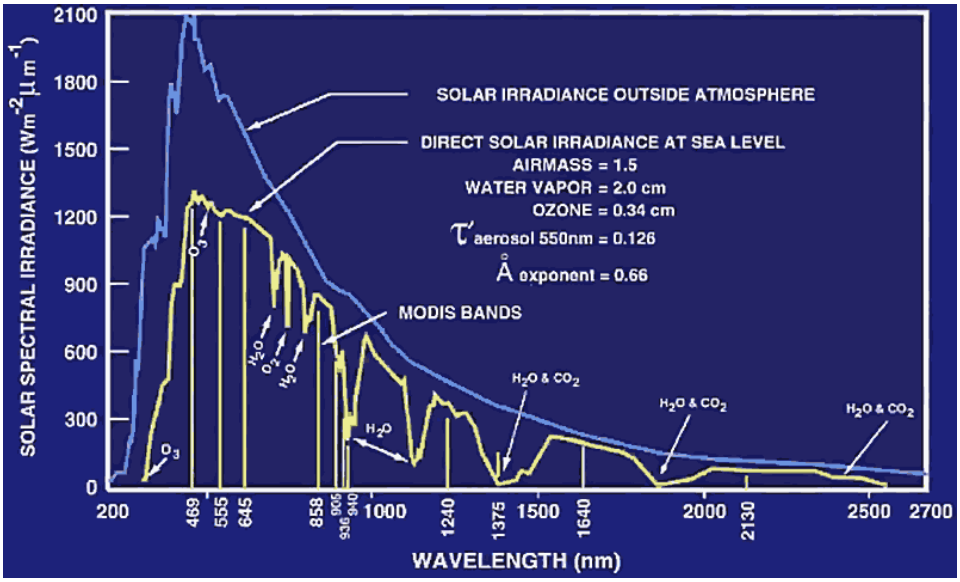

Figure 57. Solar Spectral Irradiance (NASA).

LIST OF REFERENCES

1. Missile Defense Agency (MDA), "Ballistic Missile Defense System overview (BDMS)," 15 Mar. 2005. Retrieved May 1, 2007 from http://www.mda.mil.html.

2. B. F. Levine, "Quantum-well infrared photodetectors," *Journal of Applied Physics*, Vol.74, No.8, Oct. 1993.

3. S. D. Gunapala, et al., "1024 × 1024 pixel mid-wavelength and long-wavelength infrared QWIP focal plane arrays for imaging applications," *Semiconductor Science & Technology* Vol.20, pp.473-480, 2005.

4. M. Z. Tidrow, "New infrared sensors for ballistic missile defense," Quantum Sensing and Nanophotonic Devices II, *Proceedings of SPIE* Vol. 5732, Bellingham WA, 2005.

5. D. Gavalas, et al., "Clustering of Mobile Ad Hoc Networks: An Adaptive Broadcast Period Approach," *IEEE ICC Proceedings*, pp.4034-4039, 2006.

6. J. Y. Yu and P. H. J. Chong, "A Survey of Clustering Schemes for Mobile Ad Hoc Networks," *IEEE Communications Surveys & Tutorials*, Mar. 2005.

7. B. Krishnamachari, D. Estrin, and S. Wicker, "Modeling Data-Centric Routing in Wireless Sensor Networks," *Proceedings of the IEEE INFOCOM*, 2002.

8. W. Heinzelman, J. Kulik, and H. Balakrishnan, "Adaptive Protocols for Information Disseminating in Wireless Sensor Networks," *Proceedings of the IEEE Mobicom*, pp. 174-185, Aug. 1999.

9. C. Intanagonwiwat, R. Govindan, D. Estrin, and J. Heidemann, "Directed Diffusion for Wireless Sensor Networking," *IEEE/ACM Transactions on Networking*, Vol.11, No.1, pp. 2-16, Feb.2003.

10. B. Krishnamachari, D. Estrin, and S. Wicker, "The impact of Data Aggregation in Wireless Sensor Networks," *Proceedings of the IEEE 22nd ICDCSW*, 2002.

11. L. Kleinrock and F. A. Tobagi, "Packet Switching in Radio Channels: Part I-Carrier Sense Multiple-Access Modes and their Throughput-Delay Characteristics," *IEEE Transactions on Communications*, Vol. Com-23, No.12, Dec. 1975.

12. S. S. Lam, "Delay Analysis of a Time Division Multiple Access (TDMA) Channel," *IEEE Transactions on Communications*, Vol. Com-25, No.12, Dec. 1977.

13. M. Z. Tidrow and W. R. Dyer, "Infrared Sensors for ballistic missile defense," *Infrared Physics & Technology*, Vol.42, pp.333-336, 2001.

14. D. W. Wilmot, W. R. Owens, and R. J. Shelton, *Electro-optical Systems Handbook Vol. 7: Countermeasure Systems*, Environmental Research Institute of Michigan, Ann Arbor, Michigan and SPIE Optical Engineering Press, Bellingham, Washington, 1996.

15. S. Blackman and R. Popoli, *Modern Tracking Systems*, Artech House, 1999.

16. H. E. Evans, et al., "The theory of single sensor altitude measurement," *Proceedings of IEEE National Aerospace and Electronics*, pp.851-8, May 1995.

17. E. L. Dereniak and G. D. Boreman, *Infrared Detectors and Systems*, Wiley, 1996

18. M. P. Touse, G. Karunasiri, and K. R. Lantz, "Near and mid-infrared detection using GaAs/$In_xGa_{1-x}As$/$In_yGa_{1-y}As$ multiple step quantum wells," *American Institute of Physics, Applied Physics Letters*, Vol.86, 2005.

19. S. D. Gunapala, et al., "Four-band quantum well infrared photodetector array," *Infrared Physics & Technology*, Vol.44, pp.369-375, 2003.

20. S. D. Gunapala, et al., "Quantum well infrared photodetector research and development at Jet Propulsion Laboratory," *Infrared Physics & Technology*, Vol.42, pp.267-282, 2001.

21. A. R. Jha, *Infrared Technology Applications to Electro-optics, Photonic Devices, and Sensors,* Wiley, 2000.

22. F. Neri, *Introduction to Electronic Defense Systems*, Artech House, 2001.

23. F. L. Pedrotti and L. S. Pedrotti, *Introduction to Optics*, Prentice Hall, 1993.

24. J. T. Caulfield, "Next Generation IR Focal Plane Arrays and Applications," *IEEE 32nd Applied Imagery Pattern Recognition Workshop*, 2003.

25. Jane's Strategic Weapon Systems. Retrieved May 21, 2007 from http://jsws.janes.com/public/jsws/index.shtml

26. D. Niculescu, "Communication paradigms for sensor networks," *IEEE Communications Magazine,* Vol.43, No.3, pp. 116-122, March 2005.

27. J. N. Al-Karaki and A. E. Kamal, "Routing techniques in wireless sensor networks: a survey," *IEEE Wireless Communications*, Vol.11, No.6, pp. 6-28, Dec. 2004.

28. J. Moy, “Open Shortest Path First (OSPF) Version 2”, IETF-Request for Comment (RFC) 1247, Jul. 1991.

29. R. W. Stevens, *TCP/IP Illustrated, Volume 1 – The Protocols*, Addison Wesley, 1994.

30. W. Stallings, *Wireless Communications & Networks*, Pearson Prentice Hall, 2005.

31. M. Tummala, Notes for EC4940 *(Ad-Hoc Wireless Networking)*, Naval Postgraduate School, 2006 (unpublished).

32. C. Perkins, et al., “Ad hoc On-Demand Distance Vector (AODV) Routing,” IETF-Request for Comment (RFC) 3561, Jul. 2003.

33. L. Kleinrock, *Queuing Systems, Volume I: Theory*, Wiley, 1975.

34. T. O. Walker, M. Tummala, and B. Michael, “A Distributed Medium Access Control Protocol for Wireless Networks of Cooperative Radar Systems,” *Proceedings of the IEEE International Conference on Systems of Systems Engineering*, San Antonio, TX, April 2007.

35. P. Katopodis, G. Katsis, T. O. Walker, M. Tummala, B. Michael, “A Hybrid, Large-scale Wireless Sensor Network for Missile Defense,” *Proceedings of the IEEE International Conference on Systems of Systems Engineering*, San Antonio, TX, April 2007.

36. W. Stallings, *Data and Computer Communications*, Pearson Prentice Hall, 2004.

37. B. Sklar, *Digital Communications – Fundamentals and Applications*, Prentice Hall PTR, 2001.

38. OPNET Technologies Inc., “Modeler Documentation Set”, Version: 12.0, 2006.

THIS PAGE INTENTIONALLY LEFT BLANK

INITIAL DISTRIBUTION LIST

1. Defense Technical Information Center
   Ft. Belvoir, Virginia

2. Dudley Knox Library
   Naval Postgraduate School
   Monterey, California

3. Ms. Deborah Stiltner
   Missile Defense National Team
   Crystal City, Virginia

4. Hellenic Navy General Staff (HNGS)
   Athens, Greece

5. Murali Tummala
   Naval Postgraduate School
   Monterey, California

6. Gamani Karunasiri
   Naval Postgraduate School
   Monterey, California

7. Bret Michael
   Naval Postgraduate School
   Monterey, California

8. Owens Walker
   Naval Postgraduate School
   Monterey, California

9. Panagiotis Katopodis
   Naval Postgraduate School
   Monterey, California